THESIS

# IMPACTS OF CLIMATE CHANGE ON THE HYDROLOGIC RESPONSE OF HEADWATER BASINS IN COLORADO

Submitted by

Caleb R. Foy

Department of Civil and Environmental Engineering

In partial fulfillment of the requirements

For the Degree of Master of Science

Colorado State University

Fort Collins, Colorado

Fall 2010

COLORADO STATE UNIVERSITY

July 9, 2010

WE HERBY RECOMMEND THAT THE THESIS PREPARED UNDER OUR SUPERVISION BY CALEB R. FOY ENTITLED IMPACTS OF CLIMATE CHANGE ON THE HYDROLOGIC RESPONSE OF HEADWATER BASINS IN COLORADO BE ACCEPTED AS FULFILLING IN PART REQUIREMENTS FOR THE DEGREE OF MASTER OF SCIENCE.

Committee on Graduate Work

_____
Stephanie Kampf

_____
Jorge Ramírez

_____
Advisor: Mazdak Arabi

_____
Department Head: Luis Garcia

ABSTRACT OF THESIS

IMPACTS OF CLIMATE CHANGE ON THE HYDROLOGIC RESPONSE OF HEADWATER BASINS IN COLORADO

The headwater basins of Colorado are heavily relied upon for freshwater resources on an annual basis. However, knowledge concerning generation of such resources, and implications of climate change on their availability in the future, is not well understood. Thus, this research has been undertaken to develop, calibrate, and test a comprehensive process-based model in four mountainous watersheds of Colorado, and investigate the potential impacts of changing climate on hydrologic response in these basins. Specifically, the four study watersheds considered for analysis include the Cache la Poudre, Gunnison, San Juan and Yampa River basins. Calibration of the model compared several parameter optimization techniques for performance in each of the study basins, which included the more common Shuffled Complex Evolution – University of Arizona (SCE-UA) method and a Markov Chain Monte Carlo (MCMC) method known as the Gibbs Sampler Algorithm (GSA). Fully calibrated and tested models were driven by a suite of 112 climate projections, downscaled both spatially and temporally, and were run on a daily time-step for a period of 90 years from 2010 – 2099.

Results from model calibration indicate GSA outperformed SCE-UA in a majority of the study basins, in addition to revealing promising results from a two-stage method that combined the strengths of the two techniques. Error statistics showed very good

(Nash-Sutcliffe coefficient of efficiency > 0.75 and relative error < +/- 10%) performance of monthly streamflow simulations compared to naturalized flows at the outlet of each watershed over a period of 16 years (1990 – 2005). Additionally, the models provided satisfactory results for simulating monthly streamflow at multiple sites nested within each watershed, which increased confidence in model parameterization and representation of dominant hydrologic processes. Results indicate that on an average annual basis, 55% – 65% of precipitation goes to evapotranspiration, and lateral flow contributes to between 64% and 82% of gross water yield. Results from future simulations over the course of the 21$^{st}$ century indicate inconsistent responses in streamflow to increasing temperature and variable precipitation projections. However, results did show consistency in the Yampa River basin, where 71 out of 112 future projections resulted in statistically significant ($\alpha$<0.1) positive trends of average annual streamflow. Furthermore, all study basins exhibited a decreasing ratio of precipitation to potential evapotranspiration from emissions scenario ensemble averages, which suggest Colorado basins will become more arid over the 21$^{st}$ century. Future forecasting of water availability in Colorado may benefit from this research, as specific climate projections were provided that resulted in consistent responses (increasing and decreasing) in streamflow across all watersheds. Implications of this study are considerable, as management of water resources, both within the state and across the West, will be affected by freshwater availability in headwater basins of Colorado in the future.

Caleb R. Foy
Department of Civil and Environmental Engineering
Colorado State University
Fort Collins, CO 80523
Fall 2010

ACKNOWLEDGEMENTS

This project was funded by the Department of Civil and Environmental Engineering at Colorado State University. First of all, I would like to acknowledge the time and support provided by my advisor, Dr. Mazdak Arabi, in addition to my committee members, Dr. Stephanie Kampf and Dr. Jorge Ramírez, for their comments and critiques regarding my research. I would also like to acknowledge support provided by the environmental Risk Assessment & Management System (eRAMS) group, especially from Haw Yen and Pranay Sanadhya. Lastly, I would like to acknowledge Northern Water and the Colorado Division of Water Resources for access to naturalized streamflow data as well as the modeling groups, the Program for Climate Model Diagnosis and Intercomparison (PCMDI) and the WCRP's Working Group on Coupled Modelling (WGCM) for their roles in making available the WCRP CMIP3 multi-model dataset. Support of this dataset is provided by the Office of Science, U.S. Department of Energy.

TABLE OF CONTENTS

LIST OF FIGURES

LIST OF TABLES

## CHAPTER 1: INTRODUCTION

Freshwater is one of the most basic necessities required to sustain all forms of life on this planet. Not only are freshwater resources needed to sustain all living organisms, but access to them is needed for nearly all human activities. In fact, the United Nations recently regarded access to safe freshwater as a universal human right (United Nations Committee on Economic, 2003). However, access to freshwater, let alone safe and usable freshwater, is far from secure as the 21$^{st}$ century progresses. More than one-sixth of the world's population live in glacier- or snowmelt-fed river basins, where impacts of climate change, resulting from observed and projected increases in temperature and precipitation variability, will be potentially felt through alterations to availability of freshwater resources (Kundzewicz et al., 2007). Not only is future climate change predicted to affect the mean hydrology of river basins, but it is also likely to affect the frequency and magnitude of extreme hydrologic events (Praskievicz and Chang, 2009). Thus, hydrologic modeling has increasingly been recognized as an important tool for improved understanding of the processes involved in generation of freshwater resources, as well as prediction of the potential impacts from changing climate and land use on such supplies (Praskievicz and Chang, 2009).

A majority of the watersheds in the western United States are prime examples of complex systems. The snow-dominated mountainous terrain which characterize such basins make simulation of hydrologic processes difficult, let alone projections of future

conditions. Additionally, effective water management relies on accurate representation of mountainous watersheds in this region, where 50-70% of the precipitation may fall in the form of snow (Serreze et al., 1999), and the seasonal snowmelt of the spring and early summer may account for 50-80% of the total annual runoff (Stewart et al., 2004). Therefore, it is expected that policy makers and stakeholders of the present and future will be looking to scientists for explanations and predictions concerning the availability of the freshwater resources in order to make informed decisions as the 21$^{st}$ century progresses.

The future availability of freshwater is especially important in the headwater basins of Colorado. The headwater basins of Colorado are located primarily on and near the Continental Divide, of which those on the western side drain into the Upper Colorado River (Figure 1.1). Thus, there is a great deal of interest concerning the future yield of Colorado watersheds, especially those draining into the Upper Colorado River, as they provide many of the surrounding drier states (e.g. Arizona, New Mexico, Utah, and California) a substantial amount of water on an annual basis. However, the future of such supplies is also extremely important within the state due to a majority of Colorado's population residing east of the Continental Divide in the Front Range. These areas typically receive considerably less precipitation than those on the Western Slope, and will continue to rely upon the transfer of foreign water, across the divide, to meet increasing agricultural, municipal, environmental, and recreational demands.

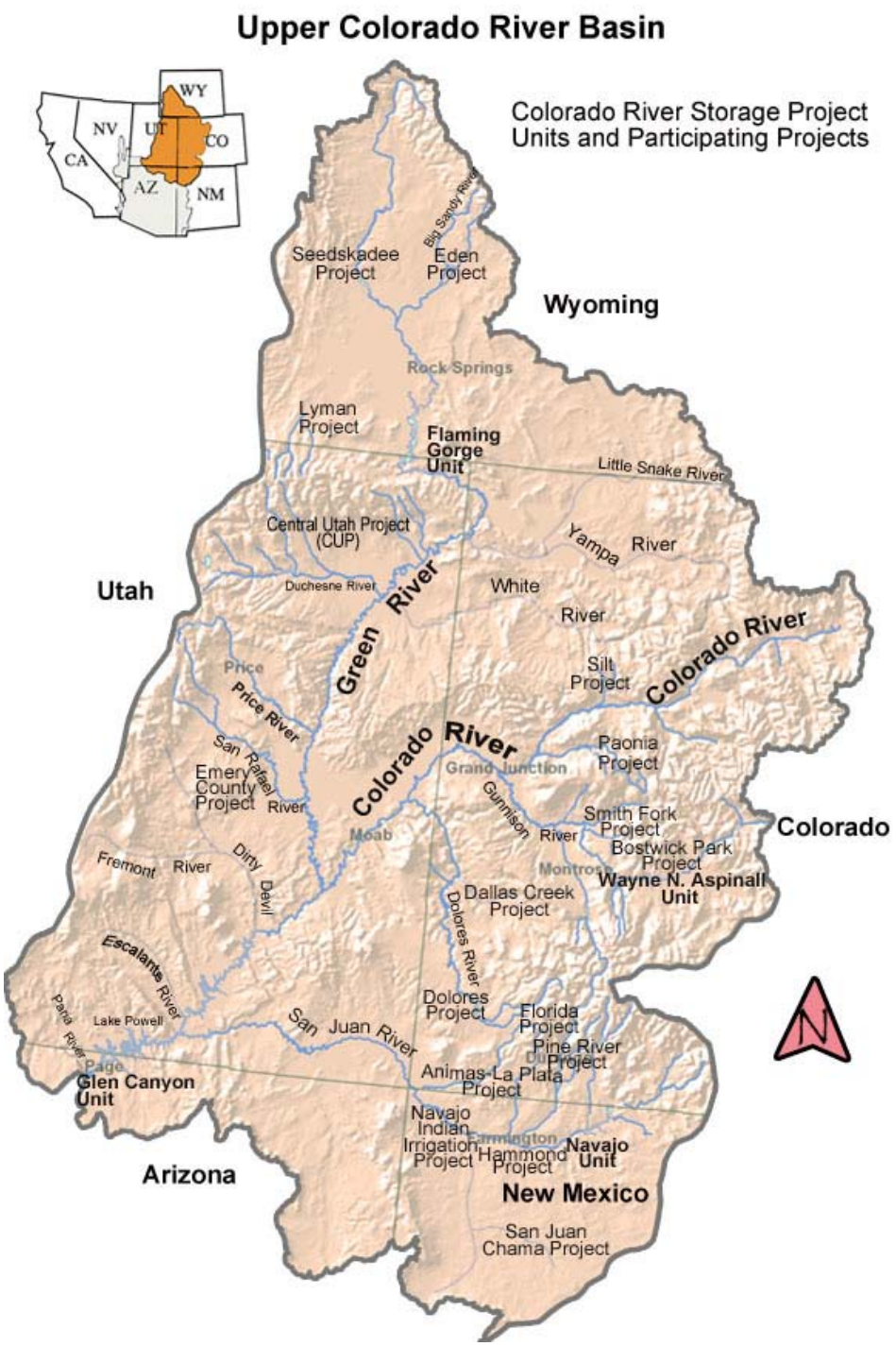


**Figure 1.1 –** Spatial extent and major tributaries of the Upper Colorado River basin. Map courtesy of Bureau of Reclamation (2009).

Existing studies concerning the impacts of climate change on the hydrology and water resources of Colorado have typically been undertaken at very coarse spatial scales, with grid cells ranging in size from as large as several hundred miles (e.g. Milly et al.,

2005), to as little as eight miles (e.g. Christensen and Lettenmaier, 2007). Such studies have discerned the hydrologic response to climate change from General Circulation Model (GCM) output and macro-scale hydrologic models, respectively, and do not include comprehensive analyses of processes important at the watershed scale. Additionally, the majority of studies have focused on the Upper Colorado River basin and have neglected to analyze other headwater basins in Colorado. The overall goal of this study is also to predict the impacts of climate change on the hydrology and water resources in Colorado, but to do so at a localized, watershed scale in an attempt to provide stakeholders and decision makers the information they need at the scales they work. The four watersheds chosen for this study represent a diverse set of attributes characteristic of headwater catchments in Colorado. One area of study, the Cache la Poudre watershed, is located on the eastern side of the Continental Divide in the north-central portion of the state and provides water for a variety of uses along the Front Range. The other three study areas are located on the western side of the Continental Divide and represent three headwater tributaries of the Upper Colorado River. From north to south the tributaries include the Yampa, Gunnison, and San Juan Rivers, respectively, and provide water to the Upper Colorado River, Western Slope of Colorado, and Front Range via transbasin diversions and transfers. Thus, future availability of freshwater in these basins has important implications to many users, policymakers, and stakeholders both within the state of Colorado and across the West as a whole.

In order to determine the impacts of climate change specific to water resources of four headwater basins in Colorado, the objectives of this thesis are (i) to develop and test a comprehensive process-based watershed model that can, with a high level of

confidence, represent important hydrologic processes in the snowmelt-dominated headwater catchments of Colorado; (ii) to observe the dominance of various hydrologic fluxes in the study watersheds based on observed conditions in the past; (iii) to downscale, in space and time, an ensemble of climate projections in a manner which addresses both the error involved and uncertainty inherent in climate modeling through incorporation of numerous models and diverse emissions scenarios; and (iv) to objectively identify the direction and degree of potential impacts on water resources, namely water yield, in Colorado and associate specific climate projections with low and high conditions of freshwater availability.

This thesis is organized into two standalone chapters and the information is presented in the following manner. The second chapter describes, in detail, the framework of the hydrologic model chosen for the study, as well as the development, calibration, and validation of the model for each of the study watersheds within Colorado. The third chapter presents the future climate projections that were utilized in addition to the temporal and spatial downscaling techniques implemented, and provides results from simulations driven by each of the projections in the study basins. The fourth and final chapter concludes with a synthesis of the overall results and possible applications of the research.

## REFERENCES


Bureau of Reclamation, U.S., 2009. Upper Colorado River Basin Map.

Christensen, N.S., Lettenmaier, D.P., 2007. A multimodel ensemble approach to assessment of climate change impacts on the hydrology and water resources of the Colorado River Basin. Hydrology and Earth System Sciences, 11(4): 1417-1434.

Kundzewicz, Z.W., Mata, L.J., Arnell, N.W., Doll, P., Kabat, P., Jiménez, B., Miller, K., Oki, T., Sen, Z., Shiklomanov, I., 2007. Freshwater resources and their management. In: Parry, M.L., Canziani, O.F., Palutikof, J.P., van der Linden, P.J., Hanson, C.E. (Eds.), Climate Change 2007: Impacts, Adaptation and Vulnerability. Contribution of Working Group II to the Fourth Assessment Report of the Intergovernmental Panel on Climate Change. Cambridge University Press, Cambridge, UK, pp. 173-210.

Milly, P.C.D., Dunne, K.A., Vecchia, A.V., 2005. Global pattern of trends in streamflow and water availability in a changing climate. Nature, 438(17): 347-350.

Praskievicz, S., Chang, H., 2009. A review of hydrological modelling of basin-scale climate change and urban development impacts. Progress in Physical Geography, 33(5): 650-671.

Serreze, M.C., Clark, M.P., Armstrong, R.L., McGinnis, D.A., Pulwarty, R.S., 1999. Characteristics of the western United States snowpack from snowpack telemetry (SNOTEL) data. Water Resources Research, 35(7): 2145-2160.

Stewart, I.T., Cayan, D.R., Dettinger, M.D., 2004. Changes in snowmelt runoff timing in western North America under abusiness as usual'climate change scenario. Climatic Change, 62(1-3): 217-232.

United Nations Committee on Economic, S.a.C.R., 2003. General Comment No. 15 (2002). United Nations Economic and Social Council, Geneva, pp. 1-18.

# CHAPTER 2: HYDROLOGIC MODELING OF COLORADO WATERSHEDS

## 2.1 INTRODUCTION

Hydrologic modeling has increasingly been recognized as an important tool for improved understanding of the processes involved in generation of freshwater resources, as well as prediction of the potential impacts from changing climate and land use on such supplies (Praskievicz and Chang, 2009). Hydrologic fluxes in mountainous watersheds, often headwater basins that exhibit a steep gradient in elevation, are particularly important as these areas often provide a significant source of freshwater for more arid surrounding lowlands. In the mountainous regions of western North America, where 50-70% of the precipitation may fall in the form of snow (Serreze et al., 1999), the seasonal snowmelt of the spring and early summer may account for 50-80% of the total annual runoff (Stewart et al., 2004). In fact, all major headwater river basins in Colorado provide substantial amounts of water to surrounding western and midwestern states, including Arizona, California, Kansas, Nebraska, Nevada, New Mexico, Oklahoma, Texas, Utah, and Wyoming. Therefore, understanding and quantifying the hydrologic processes that control generation and movement of water in headwater catchments of Colorado has significant implications for management of scarce water resources in the western United States. The comprehension and ability to represent such processes is vital for the proper

and effective management of water resources, both in the present and future years to come.

Hydrologic modeling of mountainous watersheds is often complicated by confounding factors such as scarcity and inadequate distribution of high elevation meteorological stations (Stonefelt et al., 2000), poor resolution of available climatic data (Marks et al., 1992), orographic effects on both precipitation (Hjermstad, 1970) and temperature (Barry and Chorley, 1976), and presence of snow accumulation and snowmelt processes (Luce et al., 1998). In addition, in areas where storage and redistribution of snowmelt driven flows are important (e.g. headwater basins of Colorado), modeling efforts may be complicated by the intricate system of reservoirs, diversions, transfers, and other man-made structures typically present in such watersheds.

The complexity of hydrologic models, specifically those designed for basin-wide analyses, has increased significantly since creation of the first continuous watershed model in the mid-1960s, the Stanford Watershed Model (SWM) (Crawford and Linsley, 1966). Such advancement in model complexity is mainly attributable to the spread and advancement of computing technologies, which has given models the ability to simultaneously represent more processes over larger spatial scales at smaller time steps. The sheer number of contemporary hydrologic models makes it inappropriate to document each of them herein. However, a selection of those commonly used include two successors of SWM, the Hydrologic Simulation Program—Fortran (HSPF) (Bicknell et al., 1997) and the Storm Water Management Model (SWMM) (Rossman, 2009), in addition to the Precipitation-Runoff Modeling System (PRMS) (Leavesley et al., 1983), the watershed-scale model MIKE-SHE (DHI, 2004), the Variable Infiltration Capacity

(VIC) model (Liang et al., 1994; Liang et al., 1996), and the model of choice in this study, the Soil and Water Assessment Tool (SWAT) (Arnold et al., 1998). Although each of the previously mentioned models are unique in the way certain hydrologic processes are described and interactions between them are simulated, a commonality shared by all is the multitude of parameters required to describe such phenomena.

One difficulty in the application of process-based hydrologic models is parameterization of the model. Parameterization of models becomes more challenging in large complex watersheds due to the spatial variability of watershed characteristics (e.g. elevation, land use, soil, climate, etc.). Furthermore, actual measurements of physically-based parameters are subject to measurement error and issues of scaling, such that many of the parameters in a hydrologic model will not be known. The ensuing adjustment of parameters to align select model output(s) with their respective observations is performed to reduce uncertainty in both parameterization and simulation of the model, and is a process known as model calibration. Manual calibration, when a user specifies the optimal set of parameters based on experience with the model and knowledge of the processes involved, can be both subjective and time consuming depending on the user. Automatic calibration, on the other hand, requires nothing more than identification of the parameters to be calibrated along with a range of allowable values for each of them, therefore addressing the disadvantages associated with manual calibration.

Methods for automatic calibration have been evolving for over four decades, stemming from the initial works of Dawdy and O'Donnell (1965), Nash and Sutcliffe (1970), Ibbit and O'Donnel (1971), and Johnston and Pilgrim (1976). Today, one of the most widely used optimization algorithms adopted for automatic calibration of

hydrologic models is the Shuffled Complex Evolution – University of Arizona (SCE-UA) method (Duan et al., 1993; Duan et al., 1992). SCE-UA is a global optimization method that has been shown to be both robust and efficient in finding the global optimum of an objective function in the hyper-cubic parameter space of several physically-based models (e.g. Duan et al., 1992; Kuczera, 1997; Sorooshian et al., 1993). One critique of the method is the number of runs it takes to converge upon a solution, which becomes prohibitive when the number of model parameters to be estimated exceeds a dozen (Lin and Radcliffe, 2006). This critique was substantiated by an application of SCE-UA to SWAT (Eckhardt and Arnold, 2001), where it took nearly 18,000 model runs to converge to a solution of 18 parameters. Other optimization algorithms may be better suited for applications involving an abundance of parameters (e.g. SWAT), such as those that fall under the category of Markov Chain Monte Carlo (MCMC) methods, as convergence is typically not slowed by increasing dimensionality problems (Givens and Hoeting, 2005). Several of such MCMC methods have previously been applied to SWAT as parameterization tools (e.g. Kuczera and Parent, 1998; Vrugt et al., 2003; Yang et al., 2008), but one notable exception remains the Gibbs sampler algorithm (GSA), which is specifically adapted for multidimensional target distributions. To date, no attempt to implement GSA into SWAT or compare its performance to other optimization algorithms, has been found in primary literature.

There have been multiple studies involving the development, calibration, and testing of SWAT to simulate hydrology in mountainous basins across the country, and include applications in the Upper Wind River Basin, WY (Fontaine et al., 2002; Stonefelt et al., 2000), Cannonsville Reservoir Watershed, NY (Tolson and Shoemaker, 2007),

Blue River Watershed, CO (Lemonds and McCray, 2007), Tenderfoot Creek Basin, MT (Ahl et al., 2008), Dry Creek Experimental Watershed, ID (Stratton et al., 2009), and Reynolds Creek Experimental Watershed, ID (Sridhar and Nayak, 2010). However, no studies to date have been found which specifically address the suitability of SWAT to simulate hydrologic processes in the major mountainous river basins of Colorado, at the larger watershed-scale proposed herein. Additionally, many of the previous studies have applied SWAT to one watershed in a region, whereas this research addresses four watersheds within the state of Colorado. Furthermore, the SWAT model is typically calibrated and tested at a single site (the outlet) of a watershed. In an attempt to obtain higher confidence in the model's ability to accurately simulate physical processes, results from multiple sites within each of the watersheds were analyzed.

This study aims to identify critical hydrologic processes that control the generation of streamflow and movement of water at varying spatial scales within four snow-dominated, mountainous watersheds of Colorado. To this end, the following objectives are defined: (i) development of a comprehensive, process-based watershed model for each of the study watersheds through incorporation of detailed watershed characteristics and necessary modifications for mountainous basins; (ii) evaluation of the efficiency of two parameter estimation techniques, SCE-UA and GSA, for parameterization of the models using naturalized streamflows at multiple sites within each basin; and (iii) evaluation of the importance of specific hydrologic components (e.g. evapotranspiration, snow processes, groundwater processes, etc.) occurring in the complex, high-elevation watersheds of Colorado.

## 2.2 METHODS

The comprehensive, process-based watershed model SWAT was developed, calibrated, and tested in four mountain watersheds to assess and quantify the dominant hydrologic processes occurring at the watershed-scale in the headwaters of Colorado. A SWAT model was developed for each of the study basins which utilized a variety of high-resolution spatial datasets describing terrain, land cover, soil, and climatic characteristics. In order to ensure accurate representation of hydrology within the basins, the model simulations were compared to naturalized flow data at multiple locations within the watersheds. Naturalized flows reflect the records of streamflow with the influence of flow modifications removed. Two separate optimization techniques were utilized to calibrate the models on a monthly time-step over a period spanning January 1990 through December 1997, a total of 8 years. The optimal parameter sets from the calibration period were applied to the model and tested for an additional 8 years at the monthly time-step, from January 1998 through December 2005. Multiple commonly-used error statistics were computed to evaluate the performance of the model over the calibration and validation periods. The outputs of the SWAT model were analyzed to quantify and compare the dominant hydrological processes occurring in the mountainous headwater basins of Colorado.

### 2.2.1 STUDY WATERSHEDS

Four headwater catchments in the state of Colorado were considered for this study, including the Cache la Poudre, Gunnison, San Juan, and Yampa River basins (Figure 2.1). The study watersheds range in size from the 2732 $km^2$ Cache la Poudre basin to the

10,284 $km^2$ Gunnison basin. Three of the watersheds are located on the western side of the continental divide, making them tributaries of the Upper Colorado River, while only one of the watersheds is located on the eastern side of the continental divide, making it a tributary of the Mississippi River. As with many mountain watersheds located in the western United States, the four basins exhibit a wide variety of characteristics related to geology, climate, and land cover. Such variability in watershed characteristics is mainly attributable to complex terrain and high relief of elevation found within each of the basins.

*CACHE LA POUDRE RIVER BASIN*

The Cache la Poudre River basin spans two states, located primarily in northern Colorado with a small portion extending into southeastern Wyoming. The highest headwater tributaries originate in the southwest of the basin, on the eastern side of the Continental Divide in and around Rocky Mountain National Park, and drain the Mummy Range into the mainstem of the Cache la Poudre (Poudre) River. The Poudre River flows first through the Poudre Canyon before reaching the Great Plains and the Front Range municipalities of Fort Collins and Greeley, and finally its confluence with the South Platte River. For the purposes of this study, the outlet of the Cache la Poudre River basin was defined at the mouth of the Poudre Canyon at USGS Gage 06752000 (Figure 2.1).

*GUNNISON RIVER BASIN*

The Gunnison River basin rests on the west side of the Continental Divide, located centrally in the state of Colorado. The headwater tributaries of the basin originate on the western side of the Continental Divide and drain the Elk Mountains, Southern Sawatch

Range, and La Garita Mountains into the mainstem of the Gunnison River. The mainstem then flows northwest through the deep gorge of Black Canyon of the Gunnison National Park before meeting its confluence with the Colorado River just west of Grand Junction, CO. For the purposes of this study, the outlet of the Gunnison River basin was defined just upstream of Black Canyon of the Gunnison National Park, below the Gunnison Tunnel at USGS Gage 09128000 (Figure 2.1).

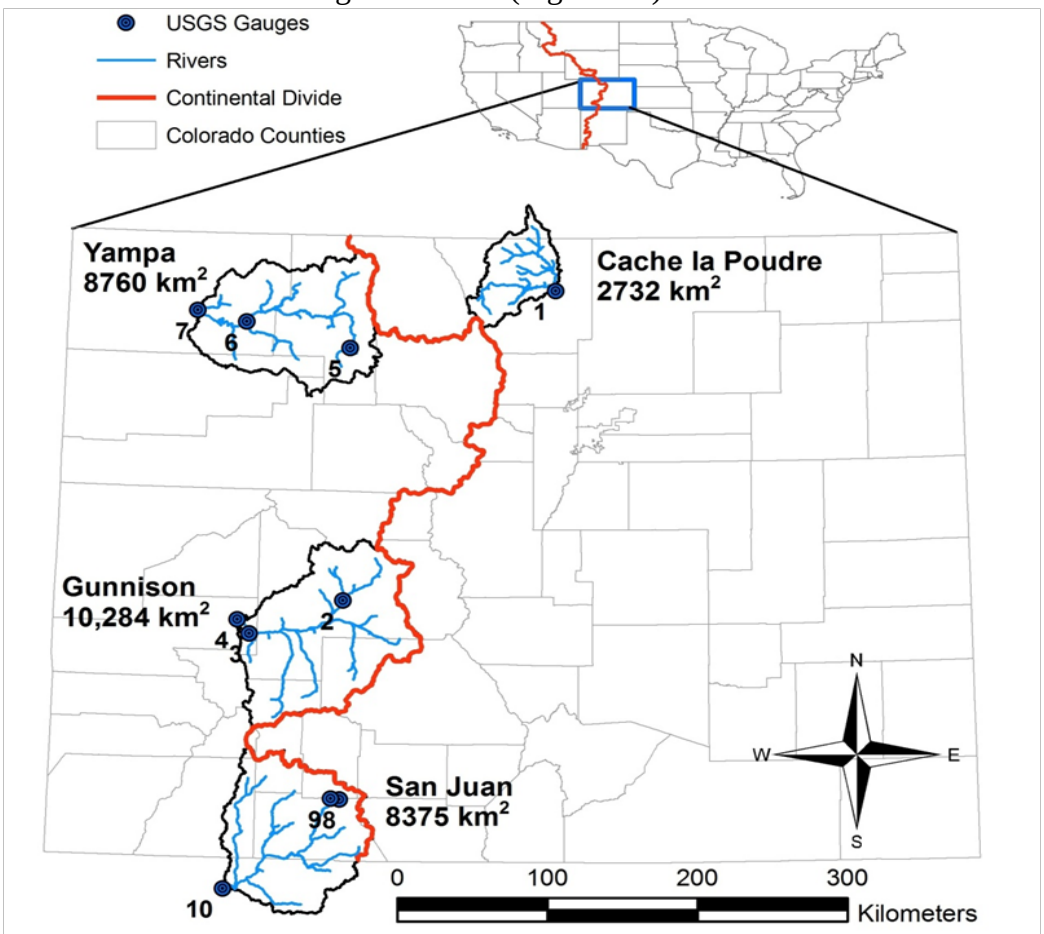


| No. | Watershed | USGS ID | Name |
|---|---|---|---|
| 1 | Cache la Poudre | 06752000 | Cache la Poudre River at Mouth of Canyon, near Fort Collins, CO |
| 2 | Gunnison | 09110000 | Taylor River at Almont, CO |
| 3 | Gunnison | 09126500 | Cimarron River at Cimarron, CO |
| 4 | Gunnison | 09128000 | Gunnison River below Gunnison Tunnel, CO |
| 5 | Yampa | 09237500 | Yampa River Below Stagecoach Reservoir, CO |
| 6 | Yampa | 09249750 | Williams Fork at Mouth, near Hamilton, CO |
| 7 | Yampa | 09251000 | Yampa River near Maybell, CO |
| 8 | San Juan | 09339900 | East Fork San Juan River near Pagosa Springs, CO |
| 9 | San Juan | 09341500 | West Fork San Juan River near Pagosa Springs, CO |
| 10 | San Juan | 09355500 | San Juan River near Archuleta, NM |

**Figure 2.1 –** Location of study basins and United States Geological Survey (USGS) surface water gauges considered during analysis.

*SAN JUAN RIVER BASIN*

The San Juan River basin flanks the west side of the Continental Divide, located primarily in southwestern Colorado with a sizable portion located in northwestern New Mexico. The headwater tributaries of the basin originate on the western side of the Continental Divide and drain the La Plata Mountains and portions of the San Juan Mountains into the mainstem of the San Juan River. The mainstem takes on many tributaries while flowing west through several states of the Four Corners region before meeting its confluence with the Colorado River as a tributary of the present-day Lake Powell. For the purposes of this study, the outlet of the San Juan River basin was defined near Archuleta, NM at USGS Gage 09355500 (Figure 2.1).

*YAMPA RIVER BASIN*

The Yampa River basin sits on the west side of the Continental Divide, nestled in the northwestern corner of Colorado and parts of southern Wyoming. The headwater tributaries of the basin originate on the western flank of the Continental Divide and drain the Elkhead Mountains, Central Park Range, and North Williams Fork Mountains into the mainstem of the Yampa River, which meanders through broad rural valleys and the desert canyons of Dinosaur National Monument before meeting its confluence with the Green River just east of the Utah state line. The Green River is a main tributary of the Colorado River, and joins it above present-day Lake Powell in Canyonlands National Park, UT. For the purposes of this study, the outlet of the Yampa River basin was defined near the town of Maybell, CO at USGS Gage 09251000 (Figure 2.1).

*CLIMATE*

The climate of mountainous watersheds in Colorado is not only highly variable amongst watersheds, but is also significantly different between locations within each watershed, even those locations in close geographic proximity. For instance in the Cache la Poudre River basin between the years 1998-2004, the average annual precipitation recorded at Deadman Hill of 721 millimeters was over twice that of the 308 millimeters of average annual precipitation recorded in Rustic (see Figure 2.2 for meteorological station locations). Not only was precipitation variable within the watershed, but during the same period, the average annual temperature at Deadman Hill (0.3 °C) was nearly six degrees Centigrade cooler than the average annual temperature in Rustic (6.0 °C). Although the two stations are relatively near one another (approximately 12 km), the variability in climate may be attributed to the difference in elevation, which is approximately 768 meters between Deadman Hill (3115.1 m) and Rustic (2347.0 m). Large gradients in elevation are typical of the mountainous watersheds of Colorado, and the distribution of elevation within each watershed may be seen in Figure 2.3.

*OROGRAPHIC EFFECTS ON PRECIPITATION AND TEMPERATURE*

It is well established that regional climate of mountainous watersheds is correlated with surface elevation. Thus, lapse rates were calculated for each of the study basins, which were used to quantify the rate at which temperature decreased and precipitation increased with increasing elevation.

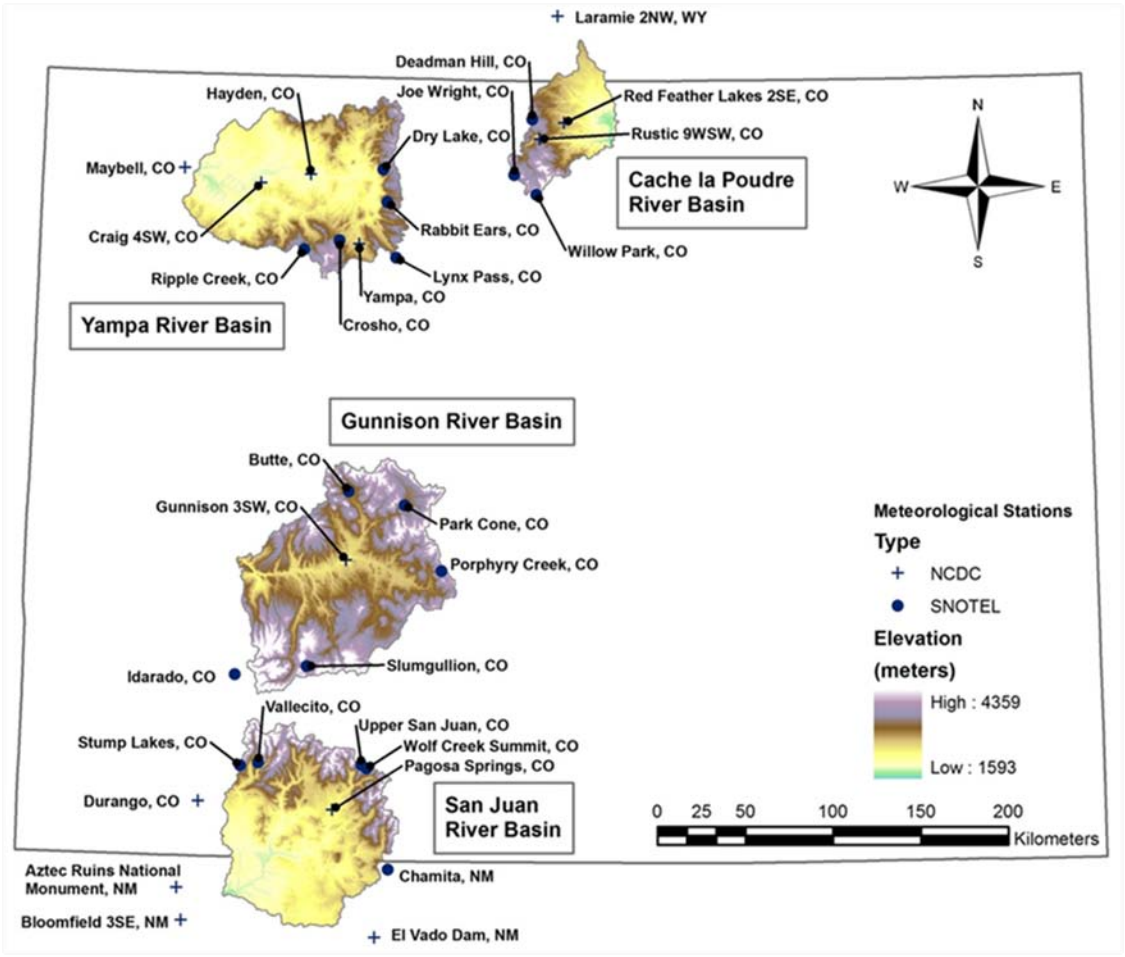


**Figure 2.2** – Topography, as represented by a digital elevation model (DEM), and location of meteorological stations (SNOTEL and NCDC) in each of the headwater basins of the Rocky Mountains, CO.

Due to the limited number of meteorological stations and also the scarcity of data, especially at SNOTEL climate stations located in higher elevations (Figure 2.2), a single lapse rate for surface temperature and a single lapse rate for precipitation was calculated in each of the study watersheds. This lapse rate was then assumed constant over the entirety of each respective watershed. The lapse rates were calculated from mean annual values averaged over a period of at least five years for precipitation and temperature, of which the period was chosen based on the most complete and reliable set of continuous years on record. This was found to be important for accurate characterization of annual

averages of temperature and precipitation, as a missing month of data could skew annual values depending on the season of that month. All meteorological stations (Figure 2.2) were utilized for the calculations with the exception of the Red Feather Lakes station in the Cache la Poudre watershed, which could not be used due to a lack of contemporary data. Graphical depictions of orographic effects on precipitation and temperature are presented in Appendix A.

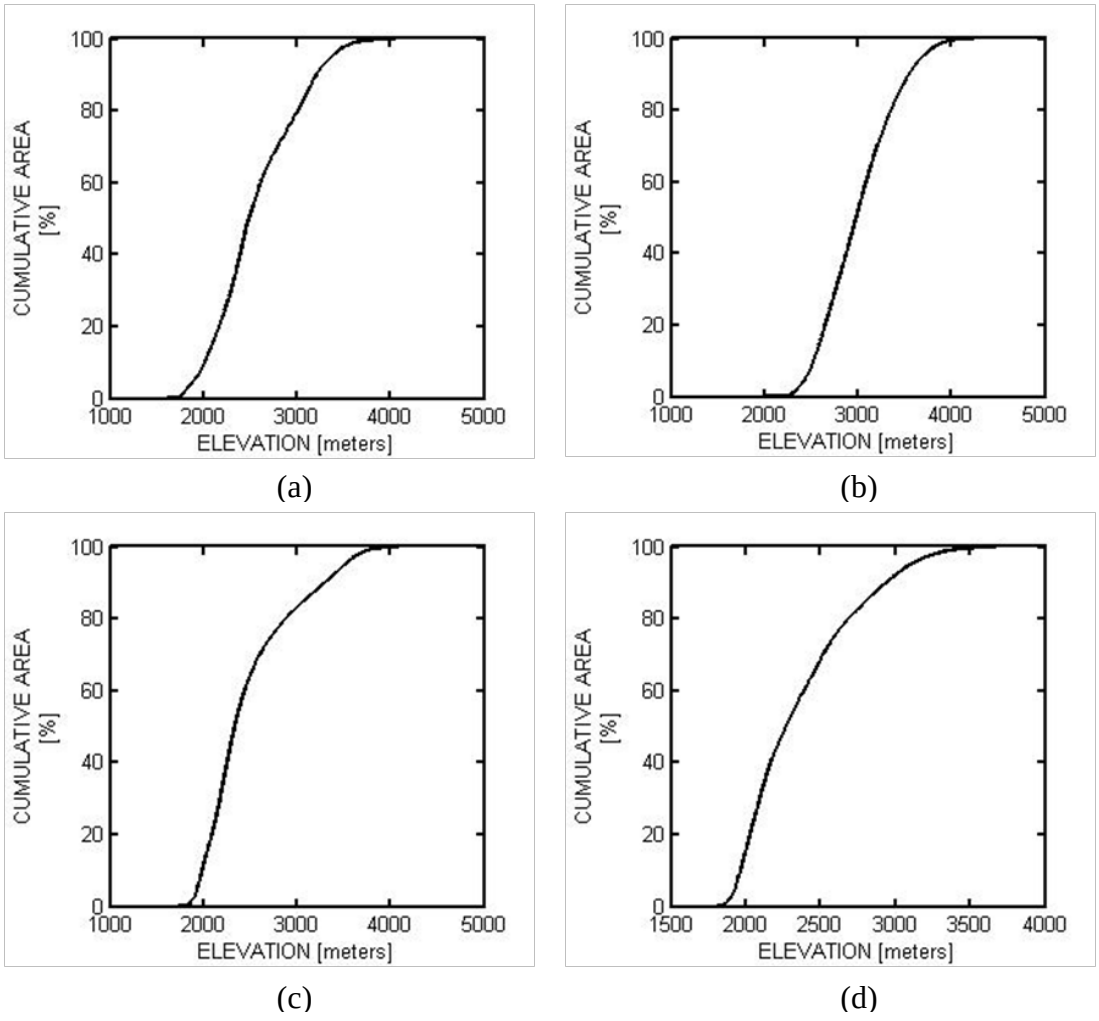


**Figure 2.3** – Hypsometric curves depicting the distribution of elevation within each of the (a) Cache la Poudre, (b) Gunnison, (c) San Juan, and (d) Yampa study basins.

Lapse rates for both temperature and precipitation varied among the study watersheds (Table 2.1). The precipitation lapse rates, which depict an increase in mean annual precipitation with an increase in elevation, varied from 353.9 mm/km in the Gunnison River Basin to 658.4 mm/km in the Cache la Poudre River Basin. The temperature lapse rates, which depict a decrease in mean annual temperature with an increase in elevation, varied from -2.7 °C/km in the Gunnison River Basin to -5.5 °C/km in the Cache la Poudre River Basin. The lapse rates computed and implemented in this study are similar to other published values including lapse rates for precipitation and temperature of 511.2 mm/km and -3.8 °C/km, respectively, in the Blue River Watershed, CO (Lemonds and McCray, 2007), and 500 mm/km and -5.0 °C/km, respectively, in the Upper Wind River Basin, WY (Fontaine et al., 2002).

**Table 2.1 –** Temperature and precipitation lapse rates representing orographic effects.

| Study Watershed | Precipitation Lapse Rate (mm/km)/$R^2$ | Temperature Lapse Rate ($^0$C/km)/$R^2$ | Period of Record | Elevation (m) |
|---|---|---|---|---|
| **Cache la Poudre** | 658.4/0.87 | -5.5/0.93 | 1998-2004 | 1594 – 4132 |
| **Gunnison** | 353.9/0.58 | -2.7/0.57 | 1996-2001 | 1982 – 4359 |
| **San Juan** | 434.9/0.79 | -5.4/0.83 | 2000-2004 | 1724 – 4280 |
| **Yampa** | 497.8/0.62 | -3.4/0.78 | 2002-2007 | 1804 – 3764 |

*LAND COVER/LAND USE*

The land cover distribution within each of the study basins was described using 2001 National Land Cover Data (NLCD 2001), and major types may be seen in Figure 2.4. At the highest elevations, land cover consists mainly of alpine tundra. Below tree line at moderate elevations, land cover consists mainly of subalpine coniferous forests and

deciduous forests. At the lowest elevations, land cover consists of shrub and scrublands, herbaceous grasslands, and pasture/hay.

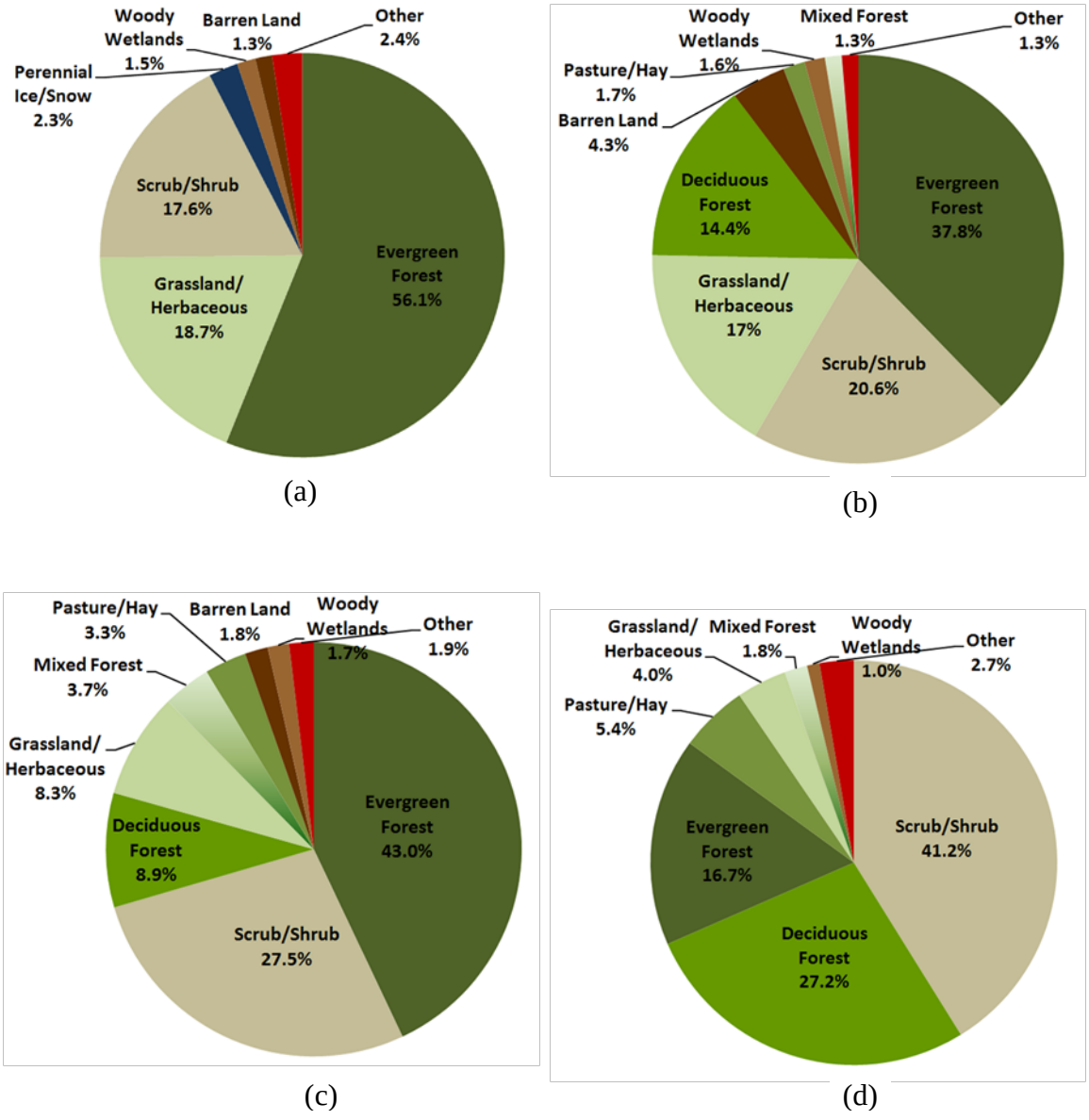


**Figure 2.4** - Distribution of land cover in the (a) Cache la Poudre, (b) Gunnison, (c) San Juan, and (d) Yampa study basins, computed from NLCD 2001.

*SOIL*

The distribution of soil within each of the study basins was described using a combination of the Soil Survey Geographic (SSURGO) Database and the State Soil Geographic (STATSGO2) Database. The distribution of the representative hydrologic soil groups is shown in Figure 2.5. The procedure utilized to combine the two datasets is outlined in the forthcoming section SWAT MODEL DEVELOPMENT, where details may be found regarding implementation of the soil databases into the SWAT model. The hydrologic soil group is a classification which refers to the drainage potential of a soil. Group A soils have the greatest ability to drain water (lowest runoff potential), and typically have less than 10% clay and more than 90% sand or gravel. Group B soils have a lower ability to drain water (moderately low runoff potential), and typically consist of 10 – 20% clay and 50 – 90% sand. Group C soils have a low ability to drain water (moderately high runoff potential), and typically consist of 20 – 40% clay and less than 50% sand. Group D soils have the lowest ability to drain water (high runoff potential), and typically consist of greater than 40% clay and less than 50% sand. In general, the soils in the study watersheds of Colorado have a relatively low ability to drain water, which is mainly attributable to the high amounts of clay found in the soils.

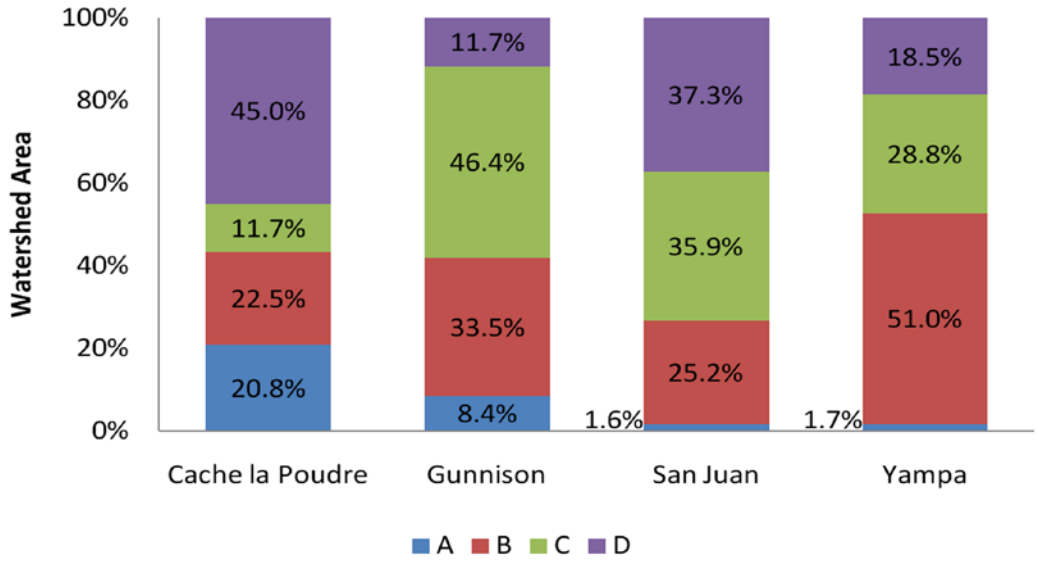


**Figure 2.5 -** Distribution of soil, as represented by hydrologic soil groups (A, B, C, and D), in each of the study basins.

### 2.2.2 HYDROLOGIC MODEL

The Soil and Water Assessment Tool Version 2005 (SWAT2005, referred to as SWAT hereafter) is a hydrologic model originally developed (as an earlier version) for the United States Department of Agriculture (USDA) Agricultural Research Service (ARS) as a tool to predict the effect of management practices on water, sediment, nutrient, and pesticide yields in agricultural basins over long periods of time (Arnold et al., 1998). Although SWAT was developed for agricultural watersheds, its application has now been extended to study the consequences of land use and climate change on hydrologic regimes (e.g. Li et al., 2009; Miller et al., 2002; Stone et al., 2001; Stonefelt et al., 2000). The model is semi-distributed, computationally efficient, process-based, and uses readily available input data (Neitsch et al., 2005), all of which assist in providing the ability to represent complex watersheds. SWAT is also a comprehensive model in that it has the ability to simulate important hydrologic processes such as surface runoff, return flow,

percolation, evapotranspiration, snow accumulation, snowmelt, and sediment movement, in addition to other agricultural processes such as crop growth and nutrient and pesticide loading (Figure 2.6).

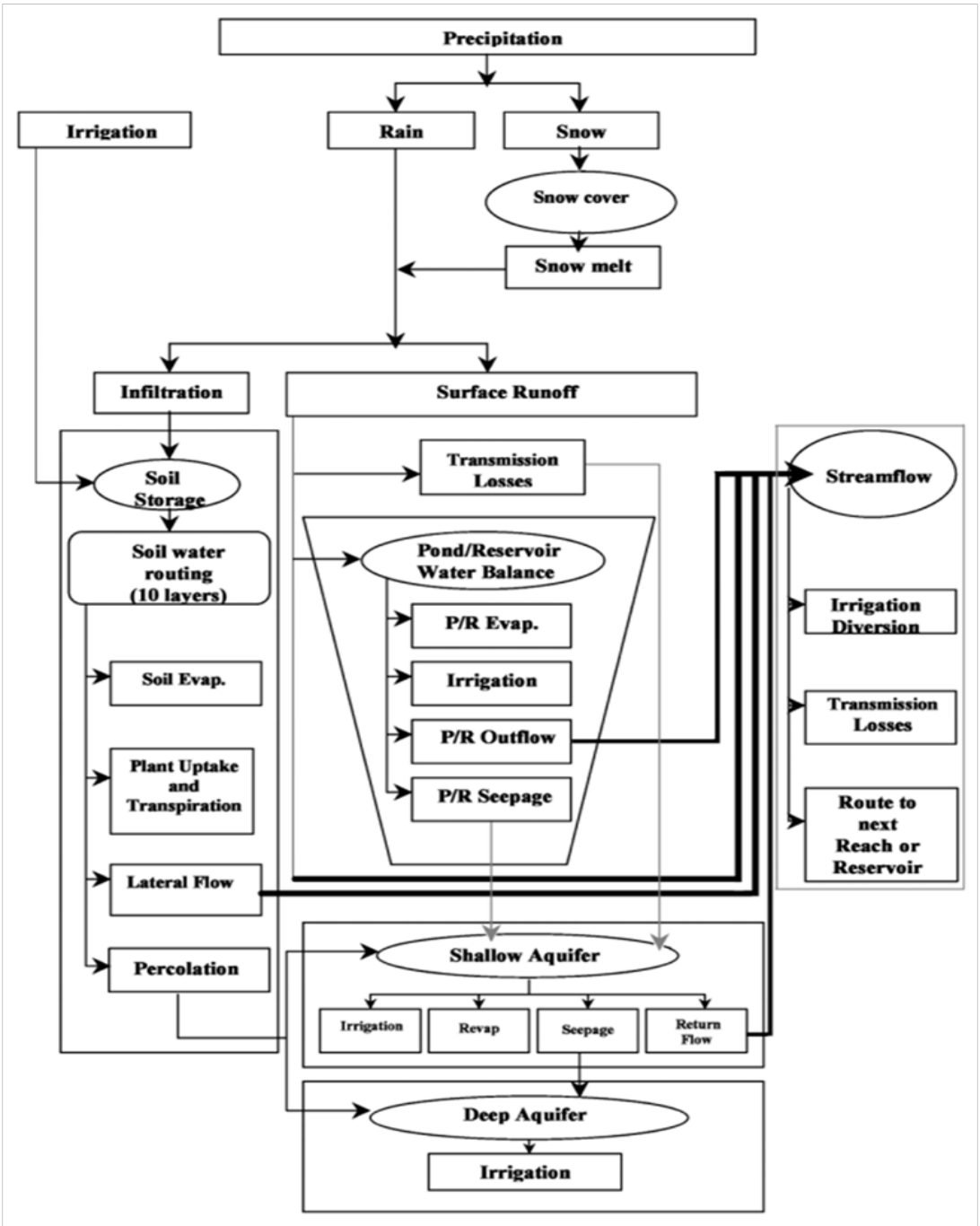


**Figure 2.6** – Schematic of the hydrologic process and pathways which are simulated in SWAT. Figure adapted from Eckhardt and Arnold (2001).

SWAT is a semi-distributed hydrologic model based on two levels of subdivision within a watershed. The first level of subdivision is the subbasin, which are linked together by main channel segments, or reaches. Each of the subbasins may be thought of as an individual unit, as they may be defined with unique climate and hydrologic properties. Within a subbasin, further partitioning is performed into areas with unique combinations of land use, management, and soil attributes, referred to as hydrologic response units (HRUs). The SWAT model simplifies runs by lumping together identical HRUs within a subbasin into single, non-interacting units of response (Neitsch et al., 2004), which in turn provides the model greater computational efficiency. Loadings of water, sediment, nutrients, etc. are aggregated at the HRU level, where they are transferred to the respective subbasin. From the subbasin-level, the constituents are delivered to the main channel reach at each subbasin outlet, from which they are routed to the outlet of the entire watershed.

*PHYSICAL BASIS*

SWAT is a physically-based hydrologic model in that most of its parameters can be measured in the field and physically-based equations are used to represent hydrologic processes, as opposed to empirical, regression-based equations. For example, the land phase of the hydrologic cycle is based on the water balance equation within each HRU (Neitsch et al., 2005):

$$SW_t = SW_0 + \sum_{i=1}^{t} \left(R_{day} - Q_{surf} - E_a - w_{seep} - Q_{gw}\right) \qquad \textit{Equation 2.1}$$

where $SW_t$ is the final soil water content on day $t$ (mm of water), $SW_0$ is the initial soil water content (mm of water), $t$ is the time (days), $R_{day}$ is the amount of precipitation on

day $i$ (mm of liquid water), $Q_{surf}$ is the amount of surface runoff on day $i$ (mm of water), $E_a$ is the amount of evapotranspiration (ET) on day $i$ (mm of water), $w_{seep}$ is the amount of water entering the vadose zone from the soil profile on day $i$ (mm of water), and $Q_{gw}$ is the amount of return flow on day $i$ (mm of water).

Potential evapotranspiration (PET) may be modeled in SWAT through the application of one of three physically-based methods: the Penman-Monteith method (Allen, 1986; Allen et al., 1989; Monteith, 1965), the Priestley-Taylor method (Priestley and Taylor, 1972), and the Hargreaves method (Hargreaves and Samani, 1985). Each of the methods requires a different amount of input data. The Penman-Monteith method requires solar radiation, air temperature, relative humidity, and wind speed, the Priestley-Taylor method requires solar radiation, air temperature, and relative humidity, while the Hargreaves method requires air temperature. The Penman-Monteith method is the default SWAT method for simulating PET, and was utilized in all watersheds except for the Cache la Poudre, where the Hargreaves method yielded better results.

*GROUNDWATER PROCESSES*

Water that reaches the soil has several pathways for movement in SWAT. The first pathway is removal from the soil, either through plant transpiration or evaporation. The second pathway is that of subsurface lateral flow, where water moves through the saturated soil profile and is ultimately contributed back to streamflow further down in the basin. The final pathway available to water that reaches the soil profile is aquifer recharge, where water percolates through the entire profile and is made available to the underlying aquifer as recharge.

Subsurface lateral flow is typically significant in areas with soils having high hydraulic conductivities and an impermeable or semi-permeable layer at a shallow depth (Neitsch et al., 2005), and is analogous to saturated subsurface flow. The SWAT model simulates such flow using a kinematic storage model developed by Sloan et al. (1984; 1983), from which the net daily discharge of subsurface lateral flow at the hillslope outlet, $Q_{lat}$ (mm), is calculated within each HRU as:

$$Q_{lat} = 0.024\left(\frac{2 * SW_{ly,excess} * K_{sat} * slp}{\emptyset_d * L_{hill}}\right) \qquad \textit{Equation 2.2}$$

where $SW_{ly,excess}$ is the specific drainable volume of water stored in the saturated zone of the hillslope per unit area (mm), $K_{sat}$ is the saturated hydraulic conductivity of the soil (mm/hr), *slp* (SWAT parameter SLOPE) is the slope (m/m), $\emptyset_d$ is the drainable porosity of the soil (mm/mm), and $L_{hill}$ is the hillslope length (m).

In large subbasins where not all subsurface lateral flow will reach the main channel in one day, a portion of the flow is lagged, or stored, for later release. The lateral flow released to the main channel on a given day, $Q_{lat,channel}$, within each subbasin is:

$$Q_{lat,channel} = \left(Q'_{lat} + Q_{latstor,i-1}\right)\left(1 - exp\left[\frac{-1}{TT_{lag}}\right]\right) \qquad \textit{Equation 2.3}$$

where $Q'_{lat}$ is the amount of subsurface lateral flow generated in a subbasin (summed across all HRUs within the subbasin) on a given day (mm), $Q_{latstor,\ i\text{-}1}$ is the amount of subsurface lateral flow stored from the previous day (mm), and $TT_{lag}$ is the travel time of the subsurface lateral flow (days).

SWAT represents subsurface hydrologic processes of aquifers through application of a kinematic storage model, which is based on conservation of mass (of water). Such processes are represented within the model at the subbasin level, where water percolating

through the entire soil profile may enter one or two aquifers; the shallow aquifer, an unconfined aquifer that contributes water to baseflow of the stream on the surface, and/or the deep aquifer, a confined aquifer where the water is assumed lost to the system (assumed to contribute to streamflow at a location further downstream of the watershed boundaries). The water balance for the shallow aquifer within each HRU is:

$$aq_{sh,i} = aq_{sh,i-1} + w_{rchrg,sh} - Q_{gw} - w_{revap} - w_{pump,sh} \qquad \textit{Equation 2.4}$$

where $aq_{sh,i}$ is the amount of water stored in the shallow aquifer on day $i$ (mm), $aq_{sh,i-1}$ is the amount of water stored in the shallow aquifer on day $i$-1 (mm), $w_{rchrg,sh}$ is the amount of recharge entering the shallow aquifer on day $i$ (mm), $Q_{gw}$ is the groundwater flow, or baseflow, into the main channel on day $i$ (mm), $w_{revap}$ is the amount of water moving up into the soil profile in response to water deficiencies on day $i$, and $w_{pump,sh}$ is the amount of water pumped from the shallow aquifer on day $i$ (mm).

The aquifer percolation coefficient, $\beta_{deep}$, determines the amount of total recharge from the soil profile, $w_{rchrg}$ (mm), which is percolated to the deep aquifer within each HRU:

$$w_{deep} = \beta_{deep} \times w_{rchrg} \qquad \textit{Equation 2.5}$$

where $w_{deep}$ is the amount of water percolating into the deep aquifer on day $i$. The remainder of the total recharge which does not enter the deep aquifer is allocated to the shallow aquifer, as $w_{rchrg,sh}$.

*SNOW-RELATED PROCESSES*

SWAT has the ability to represent several hydrologic processes specifically related to snow, including snow accumulation, snow distribution/cover, and snowmelt. Accounting

for snow hydrology is important, especially in the mountainous watersheds of Colorado where a substantial portion of the annual precipitation falls as snow over the winter months. Precipitation is simulated as snowfall when the mean daily air temperature is less than the snowfall threshold temperature (SWAT parameter SFTMP).

SWAT stores snowfall on the ground in the form of a snowpack, which is described by the snow water equivalent it holds. The daily mass balance for the snowpack within each HRU is represented as:

$$SNO_i = SNO_{i-1} + R_{day,i} - E_{sub,i} - SNO_{mlt,i} \qquad \textit{Equation 2.6}$$

where *SNO* is the snow water equivalent of the snowpack on day *i* (mm), $R_{day}$ is the amount of precipitation falling as snow on day *i* (mm), $E_{sub}$ is the amount of sublimation on day *i* (mm), and $SNO_{mlt}$ is the amount of snowmelt on day *i* (mm).

The snowpack of a subbasin is rarely uniform in distribution, and is often complicated by processes such as drifting and shading in complex topography. Thus, the areal coverage of the snowpack in a subbasin is dependent upon an areal depletion curve, which SWAT bases on a natural logarithm model, to correlate the areal coverage of the snowpack with the amount of snow present in the subbasin. A threshold depth of snow (SWAT parameter $SNO_{100}$) determines the amount of snow above which there will be 100% cover in a subbasin.

Daily snowmelt is modeled in SWAT as a function of maximum air temperature, snowpack temperature, melting threshold temperature, snow cover, and snow melting rate within each HRU as:

$$SNO_{mlt} = b_{mlt} \times sno_{cov} \times \left[\frac{T_{snow} + T_{max}}{2} - T_{mlt}\right] \qquad \textit{Equation 2.7}$$

where $SNO_{mlt}$ is the amount of snowmelt in a day, $b_{mlt}$ is the melt fact (mm/day-°C), $sno_{cov}$ is the fraction of the HRU area covered by snow, $T_{snow}$ is the snow pack temperature (°C), $T_{max}$ is the maximum daily air temperature (°C), and $T_{mlt}$ is the threshold temperature above which snow is allowed to melt (SWAT parameter SMTMP) (°C).

*STREAMFLOW PARAMETERS*

SWAT has the ability to readily represent both snow-related and groundwater hydrologic processes through the previously discussed physically-based methods. Additional physically-based water balances are used for other components of the hydrologic cycle, and details may be found in the SWAT Theoretical Documentation (Neitsch et al., 2005). In order to represent such an array of hydrologic processes, SWAT has numerous parameters to represent the physical phenomena in which it simulates. In the present study, thirty streamflow-related parameters were adjusted for each watershed. The parameters, along with their associated minimum and maximum allowable values, descriptions, and related processes, are presented in Appendix B. The lower and upper bound of parameter values were obtained from the SWAT Theoretical Documentation (Neitsch et al., 2005). Parameters of SWAT may be defined at three spatial scales including the basin, subbasin, and HRU discretization levels. Thus, several parameters (indicated by an asterisk) have multiple values in subbasins with more than one HRU due to their dependence on land use and soil. In order to maintain the spatial variability of such parameters, they were adjusted as a fraction of their default value during optimization procedures.

*SWAT MODEL DEVELOPMENT*

The SWAT extension for ArcGIS, ArcSWAT Interface for SWAT2005 (Winchell et al., 2007), was utilized for model development in each of the four study basins. ArcSWAT is a graphical user interface which allows the user to easily assimilate the readily available input data during model development. The necessary spatial datasets and databases were collected and modified, as required by the model, before implementation into ArcSWAT. The input data, summarized in Table 2.2, were prepared as set forth in the ArcSWAT documentation (Winchell et al., 2007), and ensuing development of the model will be discussed in the following sections.

**Table 2.2** – SWAT input data.

| Data Type | Description | Access |
|---|---|---|
| Topography | 30-m DEM | http://seamless.usgs.gov/ - September, 2008 |
| Land cover | NLCD 1992; | http://www.mrlc.gov/index.php - September, 2009; |
| | NLCD 2001 | http://www.mrlc.gov/index.php - September, 2009 |
| Soil | STATSGO2; | http://soildatamart.nrcs.usda.gov/ - September, 2009; |
| | SSURGO | http://soildatamart.nrcs.usda.gov/ - September, 2009 |
| Weather | SNOTEL; | http://www.wcc.nrcs.usda.gov/snow/; September, 2008; |
| | NCDC | http://www.ncdc.noaa.gov/oa/ncdc.html - September, 2008 |

The first step in SWAT model development was to delineate the watershed as a whole, as well as the subbasins within the watershed. Delineation was performed using the interface and a 30-meter resolution Digital Elevation Model (DEM) from the U.S. Geological Survey (USGS) National Elevation Dataset (Gesch, 2007; Gesch et al., 2002). The whole watersheds were defined by their respective outlets, while subbasins were defined by outlets created at stream junctions, of which the extent is defined by a threshold area for stream initiation.

The land use/land cover attributes for each watershed were characterized by NLCD 2001 and NLCD 1992, which were produced by the Multi-Resolution Land

Characteristics Consortium (MLRC) with a methodology presented in two separate studies (Homer et al., 2004; Vogelman et al., 2001), respectively. The 1992 version of NLCD was used for model simulations during the years 1990-1997, while the 2001 version of NLCD was used for model simulations during the years 1998-present. SWAT classifies each type of NLCD land use/land cover into a corresponding type of SWAT land use/land cover (LULC) according to lookup tables, which may be found for both NLCD 1992 and NLCD 2001 in Appendix B. A thorough description of the types of land use/land cover present in each of the NLCD datasets are available in the original NLCD documentations (Homer et al., 2004; Vogelman et al., 2001).

Typically, the source for soil attributes utilized in SWAT are taken from the U.S. General Soil Map (STATSGO2), which was developed by the USDA Natural Resource Conservation Service (NRCS) National Cooperative Soil Survey (Soil Survey Staff, 2006). STATSGO2 provides a broad-based inventory of soils for the contiguous United States, Alaska, Hawaii, Puerto Rico, and the U.S. Virgin Islands in the form of geo-referenced vector and tabular digital data, and provides such soil attributes as texture, bulk density, hydraulic conductivity, and available water capacity. STATSGO2 has now been succeeded by the most detailed level of soil mapping provided by the NRCS, the Soil Survey Geographic (SSURGO) Database (Soil Survey Staff, 2009). SSURGO provides a county-level, more detailed inventory of soils for most of the contiguous United States, and is also provided in the form of geo-referenced vector and tabular digital data. Utilization of SSURGO as an alternative to STATSGO2 has the potential to not only better represent the physical properties of a basin (Anderson et al., 2006), but may lead to improvements in hydrologic simulations as well (Anderson et al., 2006; Di

Luzio et al., 2004; Wang and Melesse, 2006). Thus, in an attempt to improve simulation results, SSURGO soils were utilized wherever possible for each of the study watersheds.

In order to represent SSURGO soils in the SWAT model, a preprocessing tool was implemented. The preprocessing tool was originally developed for a similar SWAT interface, AvSWAT (Di Luzio et al., 2004; Peschel et al., 2006), and was modified for ArcSWAT as set forth by Sheshukov et al. (2009). However, due to the fine-scale resolution and continuing development of the SSURGO data, its extent does not cover the entire United States. Unfortunately, the SSURGO data has missing features which included portions of the four study watersheds in Colorado. In areas where SSURGO data was unavailable, the soil attributes were taken from STATSGO2, which created a SWAT model with the most detailed soil data available. Table 2.3 displays the difference in the number of unique soil types between STATSGO2, and the combination of SSURGO/STATSGO2 utilized in the analysis.

**Table 2.3** – Difference in resolution between soil datasets, as expressed by the number of unique soil types within each of the study basins.

| Watershed | STATSGO2 Soil Types | SSURGO / STATSGO2 Soil Types |
|---|---|---|
| **Cache la Poudre** | 10 | 164 |
| **Gunnison** | 25 | 248 |
| **San Juan** | 46 | 348 |
| **Yampa** | 25 | 317 |

With the land use and soil data input process complete, unique HRUs were defined and distributed throughout each subbasin. As previously stated, HRUs are areas with unique combinations of soil and land use, and those areas are lumped together within a subbasin to increase computation efficiency of the model. The same HRU may be distributed across a subbasin, depending on the distribution of soil and land use, in

areas that are not adjacent. The number of HRUs in a subbasin is determined by the number of unique combinations of soil and land use that are present. Threshold levels for both soil and land use may be implemented to avoid distribution of very small HRUs with little effect on model simulations. The ArcSWAT Documentation (Winchell et al., 2007), recommends a land use threshold of 20% and a soil threshold of 10% as default values. The land use threshold specifies a value below which the areal coverage of a given land use is neglected. For example, the 20% land use threshold indicates that all land uses that cover less than 20% of a subbasin will be neglected, of which the area will be reapportioned to all remaining land uses. The soil threshold eliminates minor soils within each remaining land use whose areal coverage is less than the value. Thus, a 10% threshold eliminates all soils which cover less than 10% of a given land use. In order to avoid oversimplifying the complex distribution of soil and land use within the study watersheds of Colorado, thresholds of 10% and 5% were applied to land use and soils, respectively, which limited the number of HRUs, land use types, and soil types modeled in each basin (Table 2.4).

**Table 2.4 –** Distribution of subbasins, HRUs, and types of land use and soil (before and after application of thresholds), within each of the study basins.

| Watershed | Subbasins | HRUs[1] | | Land Use Types[2] | | Soil Types[3] | |
|---|---|---|---|---|---|---|---|
| | | Pre-[4] | Post-[5] | Pre-[4] | Post-[5] | Pre-[4] | Post-[5] |
| **Cache la Poudre** | 33 | 4,269 | 350 | 14 | 6 | 164 | 72 |
| **Gunnison** | 39 | 7,259 | 518 | 15 | 7 | 248 | 125 |
| **San Juan** | 25 | 5,677 | 316 | 15 | 8 | 348 | 110 |
| **Yampa** | 29 | 9,170 | 336 | 15 | 5 | 317 | 122 |

**[1]Number of HRUs created with SWAT LULC classification derived from NLCD 2001.**
**[2]Number of SWAT LULC types.**
**[3]Number of soil types derived from the combination SSURGO/STATSGO2 coverage.**
**[4]Pre- refers to pre-threshold application.**
**[5]Post- refers to post-threshold application.**

The SWAT model requires climatic data in the form of daily values of precipitation, maximum temperature, minimum temperature, solar radiation, relative

humidity, and wind speed. This data may be provided to the model in one of two ways; through generation of the data by the internal WXGEN weather generator model (Sharpley and Williams, 1990), or through provided measurements taken at nearby weather stations. Daily measurements of precipitation, maximum temperature, and minimum temperature from stations in and around the study watersheds were available from the National Climatic Data Center (NCDC) archives (Satellite and Information Service, 2009) and the NRCS Snowpack Telemetry (SNOTEL) Data Network (Natural Resources Conservation Service, 2009). The stations were selected based on proximity to/within the study basin, type of data provided (e.g. precipitation, maximum temperature, minimum temperature), length of record, and completeness of record (Appendix B). The WXGEN weather generator model was utilized to fill in missing daily values of precipitation, maximum temperature, and minimum temperature, as well as to simulate those variables not measured at stations including solar radiation, relative humidity, and wind speed. Details regarding implementation and use of the WXGEN weather generator model within SWAT may be found in the SWAT2005 Theoretical Documentation (Neitsch et al., 2005).

*INCORPORATION OF ELEVATION BANDS & LAPSE RATES*

The daily values of precipitation and temperature for a particular subbasin are taken from the meteorological station closest to the centroid of that subbasin. This implies an assumption that temperature and precipitation of a given day are not only distributed uniformly across an individual subbasin, but also across all subbasins that share a meteorological station. However, in watersheds which exhibit a steep gradient in elevation over small areas, such as the mountainous watersheds of Colorado, this

assumption may be invalid due to orographic effects. Elevation bands may be incorporated in the SWAT model during development, when necessary, in order to improve simulation of orographic effects on atmospheric and hydrologic processes (Fontaine et al., 2002).

Each subbasin within the SWAT model may be topographically discretized into a set of up to ten elevation bands. For each band, the average elevation and the percentage of subbasin area within that band must be specified. In order to distribute the orographic effects on precipitation and temperature within a subbasin as much as possible, the maximum number of ten elevation bands per subbasin was utilized in each of the watershed models. The elevation bands were created by dividing the overall relief in each subbasin (maximum elevation minus minimum elevation) by ten, which resulted in a set of ten, equal-interval bands. The temperature and precipitation of each elevation band in a subbasin are computed as:

$$T_{EB} = T + (Z_{EB} - Z)\frac{dT}{dZ} \qquad \textit{Equation 2.8}$$

$$P_{EB} = P + (Z_{EB} - Z)\frac{dP}{dZ} \qquad \textit{Equation 2.9}$$

where $T_{EB}$ is the adjusted elevation band temperature (°C), $T$ is the meteorological station temperature (°C), $Z_{EB}$ is the elevation of the center of the elevation band (m), $Z$ is the elevation of the meteorological station (m), $dT/dZ$ is the temperature lapse rate (°C/m), $P_{EB}$ is the adjusted elevation band precipitation (mm), $P$ is the meteorological station precipitation (mm), and $dP/dZ$ is the precipitation lapse rate (mm/m).

*MODELING CONSIDERATIONS FOR MOUNTAINOUS WATERSHEDS*

Previous applications of SWAT have showed that the model does not always simulate streamflow accurately in basins with freezing temperatures where snow accumulation and snowmelt processes dominate a majority of the year, such as in Pennsylvania (Peterson and Hamlett, 1998) and in Upstate New York (Tolson and Shoemaker, 2004; Tolson and Shoemaker, 2007). Thus, several modifications related to frozen soils and snowfall and snowmelt processes were incorporated into the SWAT model source code as set forth in Tolson and Shoemaker (2004).

(i) The default SWAT approach for handling soil water above field capacity in frozen soils is to assume that no subsurface lateral flow occurs, that the soil layer can hold excess water until soil saturation is reached, and that any additional percolate from above a frozen soil layer passes through the layer to become percolate to the subsequent layer. This approach results in the routing of all rainfall on a frozen and saturated soil layer directly to groundwater, which delays the transfer of water to the stream. A simple modification to the SWAT source code was made such to allow the model to predict subsurface lateral flow in frozen soils (Tolson and Shoemaker, 2004). Algorithms for partitioning of water into percolate and subsurface lateral flow were made no longer dependent on whether or not the soil is frozen.

(ii) SWAT utilizes average monthly maximum and minimum temperatures to generate weather with an internal weather generator, WXGEN, which fills in missing values at meteorological stations. Each subbasin then utilizes the precipitation, maximum temperature, and minimum temperature values from the meteorological station closest to its centroid for simulation. It was found that for scenarios where elevation

bands and lapse rates were implemented in the model, the average monthly maximum and minimum temperatures in a subbasin were not adjusted for orographic effects (Tolson and Shoemaker, 2004). Therefore, the SWAT source code was modified such that the average monthly maximum and minimum temperatures of a subbasin were adjusted using the temperature lapse rate and difference between the average elevation of the subbasin and the elevation of the meteorological station.

(iii) The SWAT default logic for estimating snowmelt was found to be inconsistent depending on whether elevation bands are utilized (Tolson and Shoemaker, 2004). For configurations that do not incorporate elevation bands, SWAT allows both snow accumulation and snowmelt to occur on the same day. Conversely, with elevation bands implemented, SWAT does not allow for both accumulation of snow and snowmelt to occur on the same day. A final modification to SWAT utilized logic from the portion of the source code which simulated elevation bands and applied it to the setting with elevation bands, which allowed for both snowfall and snowmelt to occur on the same day regardless of whether elevation bands were implemented in the model.

### 2.2.3 NATURALIZED STREAMFLOW

Diversions, transfers (both inter- and intra-basin), storage reservoirs, and irrigation canals/ditches are prevalent in the study watersheds of Colorado. A majority of the precipitation in these basins falls as snow in the winter months, and is stored as snowpack at high elevations until the annual spring melt occurs. Therefore, in order to support both agricultural and municipal use across the state (and other states), manmade structures are required to store and distribute the annual snowmelt-dominated hydrograph to other times

of the year when the demand of water exceeds its availability. Any reasonable representation of hydrologic processes in the study watersheds must take into account the impacts of such structures, either by direct representation of the features within the model itself, or by removing the effect of such features out of the streamflow record, resulting in what are referred to as naturalized streamflows. For example, one study in the Cache la Poudre River basin described several effects resulting from flow modifications including delayed hydrograph rise (in spring), decreased peak flows, and lower winter baseflows, with an average net reduction of 56 million cubic meters, or 23% of annual streamflow between 2000 and 2006 (Richer, 2009).

For each of the four study basins, the SWAT models were calibrated to monthly naturalized streamflows from multiple sites within the watersheds. While the outlet of the entire watershed was used as one of the calibration sites for each of the study basins, other sites within the watershed were chosen based on availability of data at subbasin outlets created in the modeling set up (Figure 2.1). Naturalized streamflows at the monthly time-step were obtained from Colorado's Decision Support Systems (CO Division of Water Resources and CO Water Conservation Board, 2010) for the Gunnison (1/1990-12/2005), San Juan (1/1990-12/2005), and Yampa (1/1990-12/2004) River basins. Naturalized flow data for the Cache la Poudre River basin (1/1990 – 12/2005) were obtained from the Northern Colorado Water Conservancy District (Northern Water, 2009). Graphs of naturalized versus measured streamflows at the USGS gauges used for monthly calibration may be found herein (Figure 2.7) for the watershed outlets, while graphs for sites within the watersheds may be found in Appendix A.

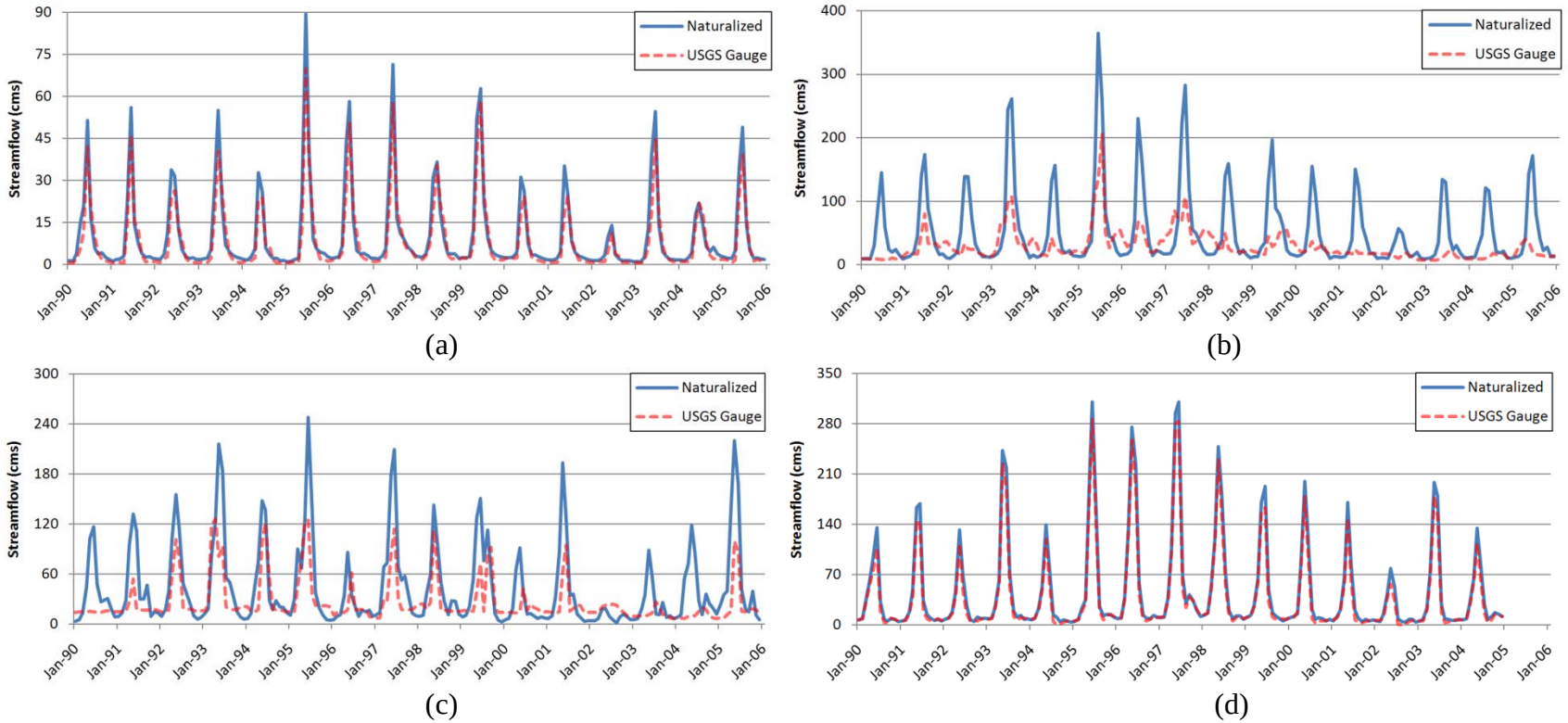


**Figure 2.7 –** The impact of diversions, transfers, and reservoirs on streamflow, as shown by a comparison between naturalized streamflow and measured streamflow recorded at (a) USGS 06752000 – Cache la Poudre River, (b) USGS 09128000 – Gunnison River, (c) USGS 09355500 – San Juan River, and (d) USGS 09251000 – Yampa River.

### 2.2.4 CALIBRATION & TESTING

The ability of a hydrologic model to accurately simulate physical phenomena, especially a comprehensive, semi-distributed model in a complex mountain watershed, depends on the knowledge and skill of the user to both identify and provide values for the set of parameters that result in the most accurate model outputs, a process referred to as manual calibration. Thus, the manual calibration process may not only be subjective, depending on the user, but may also be an extremely time consuming process, depending on the complexity of the model and number of parameters. In order to avoid the difficulties and subjectivity associated with the manual calibration process, automated methods have been developed to calibrate hydrologic models, including specific applications to SWAT, of which two unique methods will be analyzed in this study.

*SCE-UA ALGORITHM*

One of the parameter optimization procedures consisted of an application of the Shuffled Complex Evolution - University of Arizona (SCE-UA) method, as first proposed by Duan et al. (1993; 1992) and reviewed in Duan et al. (1994). The SCE-UA procedure combines the concept of the simplex procedure (Nelder and Mead, 1965) with concepts of controlled random search (Price, 1987), competitive evolution (Holland, 1975), and complex shuffling (Duan et al., 1992). The SCE-UA methodology begins with a random sample of a number of points from a feasible parameter space, as defined by the range of allowable parameter values (Appendix B). The sampled points are sorted based on an objective function value, and are further partitioned into complexes containing a fixed number of points. Each complex is then evolved, separately, by a defined number of evolution steps, and complex shuffling is performed. Convergence is satisfied when

either the maximum number of trials has been met, or when improvement of the objective function value is less than a defined percentage within shuffling loops.

Previous applications of SCE-UA as a calibration procedure for streamflow parameterization have proven to be successful in the SWAT modeling framework and include studies in two central German catchments (Eckhardt and Arnold, 2001; Eckhardt et al., 2005), the Luohe River basin (Zhang et al., 2007), and the Dill catchment in mid-Hesse, Germany (Pohlert et al., 2005). Additional studies documenting the application of SCE-UA in SWAT may be found in Gassman et al. (2007).

*GIBBS SAMPLER ALGORITHM*

The performance of the Gibbs Sampler Algorithm (GSA), a Markov Chain Monte Carlo (MCMC) method, was compared with the performance of SCE-UA to establish guidelines for the use of these methods for calibration of watershed models in mountainous basins. The MCMC methods, as a whole, are generally distinguished from other Monte Carlo numerical optimization techniques in that they are iterative in nature, relatively easy to customize and implement, and are able to handle high dimensionality problems without slowing convergence (Givens and Hoeting, 2005). The basic premise behind all MCMC methods is the construction of an irreducible, aperiodic Markov chain which has the target distribution as its equilibrium, or stationary distribution. A variety of methods have been proposed for the construction of such chains, with one of the simplest, and arguable the most popular classes of methods being based on the Metropolis algorithm (Metropolis et al., 1953). GSA is a special application of the Metropolis algorithm that sequentially samples each parameter's conditional distribution in order to create a Markov chain, which makes it specifically tailored to problems with

high dimensionality and multiple target distributions. The basic GSA utilized in this study simply starts in a random point of hyper-cubic parameter space, and adjusting one parameter at a time, moves through space until convergence is satisfied.

*COMPARISON OF OPTIMIZATION METHODS*

In order to determine which optimization method is better suited for the study watersheds of Colorado, a side-by-side performance evaluation was made between the two techniques. This comparison was made in each of the study basins, and utilized an identical initial parameter set and same number of runs for each method (2,500). Thus, both convergence speed and the ability to obtain a local optimum were compared between the calibration techniques. A third method was also compared, which combined both SCE-UA and GSA techniques. Two-stage optimization routines that incorporate more than one method are rarely utilized, but one such study was found by Lin and Radcliffe (2006), who combined SCE-UA and a local search method based on a variant of the Levenberg-Marquart method to calibrate SWAT. The two-stage calibration procedure in this study consisted of an initial 1,250 runs with SCE-UA. The optimal parameter set from those 1,250 runs was taken and used as the initial parameter set for GSA, which was then ran for an additional 1,250 runs for a combined method total of 2,500 runs. Results from each of the three methods were then compared to determine if either of the three significantly outperformed the others in the mountainous headwater basins of Colorado.

*ERROR STATISTICS*

Five error statistics were utilized to determine how accurately SWAT was representing hydrologic processes, through comparison of observed and simulated streamflows in each of the four study basins. The relative error (*RE*) is a measure of goodness of fit between simulated and observed streamflows, and is expressed as a percentage by:

$$RE\ (\%) = \frac{\sum_{i=1}^{n}(Q_i - \widehat{Q}_i)}{\sum_{i=1}^{n} Q_i} \times 100 \qquad \textit{Equation 2.10}$$

where $Q_i$ and $\widehat{Q}_\iota$ refer to the observed and simulated streamflows, respectively, and *i* refers to the time (month).

The bias (*BIAS*) is a measure of whether or not simulated streamflows have a tendency of being above or below observed values. A negative bias would result from overestimation of observed steamflows, while a positive bias would result from underestimation of streamflows. The bias is calculated as:

$$BIAS = \frac{1}{n}\sum_{i=1}^{n}(Q_i - \widehat{Q}_\iota) \qquad \textit{Equation 2.11}$$

where *n* refers to the number of time steps under analysis.

The root mean square error (*RMSE*) is a measure of the error between simulated and observed streamflows, with respect to both magnitude and timing, and is found as:

$$RMSE = \sqrt{\frac{1}{n}\sum_{i=1}^{n}(Q_i - \widehat{Q}_i)^2} \qquad \textit{Equation 2.12}$$

The coefficient of correlation ($R^2$) is a measure of how well the observed and simulated streamflows are correlated, and is defined as:

$$R^2 = \frac{1}{n-1}\sum_{i=1}^{n}\left(\frac{Q_i - Q_{mean}}{s_Q}\right)\left(\frac{\hat{Q}_i - \hat{Q}_{mean}}{s_{\hat{Q}}}\right) \qquad \textit{Equation 2.13}$$

where $Q_{mean}$ and $\hat{Q}_{mean}$ refer to the averages of the observed and simulated discharges, respectively, and $s_Q$ and $s_{\hat{Q}}$ refer to the standard deviations of the observed and simulated discharges, respectively.

A final measure of goodness of fit that is commonly used in hydrologic modeling is the Nash-Sutcliffe efficiency coefficient ($E_{NS}$). Originally developed by Nash and Sutcliffe (1970), $E_{NS}$ is a measure of how well the plot of observed versus simulated streamflows fits the 1:1 line. The coefficient is identified as:

$$E_{NS} = 1 - \frac{\sum_{i=1}^{n}(Q_i - \hat{Q}_i)^2}{\sum_{i=1}^{n}(Q_i - Q_{mean})^2} \qquad \textit{Equation 2.14}$$

The $E_{NS}$ measure ranges between -∞ and 1, with 1 corresponding to perfect agreement.

*PERFORMANCE RATINGS*

Although all five error statistics were analyzed in this study, RE and $E_{NS}$ were considered the primary measures and used to rate the performance of the models. A review of published literature revealed performance ratings of very good ($E_{NS}$>0.75, |RE|<10%), good (0.65<$E_{NS}$<0.75, 10%<|RE|<15%), satisfactory (0.5<$E_{NS}$<0.65, 15%<|RE|<20%), and unsatisfactory ($E_{NS}$<0.5, |RE| >25%) for monthly simulations of streamflow (Moriasi et al., 2007; Santhi et al., 2001).

*MULTISITE CALIBRATION AND TESTING*

Calibration of the SWAT models specifically refers to the fine-tuning of 30 streamflow parameters within their acceptable ranges in order to obtain simulation of monthly streamflows that closely agree with observed (naturalized) streamflows. For each of the

study catchments, calibration to monthly naturalized flow was performed for a period of 8 years (January 1, 1990 - December 31, 1997) after a 2 year warm-up period (January 1, 1988 – December 31, 1989), which was implemented to adjust the initial storage conditions of the watersheds. The calibration process was performed for multiple sites within each of the watersheds (except for the Cache la Poudre which only had naturalized flow for a single site) based on minimization of the objective function (*f*) defined as:

$$f = 1 - E_{NS} = \frac{1}{M}\sum_{j=1}^{M}\frac{\sum_{i=1}^{n}(Q_{i,j} - \hat{Q}_{i,j})^2}{\sum_{i=1}^{n}(Q_{i,j} - Q_{mean,j})^2} \qquad \textit{Equation 2.15}$$

where *M* reflects the number of calibration sites within each watershed (i.e. *M* equals 1 in the Cache la Poudre watershed and *M* equals 3 for all other study basins). Due to the period chosen for calibration, the SWAT models developed for this period utilized NLCD 1992 as an input for land use/land cover.

The three optimization methods previously described were run for 2,500 evaluations. In addition, as the results show it, it appears as if convergence was met by 2,500 runs. However, in an attempt to parameterize the models as well as possible, a fourth automatic calibration procedure was used. This procedure used the best parameter set from SCE-UA after 2,500 runs, and applied it to GSA, which was run for an additional 2,500 runs for a total of 5,000 trials. The optimal parameter set was then chosen from the results of this procedure. Measures other than the objective function *f*, including RE, BIAS, RMSE, and $R^2$, were analyzed for performance of the model. Specifically the calibration run that resulted in the lowest RE, in addition to an $E_{NS}$ comparable to the best calibrated $E_{NS}$, was chosen as the optimal parameter set. This

ensured that the error between simulated and observed streamflows was minimized while still maintaining a correlation comparable to the optimal objective function.

Testing, or validation, of the SWAT model refers to the application of an optimal parameter set (obtained from calibration) to a period of time other than that of calibration, and is often used as evidence for the performance of the model. In this application, testing of the SWAT models was performed by utilizing the set of parameters which resulted in the best simulation from the calibration period, and applying them to the models for a period immediately following the calibration period. In the Cache la Poudre, Gunnison, and San Juan River basins the model was validated for a period of 8 years (January 1, 1998 – December 31, 2005). Due to unavailability of naturalized streamflow for latter half of 2005, the Yampa River basin model was validated for a period of 7 years immediately following the calibration procedure (January 1, 1998 – December 31, 2004). For validation, separate SWAT models different from the models used during the calibration period were developed which utilized NLCD 2001 as an input for land use/land cover, and therefore required a 2 year warm-up period (January 1, 1996 – December 31, 1997) before testing.

## 2.3 RESULTS & DISCUSSION

Three techniques of parameter optimization were compared for performance during calibration of the hydrologic model SWAT in four separate watersheds of Colorado. Results indicate that GSA outperformed SCE-UA in three watersheds, and similar results were obtained in the fourth. GSA appeared to converge to an optimal solution faster than GSA, in addition to finding a better overall solution. The optimal parameter sets from

eight years of calibration over the 1990 – 1997 period were obtained, and tested for an addition seven (Yampa) or eight years over the 1998 – 2005 period. Simulated monthly streamflows at multiple sites within each of the watersheds compared favorably to observed (naturalized) streamflows, with $E_{NS}$ values of 0.70 to 0.90 obtained at the watershed outlets over the calibration period. Several dominant hydrologic components including subsurface lateral flow, surface runoff, baseflow, and evapotranspiration were quantified, both over an annual and monthly basis, which showed their relative importance within semi-arid mountainous watersheds characteristic of the western United States.

### 2.3.1 CALIBRATION & TESTING

*COMPARISION BETWEEN OPTIMIZATION METHODS*

Two separate optimization techniques, SCE-UA and GSA, were compared for performance in a SWAT framework applied to four watersheds in Colorado. The progression of the two calibration procedures for each of the watersheds is shown in Figure 2.8, below, in addition to the performance of a method which utilized both techniques (SCE-UA for 1,250 runs followed by GSA for 1,250 runs).

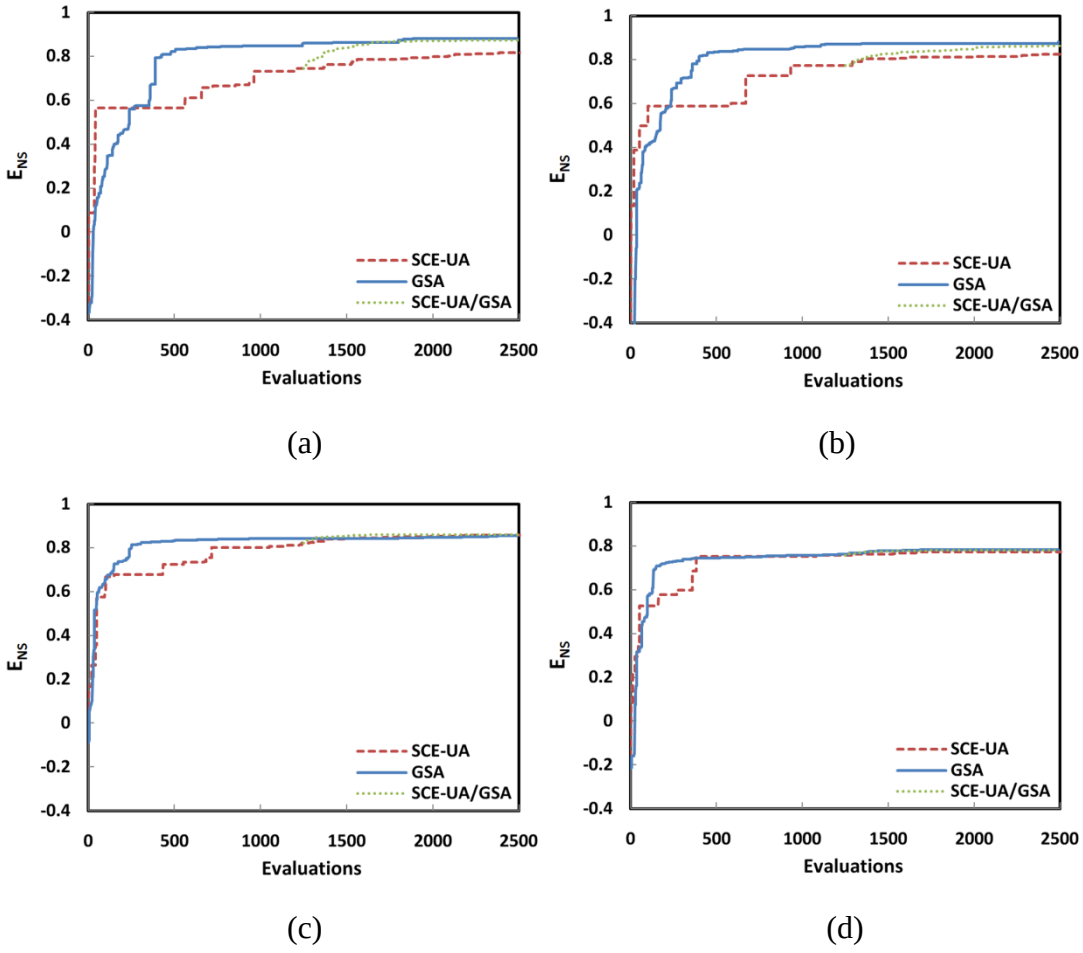


**Figure 2.8** – Comparison of the two calibration techniques and a third combined method for the (a) Cache la Poudre, (b) Gunnison, (c) San Juan, and (d) Yampa River basins.

Table 2.5 presents the best objective function value at 500 model evaluation increments. It is apparent that GSA outperforms SCE-UA in both convergence speed and ability to obtain a better solution in the majority of study watersheds. Two notable exceptions occurred in the San Juan and Yampa watersheds. In the San Juan watershed, SCE-UA was able to obtain a better solution overall, but GSA was able to converge much faster ($E_{NS}$ = 0.833 after 500 GSA runs compared to $E_{NS}$ = 0.724 after 500 SCE-UA runs). In the Yampa basin, both methods achieved comparable results and neither was determined to significantly outperform the other.

**Table 2.5** - Progression of individual calibration techniques.

| Watershed | Method | 500 Runs | 1000 Runs | 1500 Runs | 2000 Runs | 2500 Runs |
|---|---|---|---|---|---|---|
| **Cache la Poudre** | SCE-UA | 0.5657 | 0.7324 | 0.7635 | 0.7997 | 0.8164 |
| | GSA | 0.8223 | 0.8466 | 0.8616 | 0.8810 | 0.8811 |
| | Combined | 0.5657 | 0.7324 | 0.8385 | 0.8716 | 0.8736 |
| **Gunnison** | SCE-UA | 0.5868 | 0.7728 | 0.8026 | 0.8123 | 0.8242 |
| | GSA | 0.8352 | 0.8587 | 0.8727 | 0.8733 | 0.8800 |
| | Combined | 0.5868 | 0.7728 | 0.8266 | 0.8538 | 0.8625 |
| **San Juan** | SCE-UA | 0.7235 | 0.8019 | 0.8393 | 0.8520 | 0.8582 |
| | GSA | 0.8329 | 0.8411 | 0.8421 | 0.8465 | 0.8557 |
| | Combined | 0.7235 | 0.8019 | 0.8543 | 0.8597 | 0.8603 |
| **Yampa** | SCE-UA | 0.7526 | 0.7529 | 0.7633 | 0.7727 | 0.7736 |
| | GSA | 0.7459 | 0.7576 | 0.7774 | 0.7837 | 0.7842 |
| | Combined | 0.7526 | 0.7529 | 0.7760 | 0.7813 | 0.7816 |

From the results the usefulness of the third method that combined SCE-UA and GSA might be questioned, as it rarely outperformed the other two methods. The one instance when the combined method did outperform either standalone technique was in the San Juan watershed, but results indicated only a marginally superior performance. The theory behind the combination of the two methods is to take advantage of the strengths in each. SCE-UA is a proven global optimization algorithm, which has been applied in many areas of modeling and is thus well documented. GSA, on the other hand, is more of a local optimization algorithm which is able to handle higher dimensionality parameter space without slowing convergence, and does not seem to be as well documented in application. After analysis of the comparisons between methods, it was certainly appealing to solely use GSA for optimization of SWAT. However, in doing so there runs the risk of getting caught in a local "pit" that is not the true unique global optimum (assuming one exists). Thus, SCE-UA was utilized for the first 1,250 runs not to obtain such a global optimum, but to assist in finding a reasonable starting point for the more powerful GSA algorithm. This is not a novel approach in automatic calibration as it

has been previously applied (with a different second-stage algorithm used) to SWAT in a northern Georgia watershed (Lin and Radcliffe, 2006).

*OPTIMAL PARAMETER SETS*

In each watershed, a set of 30 SWAT streamflow parameters was adjusted through automatic calibration techniques. The optimal parameter set which resulted in monthly simulations of streamflow that most closely matched observed (naturalized) streamflows was chosen based on analysis of performance measures, with particular attention paid to $E_{NS}$ and RE. Although 30 parameters were adjusted in calibration, only some of them bear significant influences on streamflow outputs of the model. The importance of model parameters reflects the dominance of physical processes that they represent. A previous study involving a sensitivity analysis of SWAT parameters in the four basins of this study showed both sensitivity of and interaction effects between parameters representing groundwater and snow processes (Sanadyha, 2009). Table 2.6, below, displays the optimized value from a selection of these parameters in each study basin.

**Table 2.6** – Calibrated SWAT streamflow parameters for each of the study basins.

| Parameter | Cache la Poudre | Gunnison | San Juan | Yampa |
|---|---|---|---|---|
| **SFTMP (°C)** | 2.480 | 4.912 | 2.014 | 4.968 |
| **SMTMP (°C)** | 3.331 | 3.415 | 3.703 | 3.131 |
| **SNOCOVMX (mm)** | 299.450 | 625.833 | 646.677 | 554.757 |
| **SNO50COV** | 0.569 | 0.304 | 0.323 | 0.441 |
| **ALPHA_BF (days)** | 0.245 | 0.285 | 0.524 | 0.573 |
| **CH_KII (mm/hr)** | 264.347 | 102.834 | 430.087 | 428.686 |
| **CH_KI (mm/hr)** | 299.398 | 299.379 | 299.619 | 299.840 |

The first four parameters in Table 2.6 correspond to snow-related processes, and include the snow fall temperature (SFTMP), the threshold temperature for snowmelt (SMTMP), the snow water equivalent corresponding to 100% snow cover

(SNOCOVMX), and the fraction of SNOCOVMX resulting in 50% snow cover (SNO50COV). The relative values of these parameters were mostly consistent between the study basins, which suggest the dominant hydrologic processes within each of the basins are similar. Two notable exceptions include SFTMP, which was approximately twice as high in the Gunnison and Yampa basins than in the Poudre and San Juan basins, and SNOCOVMX, which was significantly lower in the Poudre basin than the other three. Additionally, the last four parameters in the table correspond to the flow of water either on the surface or underground, and include the baseflow recession constant (ALPHA_BF), the effective hydraulic conductivity of the alluvium in the main channel reach (CH_KII) and the effective hydraulic conductivity of the tributary channels (CH_KI). The values obtained for ALPHA_BF within each study watershed indicate relatively slow groundwater flow responses to aquifer recharge, as expected in large and geologically complex watersheds. The values of CH_KI and CH_KII are relatively high and correspond to channels with higher loss rates often composed of coarse materials, such as the headwater streams of Colorado.

*STREAMFLOW SIMULATIONS*

The optimal parameter sets found for each study basin resulted in streamflow simulations with nearly all satisfactory performance over the calibration and testing periods. Figure 2.9 displays the simulated and observed streamflows at each of the study watershed outlets over the study period, while Table 2.7 presents a summary of supplementary error statistics. Additional figures presenting simulated and observed streamflows at sites within each watershed may be found in Appendix A.

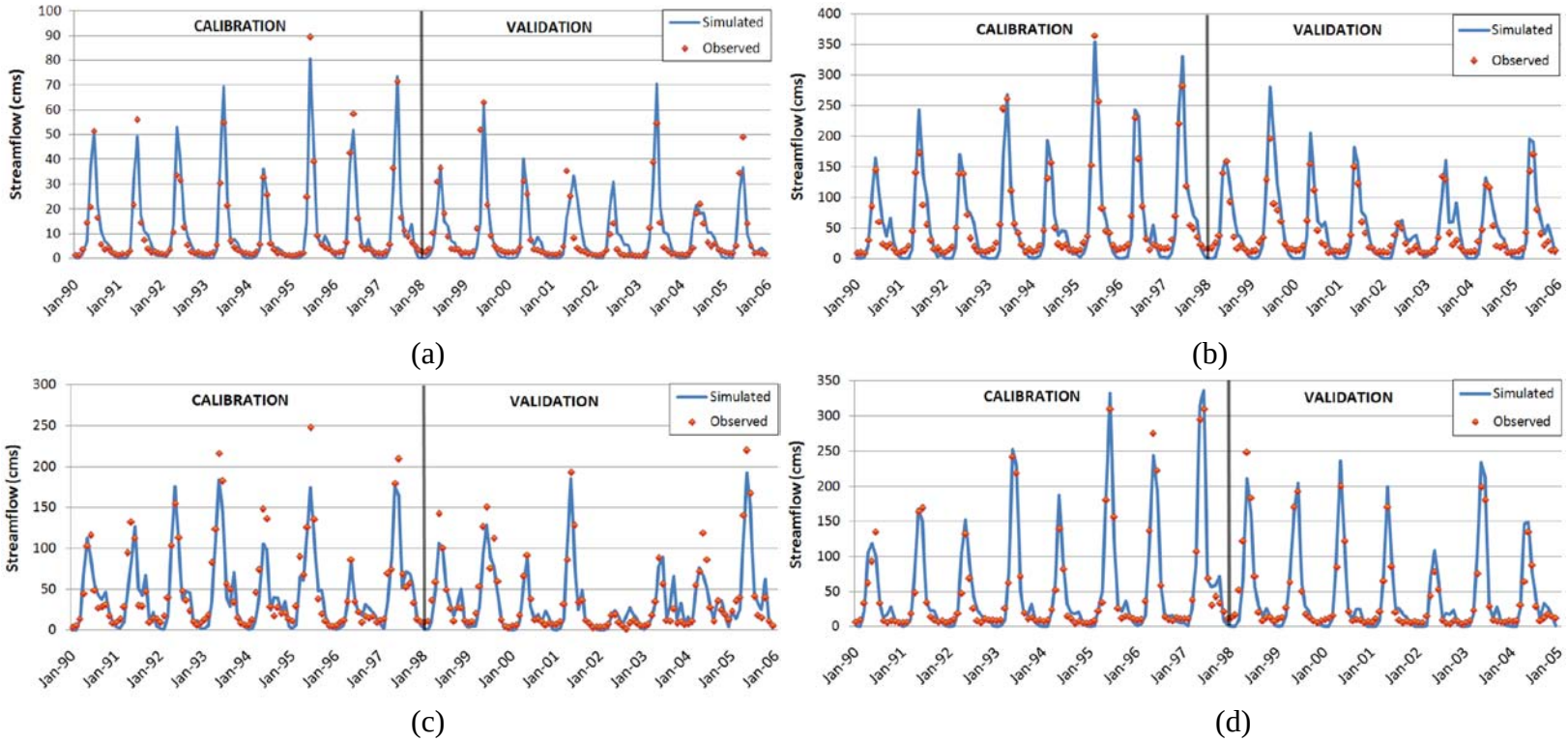


**Figure 2.9 –** A time series comparing SWAT streamflow simulations with naturalized streamflows at each of the study watershed outlets (a) Cache la Poudre – USGS 06752000 (b) Gunnison – USGS 09128000 (c) San Juan – USGS 09355500 (d) Yampa – USGS 09251000.

**Table 2.7** – Error statistics between observed and simulated monthly streamflows for both the calibration and validation periods. Performance ratings include very good (green), good (orange), satisfactory (yellow), and unsatisfactory (red shade).

| | | Calibration Period | | | | | Validation Period | | | | |
|---|---|---|---|---|---|---|---|---|---|---|---|
| **Basin** | **USGS ID** | **RE** | **BIAS** | **RMSE** | **R2** | **$E_{NS}$** | **RE** | **BIAS** | **RMSE** | **R2** | **$E_{NS}$** |
| Cache la Poudre | **06752000** | **-4.817** | **-0.546** | **4.549** | **0.967** | **0.926** | **-2.987** | **-0.274** | **7.172** | **0.848** | **0.698** |
| Gunnison | **09128000** | **-3.881** | **-2.314** | **24.360** | **0.995** | **0.885** | **-15.920** | **-6.850** | **24.620** | **0.935** | **0.704** |
| | 09110000 | 1.587 | 0.163 | 5.275 | 0.961 | 0.832 | -8.115 | -0.569 | 4.728 | 0.965 | 0.455 |
| | 09126500 | 2.258 | 0.103 | 1.777 | 0.951 | 0.904 | -3.648 | -0.131 | 2.201 | 0.891 | 0.684 |
| San Juan | **09355500** | **9.655** | **4.793** | **20.140** | **0.934** | **0.860** | **8.353** | **3.152** | **15.650** | **0.946** | **0.883** |
| | 09341500 | -1.268 | -0.063 | 2.225 | 0.944 | 0.880 | -12.100 | -0.467 | 2.555 | 0.922 | 0.742 |
| | 09339900 | -10.130 | -0.280 | 1.410 | 0.943 | 0.853 | -10.220 | -0.220 | 0.872 | 0.969 | 0.917 |
| Yampa | **09251000** | **-5.114** | **-2.606** | **16.440** | **0.978** | **0.951** | **-6.281** | **-2.611** | **17.940** | **0.959** | **0.903** |
| | 09249750 | -32.560 | -2.107 | 3.870 | 0.952 | 0.849 | -24.710 | -1.349 | 3.562 | 0.923 | 0.794 |
| | 09237500 | 22.230 | 0.789 | 1.723 | 0.899 | 0.710 | 26.130 | 0.776 | 1.393 | 0.891 | 0.631 |

Error statistics between simulated and observed (naturalized) streamflows (Table 2.7) were nearly all considered satisfactory. At the outlet of each watershed $E_{NS}$ varied between 0.86 and 0.95 during the calibration period and between 0.70 and 0.90 during the validation period. Generally, the models performed slightly better during the calibration period, but performance measures from the validation period indicated a satisfactory level of model parameterization at nearly all sites. Overall, the results compare favorably with those from other SWAT simulations of monthly streamflow in mountainous watersheds including an $E_{NS}$ = 0.71 over an 11 year period in a small watershed in Colorado (Lemonds and McCray, 2007), $E_{NS}$ = 0.86 over a 6 year period in the Upper Wind River basin of Wyoming (Fontaine et al., 2002), and $E_{NS}$ = 0.79 over a 4 year period in the Dry Creek Experimental Watershed of Idaho. This is consistent with the finding of Ahl et al. (2008), who concluded that SWAT is able to predict hydrologic processes in snow-dominated mountain watersheds with performance levels similar to those from the agriculture-dominated basins it was originally designed for.

In basins with multiple calibration points, a range of performance between sites was observed. Typically, the outlet of the entire basin typically had better error statistics than sites within the watershed, as shown in the Yampa basin with $E_{NS}$ = 0.95 at the outlet and $E_{NS}$ = 0.85 and 0.71 at two sites within. One reason for a discrepancy between results at different sites within a basin may have to do with the rectification of spatial scales within the framework of a watershed model. When a parameter is defined it is often applied over the entire watershed, regardless of the size and characteristics of the computational unit. This is the case for the majority of parameters in SWAT except for a select few (marked by an asterisk in Table 2.2) that have different values depending on

the soil and land use characteristics of the respective HRU (e.g. CN_F). The results showing better model performance at the outlet of the watershed relative to performance within individual subbasins are therefore unsurprising. This confirms that the application of a single parameter value represented over an entire watershed will not necessarily be appropriate for the smaller scale, heterogeneous HRU and subbasin areas.

### 2.3.2 QUANTIFICATION OF HYDROLOGIC PROCESSES

The simulations from each SWAT model were analyzed on a monthly basis in order to determine and quantify dominant hydrologic processes occurring in the mountainous headwater catchments of Colorado. Results were taken from simulations over a period of 16 years (1990 – 2005) in the Cache la Poudre, Gunnison, and San Juan River basins and from simulations ran over a period of 15 years (1990 – 2004) in the Yampa River basin.

*DOMINANT PROCESSES IN MOUNTAIN WATERSHEDS*

Figure 2.10 displays the average annual proportion of precipitation that went to ET, gross water yield, and other losses during the 16 year (15 year in Yampa) period of study. The amount of basin-averaged annual precipitation varied among study watersheds from approximately 475 mm in the Cache la Poudre watershed to nearly 660 mm in the Yampa watershed. Due to the location of the Poudre watershed on the eastern side of the Continental Divide, it had the lowest average annual precipitation out of all study watersheds.

Annual average percentages of precipitation that went to ET ranged between 55% in the Gunnison River basins to 65% in the Cache la Poudre River basin. Other losses accounted for between 3% and 12% of annual precipitation, and include soil water

storage and contribution to the deep aquifer, which is assumed not to contribute to streamflow within the watershed and is therefore lost to the system in SWAT. Typical gross water yield in each basin was on average between 30% and 38% of annual precipitation. However, it is noted that gross water yield was quantified before transmission losses were removed. Transmission losses represent the movement of water from the stream channel to the shallow aquifer, and are typically larger in areas with ephemeral and/or intermittent streams and lower groundwater tables. Thus, the net yield is the amount of water that leaves the basin and would be calculated by subtracting transmission losses from gross yield.

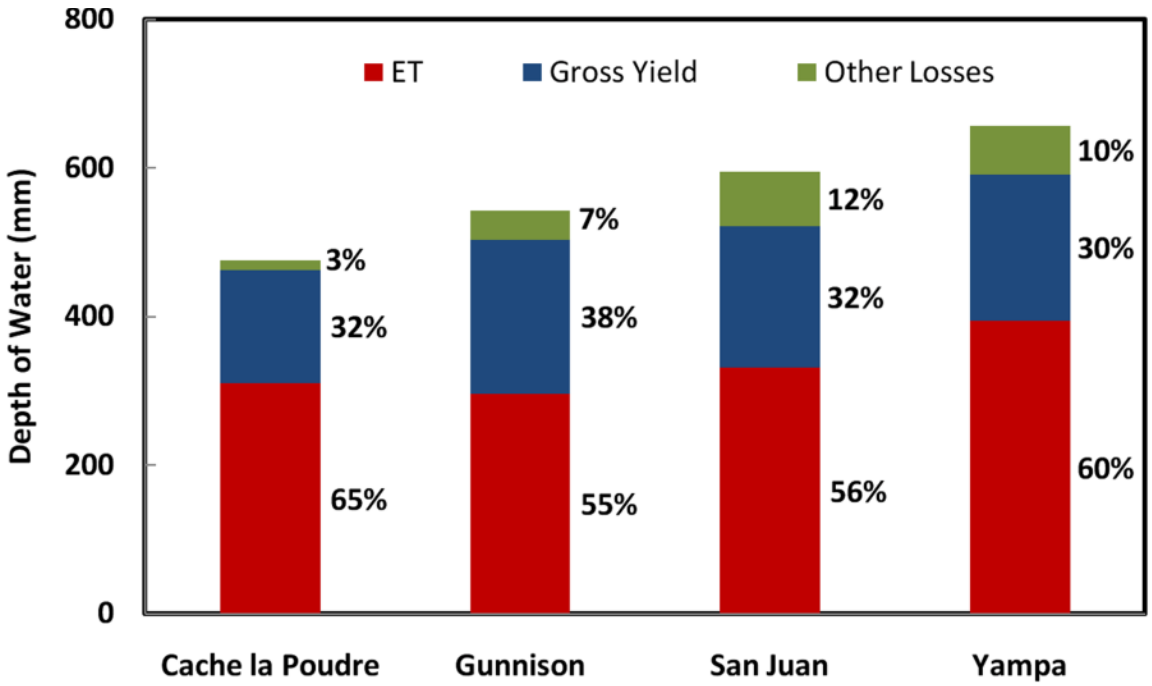


**Figure 2.10** – Hydrologic budgets displaying the fate of precipitation in the (a) Cache la Poudre (b) Gunnison (c) San Juan and (d) Yampa River watersheds. Each hydrologic component was averaged over an annual basis from 1990 – 2005 (1990 – 2004 in Yampa).

Figure 2.11 displays the average annual proportion of gross yield that came from surface runoff, subsurface lateral flow, and baseflow (groundwater contribution to the stream). It is evident that subsurface lateral flow is the dominant process that provides between 64% and 82% of the water to gross basin yield on an annual basis in the study watersheds of Colorado.

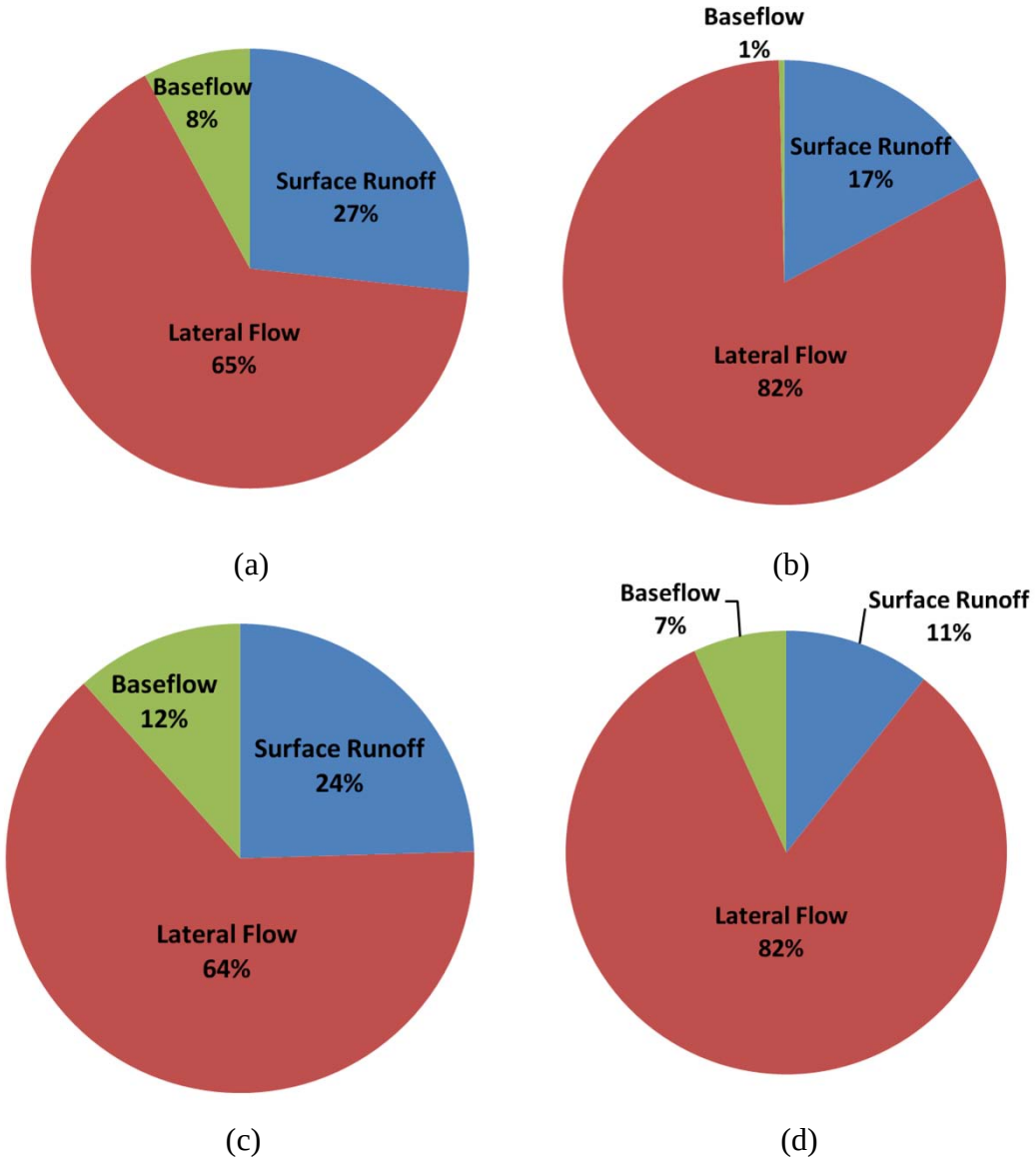


**Figure 2.11** – Average annual contribution of three major hydrologic processes to the gross water yield in the (a) Cache la Poudre, (b) Gunnison, (c) San Juan, and (d) Yampa River basins. Each process was averaged over an annual basis from 1990 – 2005 (1990 – 2004 in Yampa).

*ANNUAL HYDROLOGIC CYCLE*

The long-term monthly distributions of precipitation, snowfall, ET, and total water yield within a year are presented in Figure 2.12 for each of the study basins in Colorado over the period 1990 – 2005 (1990 – 2004 for Yampa). The monthly patterns occurring on an annual basis appear to be similar within all watersheds, and begin with the majority of precipitation falling as snow in the winter months (November – April), with little water yield anticipated during this time. Peak yield was estimated to occur in May in all four watersheds, most likely due to the rapid temperature increase and resultant snowmelt which occurs in the spring. The summer months were characterized by lower amounts of precipitation and decreasing yields, though ET continued to increase whit increasing temperatures over summer months. Interestingly, precipitation in the fall months was moderate except for in the San Juan River basin, where on average a significant amount of rain fell during August – October and coincides with the monsoon season. Both ET and water yield decreased over fall months, and precipitation began to fall as snow once again as a new calendar year approached.

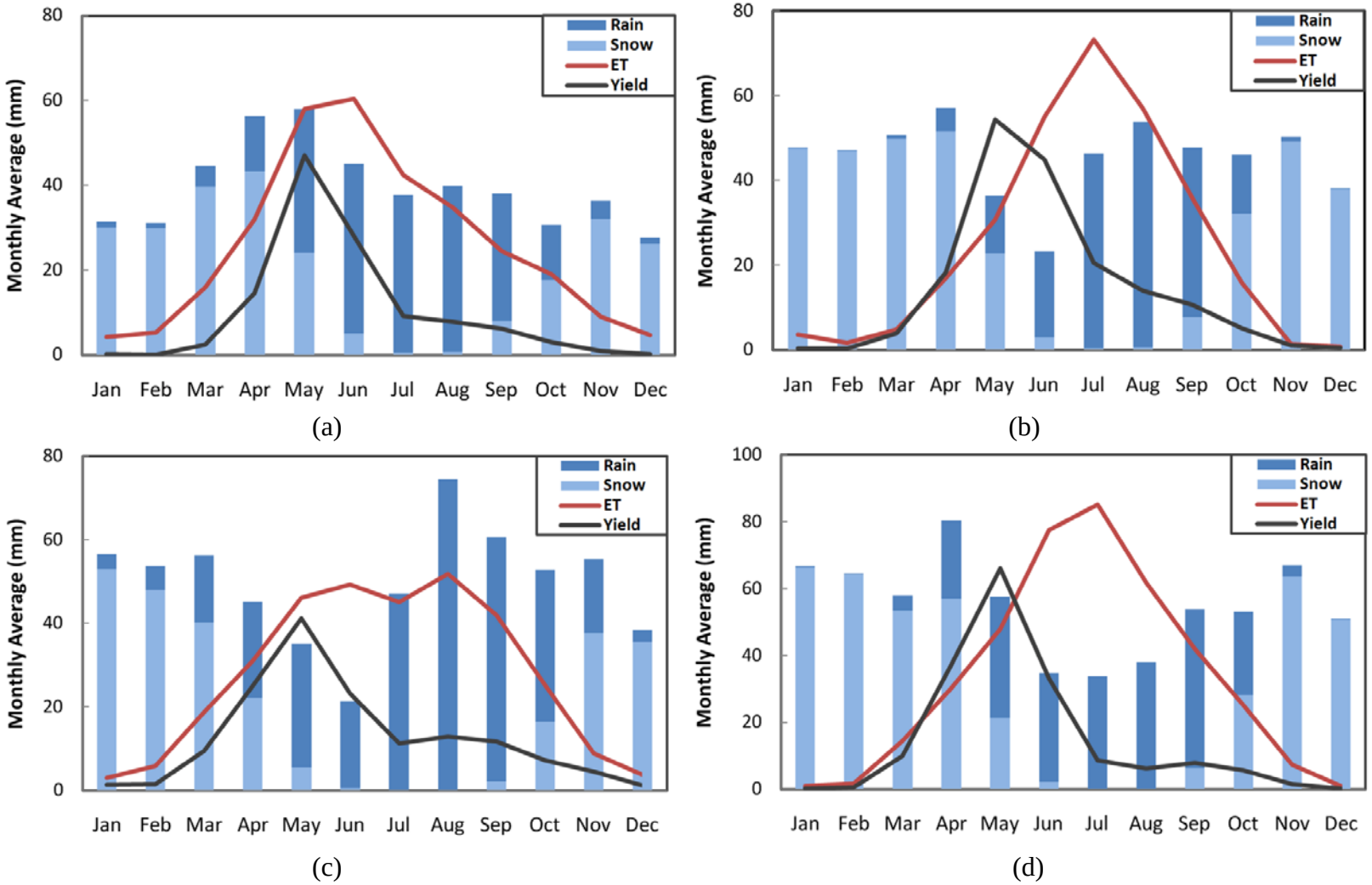


**Figure 2.12** – Long-term monthly distribution of precipitation (mm), evapotransporation (mm), and total water yield (mm) in the (a) Cache la Poudre, (b) Gunnison, (c) San Juan, and (d) Yampa watersheds during the 1990 – 2005 (1990 - 2004 in Yampa) study period.

### 2.3.3 MODEL LIMITATIONS

Figure 2.13 depicts the time series of monthly streamflow simulation error, while observed versus simulated streamflows at each of the watershed outlets are shown in Figure 2.14. Similar figures corresponding to the other calibration sites within each watershed are presented in Appendix B. Although performance measures indicated high model confidence in streamflow simulations, it was apparent that a systematic error concerning the recession of the annual snowmelt hydrograph was occurring in each of the study basins. This consistently occurring error was most pronounced in the Gunnison River basin (Figures 2.12(b), and 2.13(b)), where the recession of the snowmelt hydrograph was overestimated during the summer months (May - November), and resultant baseflow during the winter months (December - April) was underestimated. The error is systematic in that it is repeatable on an annual basis, as seen in Figure 2.12 in all four study basins. It appears as if the underestimation of streamflow in the winter months, which is most likely baseflow contributions from groundwater discharge, may have to do with the preceding overestimation of streamflow in the late spring and summer. One speculation for the cause of this is that SWAT may not be holding enough of the water from snowmelt in the aquifer, for long enough. Regardless of the cause, this shortcoming may be attributable to either a process misrepresentation within the SWAT logic or to a faulty model parameterization (or a combination of the two), and it is suggested that future work be concentrated on the representation of snowmelt and groundwater processes in mountainous watersheds.

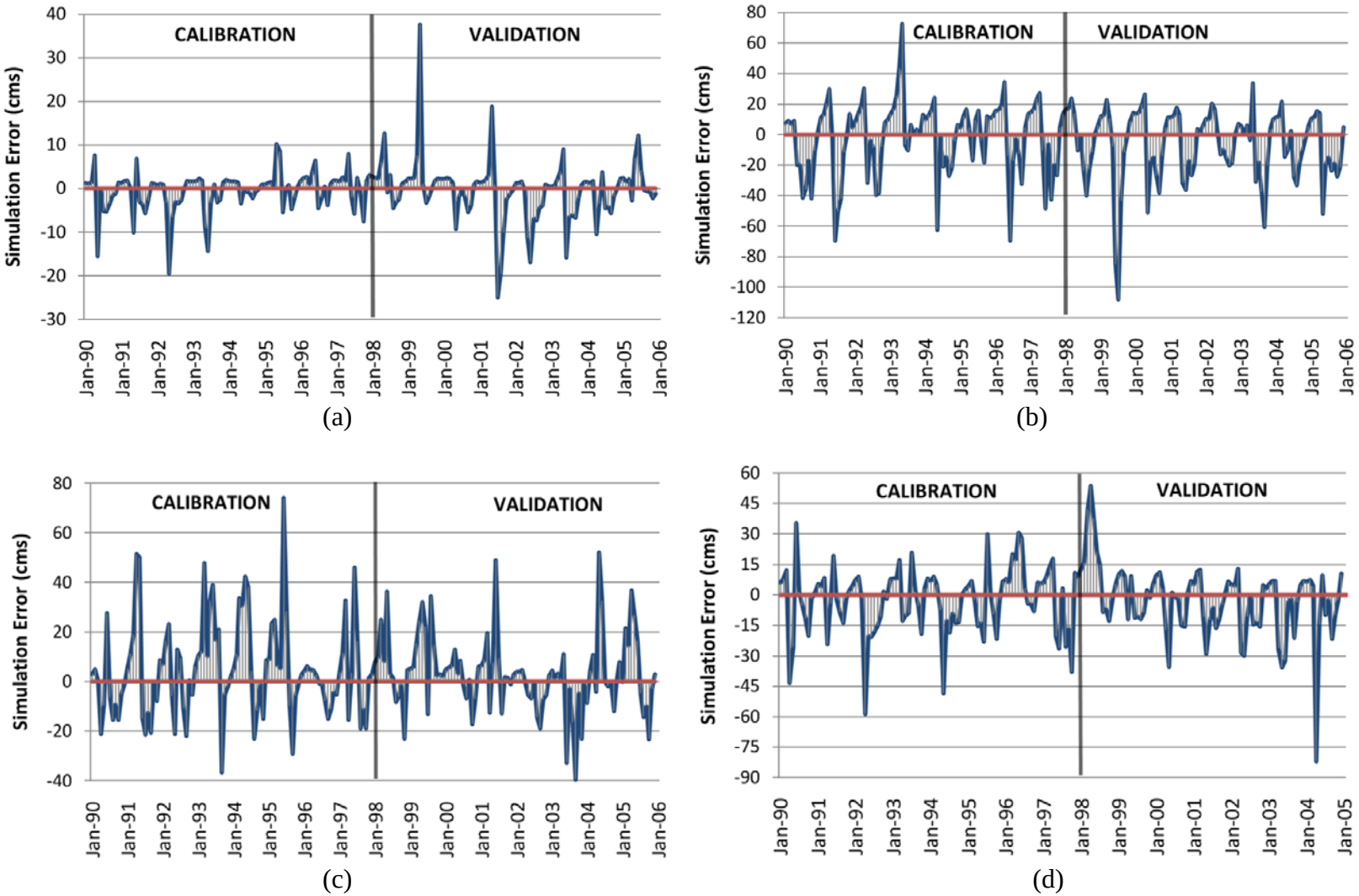


**Figure 2.13** – A time series of streamflow simulation error (error = observed – simulated) at each of the study watershed outlets (a) Cache la Poudre – USGS 06752000 (b) Gunnison – USGS 09128000 (c) San Juan – USGS 09355500 (d) Yampa – USGS 09251000.

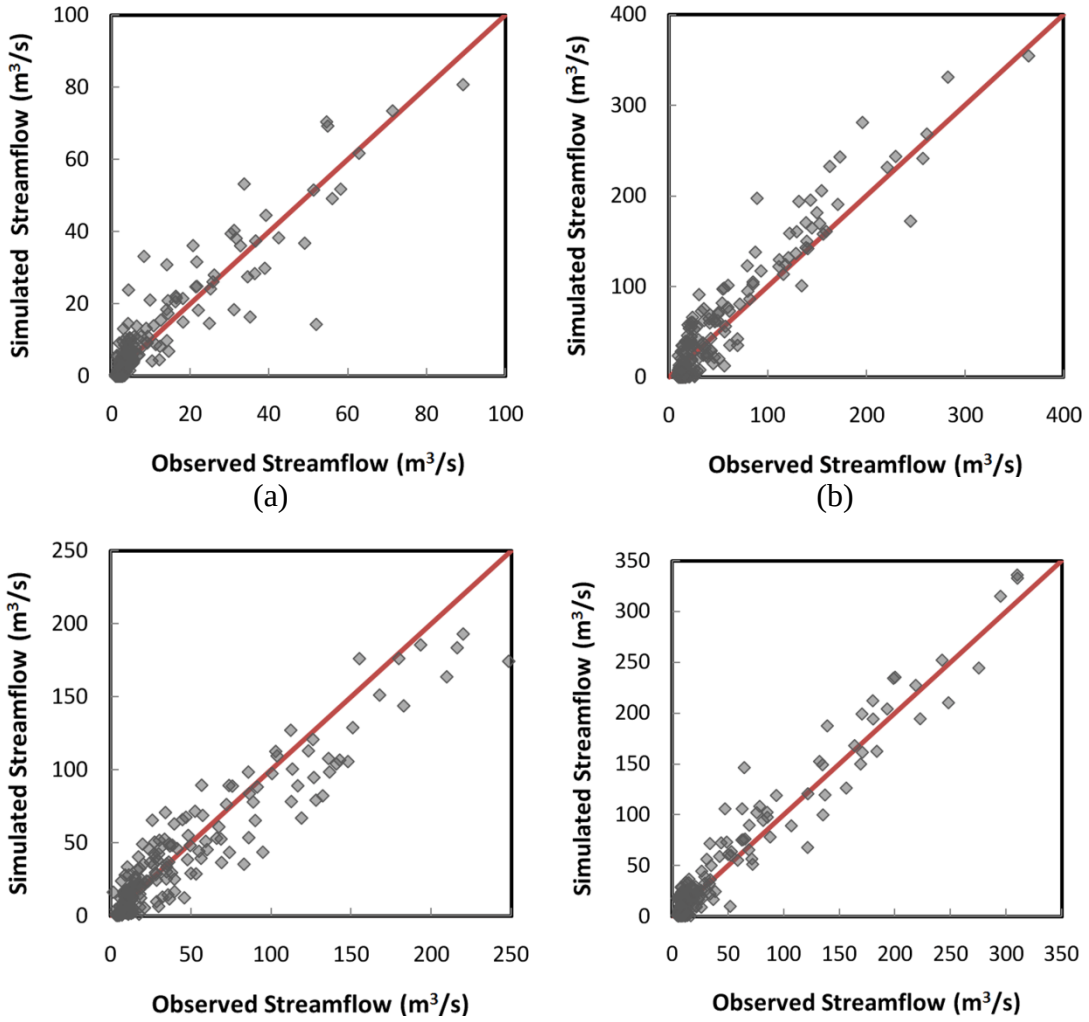


**Figure 2.14** – A plot of observed versus simulated monthly streamflows at each of the study watershed outlets over the calibration and validation periods (a) Cache la Poudre – USGS 06752000 (b) Gunnison – USGS 09128000 (c) San Juan – USGS 09355500 (d) Yampa – USGS 09251000.

## 2.4 CONCLUSIONS

The suitability of the comprehensive, process-based hydrologic model SWAT was assessed in four mountainous headwater basins of Colorado. Each model was developed utilizing detailed sets of geospatial data representing terrain, land use, soil, and climate. In order to alleviate the need to represent the complex systems of diversions, reservoirs, and irrigation canals within the study basins, the models were calibrated to naturalized

streamflow data. Three separate automatic calibration techniques including SCE-UA, GSA, and a method which combined the two were objectively compared for performance in the study watersheds. The automatic calibration techniques were applied at multiple sites within each watershed (except Cache la Poudre) to insure accurate parameterization representative of the entire watershed. GSA appeared to outperform SCE-UA in three out of the four basins, with near equal performance achieved in the fourth. The two-stage combination of SCE-UA and GSA was found to perform nearly as well as GSA alone, and was used (with a slight modification that included more model evaluations) for the final parameterization of the models. Several error measures were calculated to determine the performance of the models in simulating monthly streamflows relative to observed (naturalized) streamflows. The measures of performance, namely RE and $E_{NS}$, resulted in a relatively high level of confidence in the models. Several hydrologic components were quantified over the simulation period (1990 – 2005), and include precipitation, snow fall, ET, and resulting water yield. Subsurface lateral flow was shown to be a dominant process in all the study basins, and contributed between 64% and 82% of water to gross basin yields on an average annual basis. The results of this study indicate an overall satisfactory level of performance of SWAT in modeling monthly streamflows and dominant hydrologic components in each of the study basins, but also show a need for improvement in representation of snowmelt and groundwater processes occurring in such mountainous watersheds.

## 2.5 REFERENCES


Ahl, R.S., Woods, S.W., Zuuring, H.R., 2008. Hydrologic calibration and validation of SWAT in a snow-dominated Rocky Mountain watershed, Montana, U.S.A. . Journal of the American Water Resources Association, 44(6): 1411-1430.

Allen, R.G., 1986. A Penman for all seasons. Journal of Irrigation and Drainage Engineering, 112(4): 348-368.

Allen, R.G., Jensen, M.E., Wright, J.L., Burman, R.D., 1989. Operational estimates of reference evapotranspiration. Agronomy Journal, 81(4): 650-662.

Anderson, R.M., Koren, V.I., Reed, S.M., 2006. Using SSURGO data to improve Sacramento Model a priori parameter estimates. Journal of Hydrology, 320(1-2): 103-116.

Arnold, J.G., Srinivasan, R., Muttiah, R.S., Williams, J.R., 1998. Large area hydrologic modeling and assessment. I. Model development. Journal of the American Water Resources Association, 34(1): 73-78.

Barry, R.G., Chorley, R.J., 1976. Atmosphere, weather, and climate. Methuen, London, 432 pp.

Bicknell, B.P., Imhoff, J.C., Kittle Jr., J.L., Donigan Jr., A.S., Johanson, R.C., 1997. Hydrologic Simulation Program--Fortran, User's manual for version 11, Athens, GA.

CO Division of Water Resources, CO Water Conservation Board, 2010. Colorado's Decision Support Systems - Surface Water Model.

Crawford, N.H., Linsley, R.K., 1966. Digital simulation in hydrology: Stanford watershed model IV.

Dawdy, D.R., O'Donnell, T., 1965. Mathematical models of catchment behavior. Journal of Hydraulic Engineering, 91: 113-137.

DHI, 2004. MIKE SHE An Integrated Hydrological Modelling System - User Guide.

Di Luzio, M., Arnold, J.G., Srinivasan, R., 2004. Integration of SSURGO maps and soil parameters within a geographic information system and nonpoint source pollution model system. Journal of Soil and Water Conservation, 59(4): 123-133.

Duan, Q., Gupta, V.K., Sorooshian, S., 1993. A shuffled complex evolution approach for effective and efficient optimization. Journal of Optimization Theory Applications, 76(3): 501-521.

Duan, Q., Sorooshian, S., Gupta, V.K., 1992. Effective and efficient global optimization for conceptual rainfall-runoff models. Water Resources Research, 24(7): 1163-1173.

Duan, Q., Sorooshian, S., Gupta, V.K., 1994. Optimal use of the SCE-UA global optimization method for calibrating watershed models. Journal of Hydrology, 158: 265-284.

Eckhardt, K., Arnold, J.G., 2001. Automatic calibration of a distributed catchment model. Journal of Hydrology, 251(1-2): 103-109.

Eckhardt, K., Fohrer, N., Frede, H.-G., 2005. Automatic model calibration. Hydrological Processes, 19(3): 651-658.

Fontaine, T.A., Cruickshank, T.S., Arnold, J.G., Hotchkiss, R.H., 2002. Development of a snowfall-snowmelt routine for mountainous terrain for the soil water assessment tool (SWAT). Journal of Hydrology, 262(1-4): 209-223.

Gassman, P.W., Reyes, M.R., Green, C.H., Arnold, J.G., 2007. The Soil and Water Assessment Tool: historical development, applications, and future research directions. Transactions of the American Society of Agricultural and Biological Engineers, 50(4): 1211-1250.

Gesch, D.B., 2007. The National Elevation Dataset. In: Maune, D. (Ed.), Digital Elevation Model Technologies and Applications: The DEM Users Manual. American Society for Photogrammetry and Remote Sensing, Bethesda, Maryland, pp. 99-118.

Gesch, D.B., Oimoen, M., Greenlee, S., Nelson, C., Steuck, M., Tyler, D., 2002. The National Elevation Dataset. Photogrammetric Engineering and Remote Sensing, 68(1): 5-11.

Givens, G.H., Hoeting, J.A., 2005. Computational Statistics. John Wiley & Sons, Inc., Hoboken, NJ, 418 pp.

Hargreaves, G.H., Samani, Z.A., 1985. Reference crop evapotranspiration from temperature. Applied Engineering in Agriculture, 1(2): 96-99.

Hjermstad, L.M., 1970. The influence of meteorological parameters on the distribution of precipitation across central Colorado mountains, Colorado State University, Fort Collins, Colorado, 78 pp.

Holland, J.H., 1975. Adaptation in Natural and Artificial Systems. University of Michigan Press, Ann Arbor, MI.

Homer, C., Huang, C., Yang, L., Wylie, B., Coan, M., 2004. Development of a 2001 national landcover database for the United States. Photogrammetric Engineering and Remote Sensing, 70(7): 829-840.

Ibbitt, R.P., O'Donnell, T., 1971. Fitting Methods for Conceptual Catchment Models. Journal of Hydraulic Engineering, 97(9): 1331-1342.

Johnston, P.R., Pilgrim, D.H., 1976. Parameter optimization for watershed models. Water Resources Research, 12(3): 477-486.

Kuczera, G., 1997. Efficient subspace probabilistic parameter optimization for catchment models. Water Resources Research, 33(1): 177-185.

Kuczera, G., Parent, E., 1998. Monte Carlo assessment of parameter uncertainty in conceptual catchment models: the Metropolis algorithm. Journal of Hydrology, 211(1-4): 69-85.

Leavesley, G.H., Lichty, R.W., Troutman, B.M., Saindon, L.G., 1983. Precipitation-Runoff Modeling System: User's Manual.

Lemonds, P.J., McCray, J.E., 2007. Modeling hydrology in a small Rocky Mountain watershed serving large urban populations. Journal of the American Water Resources Association, 43(4): 875-887.

Li, Z., Liu, W.-z., Zhang, X.-c., Zheng, F.-l., 2009. Impacts of land use change and climate variability on hydrology in an agricultural catchment on the Loess Plateau of China. Journal of Hydrology, 377(1-2): 35-42.

Liang, X., Lettenmaier, D.P., Wood, E.F., Burges, S.J., 1994. A simple hydrologically based model of land surface water and energy fluxes for general circulation models. Journal of Geophysical Research, 99(14): 415–14.

Liang, X., Wood, E.F., Lettenmaier, D.P., 1996. Surface soil moisture parameterization of the VIC-2L model: Evaluation and modification. Global and Planetary Change, 13(1-4): 195-206.

Lin, Z., Radcliffe, D.E., 2006. Automatic calibration and predictive uncertainty analysis of a semidistributed watershed model. Vadose Zone Journal, 5(1): 248-260.

Luce, C.H., Tarboton, D.G., Cooley, K.R., 1998. The influence of the spatial distribution of snow on basin-averaged snowmelt. Hydrological Processes, 12(10-11): 1671-1683.

Marks, D., Dozier, J., Davis, R.E., 1992. Climate and energy exchange at the snow surface in the alpine region of the Sierra Nevada 1. Meteorological measurements and monitoring. Water Resources Research, 28(11): 3029-3042.

Metropolis, N., Rosenbluth, A.W., Rosenbluth, M.N., Teller, A.H., Teller, E., 1953. Equation of state calculations by fast computing machines. The Journal of Chemical Physics, 21(6): 1087-1092.

Miller, S.N., Kepner, W.G., Mehaffey, M.H., Hernandez, M., Miller, R.C., Goodrich, D.C., Devonald, K., Heggem, D.T., Miller, W.P., 2002. Integrating landscape assesment and hydrologic modeling for land cover change analysis. Journal of the American Water Resources Association, 38(4): 915-929.

Monteith, J.L., 1965. Evaporation and environment, The state and movement of water in living organisms. XIXth Symposium Society for Experimental Biology. Cambridge University Press, Swansea, pp. 205-234.

Moriasi, D.N., Arnold, J.G., Van Liew, M.W., Bingner, R.L., Harmel, R.D., Veith, T.L., 2007. Model evaluation guidelines for systematic quantification of accuracy in watershed simulations. Transactions of the American Society of Agricultural and Biological Engineers, 50(3): 885-900.

Nash, J.E., Sutcliffe, J.V., 1970. River flow forecasting through conceptual models part I -- A discussion of principles. Journal of Hydrology, 10(3): 282-290.

Natural Resources Conservation Service, U.S.D.A., 2009. USDA-NRCS SNOTEL Data & Products.

Neitsch, S.L., Arnold, J.G., Kiniry, J.R., Srinivasan, R., Williams, J.R., 2005. Soil and Water Assessment Tool, Theoretical Documentation, Version 2005, Temple, Texas.

Neitsch, S.L., Arnold, J.G., Kiniry, J.R., Williams, J.R., 2004. Soil and Water Assessment Tool, Input/Output File Documentation, Version 2005, Temple, Texas.

Nelder, J.A., Mead, R., 1965. A simplex method for function minimization. The Computer Journal, 7(4): 308-313.

Northern Water, 2009. Poudre River Naturalized Flow Data, Fort Collins, CO.

Peschel, J.M., Haan, P.K., Lacey, R.E., 2006. A SSURGO pre-processing extension for the ArcView Soil and Water Assessment Tool. Journal of the American Water Resources Association, 42(5): 1371-1389.

Peterson, J.R., Hamlett, J.M., 1998. Hydrologic calibration of the SWAT model in a watershed containing fragipan soils. Journal of the American Water Resources Association, 34(3): 531-544.

Pohlert, T., Huisman, J.A., Breuer, L., Frede, H.G., 2005. Modelling of point and non-point source pollution of nitrate with SWAT in the river Dill, Germany. Advances in Geosciences, 5: 7-12.

Praskievicz, S., Chang, H., 2009. A review of hydrological modelling of basin-scale climate change and urban development impacts. Progress in Physical Geography, 33(5): 650-671.

Price, W.L., 1987. Global optimization algorithms for a CAD workstation. Journal of Optimization Theory and Applications, 55(1): 133-146.

Priestley, C.H.B., Taylor, R.J., 1972. On the assessment of surface heat flux and evaporation using large-scale parameters. Monthly Weather Review, 100(2): 81-92.

Richer, E., 2009. Snowmelt Runoff Analysis and Modeling for the Upper Cache la Poudre River Basin, Colorado, Colorado State University, Fort Collins, Colorado, 117 pp.

Rossman, L.A., 2009. Storm Water Management Model, User's Manual, Version 5.0, Cincinatti, OH.

Sanadyha, P., 2009. Global Sensitivity Analysis of Hydrologic Processes in Major River Basins in Colorado, Colorado State University, Fort Collins, CO.

Santhi, C., Arnold, J.G., Williams, J.R., Dugas, W.A., Srinivasan, R., Hauck, L.M., 2001. Validation of the SWAT model on a large river basin with point and nonpoint sources. Journal of the American Water Resources Association, 37(5): 1169-1188.

Satellite and Information Service, N.O.A.A., 2009. National Climatic Data Center.

Serreze, M.C., Clark, M.P., Armstrong, R.L., McGinnis, D.A., Pulwarty, R.S., 1999. Characteristics of the western United States snowpack from snowpack telemetry (SNOTEL) data. Water Resources Research, 35(7): 2145-2160.

Sharpley, A.N., Williams, J.R., 1990. EPIC - Erosion Productivity Impact Calculator, 1. Model Documentation.

Sheshukov, A., Daggupati, P., Lee, M.C., Douglas-Mankin, K., 2009. ArcMap Tool for Pre-processing SSURGO Soil Database for ArcSWAT, 5th International SWAT Conference, Boulder, Colorado, pp. 1-8.

Sloan, P.G., Moore, I.D., 1984. Modeling subsurface stormflow on steeply sloping forested watersheds. Water Resources Research, 20(12): 1815-1822.

Sloan, P.G., Moore, I.D., Coltharp, G.B., Eigel, J.D., 1983. Modeling surface and subsurface stormflow on steeply-sloping forested watersheds, Lexington, KY.

Soil Survey Staff, N.R.C.S., 2006. U.S. General Soil Map (STATSGO2).

Soil Survey Staff, N.R.C.S., 2009. Soil Survey Geographic (SSURGO) Database.

Sorooshian, S., Duan, Q., Gupta, V.K., 1993. Calibration of rainfall-runoff models: Application of global optimization to the Sacramento soil moisture accounting model. Water Resources Research, 29(4): 1185-1194.

Sridhar, V., Nayak, A., 2010. Implications of climate-driven variability and trends for the hydrologic assessment of the Reynolds Creek Experimental Watershed, Idaho. Journal of Hydrology, 385(1-4): 183-202.

Stewart, I.T., Cayan, D.R., Dettinger, M.D., 2004. Changes in snowmelt runoff timing in western North America under abusiness as usual'climate change scenario. Climatic Change, 62(1-3): 217-232.

Stone, M.C., Hotchkiss, R.H., Hubbard, C.M., Fontaine, T.A., Mearns, L.O., Arnold, J.G., 2001. Impacts of climate change on Missouri River Basin water yield. Journal of the American Water Resources Association, 37(5): 1119-1129.

Stonefelt, M.D., Fontaine, T.A., Hotchkiss, R.H., 2000. Impacts of climate change on water yield in the Upper Wind River Basin. Journal of the American Water Resources Association, 36(2): 321-336.

Stratton, B.T., Sridhar, V., Gribb, M.M., McNamara, J.P., Narasimhan, B., 2009. Modeling the spatially varying water balance processes in a semiarid mountainous watershed of Idaho. Journal of the American Water Resources Association, 45(6): 1390-1408.

Tolson, B.A., Shoemaker, C.A., 2004. Watershed modeling of the Cannonsville Basin using SWAT2000: Model development, calibration, and validation for the prediction of flow, sediment and phosphorous transport to the Cannonsville Reservoir. Version 1.0, Cornell University.

Tolson, B.A., Shoemaker, C.A., 2007. Cannonsville Reservoir Watershed SWAT2000 model development, calibration, and validation. Journal of Hydrology, 337(1-2): 68-86.

Vogelman, J.E., Howard, S.M., Yang, L., Larson, C.R., Wylie, B.K., Van Driel, N., 2001. Completion of the 1990's National Land Cover Data set for the conterminous United States for Landsat Thematic Mapper data and ancillary data sources. Photogrammetric Engineering and Remote Sensing, 67(6): 650-662.

Vrugt, J.A., Gupta, H.V., Bouten, W., Sorooshian, S., 2003. A Shuffled Complex Evolution Metropolis algorithm for optimization and uncertainty assessment of hydrologic model parameters. Water Resources Research, 39(8): 1201-1216.

Wang, X., Melesse, A.M., 2006. Effects of STATSGO and SSURGO as inputs on SWAT model's snowmelt simulation. Journal of the American Water Resources Association, 42(5): 1217-1236.

Winchell, M., Srinivasan, R., Di Luzio, M., Arnold, J.G., 2007. ArcSWAT Interface for SWAT2005, Temple, Texas.

Yang, J., Reichert, P., Abbaspour, K.C., Xia, J., Yang, H., 2008. Comparing uncertainty analysis techniques for a SWAT application to the Chaohe Basin in China. Journal of Hydrology, 358(1-2): 1-23.

Zhang, X., Srinivasan, R., Hao, F., 2007. Predicting hydrologic response to climate change in the Luohe River basin using the SWAT model. Transactions of the American Society of Agricultural and Biological Engineers, 50(3): 901-910.

# CHAPTER 3: HYDROLOGIC RESPONSE TO CLIMATE CHANGE

## 3.1 INTRODUCTION

Freshwater is one of the most basic necessities required to sustain all forms of life on this planet. Not only are freshwater resources needed to sustain living organisms, but access to them is needed for nearly all human activities. In fact, the United Nations recently regarded access to safe freshwater as a universal human right (United Nations Committee on Economic, 2003). However, access to freshwater, let alone safe and usable freshwater, is far from secure as the 21$^{st}$ century progresses. More than one-sixth of the world's population live in glacier- or snowmelt-fed river basins, where impacts of climate change, resulting from observed and projected increases in temperature and precipitation variability, will be potentially felt through alterations to availability of freshwater resources (Kundzewicz et al., 2007). Not only is future climate change predicted to affect the mean hydrology of river basins, but it is also likely to affect the frequency and magnitude of extreme hydrologic events (Praskievicz and Chang, 2009). Thus, in order to improve understanding of the processes involved in generation of freshwater resources, as well as predict potential future conditions of such supplies, scientists must rely on hydrologic models to simulate such complex systems (Praskievicz and Chang, 2009).

On a regional scale, the presence of mountainous terrain further complicates the representation of natural phenomena. Inherent in the simulation of hydrologic processes

in such terrain, especially in the future, is a realization of the underlying connections between elevation-dependent snow processes and streamflow generation, and the role climate change and variability may play in disrupting and modifying such linkages. Snow cover plays an important role within the Earth's hydroclimatic system due to its many uniquely defining characteristics including low thermal conductivity, large spatial extent, seasonal amplitude, and longitudinal variation (Stewart, 2009). In addition, many arid and semi-arid lowland areas around the world obtain surface water from precipitation that falls on the surrounding higher elevations, mainly in the form of snow. Such is the case in the mountainous regions of western North America, where 50-70% of the precipitation may fall in the form of snow (Serreze et al., 1999), and the seasonal snowmelt of the spring and early summer may account for 50-80% of the total annual runoff (Stewart et al., 2004). Observations through the 20$^{th}$ century have characterized several trends concerning snow-related processes and streamflow generation in these areas and, generally speaking, include a decrease in spring snowpack (Hamlet et al., 2005; Mote et al., 2005), an earlier occurrence of snowmelt runoff (Cayan et al., 2001; Stewart et al., 2004), and a decrease in the ratio of snowfall to total annual precipitation (Knowles et al., 2006) due to an increase in observed winter and spring temperatures (Trenberth et al., 2007). Such regionalized trends, however, do not produce consistent hydrologic responses at the watershed scale, which is due to localized heterogeneity in geography, latitude, elevation, vegetation, and climate (Stewart, 2009).

The climate in the state of Colorado is unlike that of any other area in the United States. Characterized by high elevations and complex topography of the Rocky Mountains, the Colorado Plateau and the Continental Divide, the climate in Colorado

varies both spatially, across regions, as well as temporally, across years and decades (Ray et al., 2008). Such heterogeneity leads to difficulties in both developing representative models and forecasting of weather and climate. For instance, a recent study in the Upper Colorado River Basin predicted a multi-ensemble model average of a 6% decrease (from the 1950-1999 average baseline conditions) in runoff by the mid 21$^{st}$ century (2040-2069), while individual model predictions varied anywhere from a 40% decrease to an 18% increase in runoff over that same time period (Christensen and Lettenmaier, 2007; Ray et al., 2008). In addition, while the impact of climate change on the water resources of the Colorado River has received the most attention, climate change is projected to impact all headwaters of the state. Although the water delivered to the Upper Colorado is extremely important for the West as a whole, there is a need to direct localized attention to the watersheds of Colorado. At a state level, the yield from these basins is heavily relied upon for agricultural, municipal, and recreational uses of which demands are only projected to increase in the future.

Existing studies concerning the impacts of climate change on the hydrology and water resources of Colorado have typically been undertaken at coarse spatial scales, with model grid cells ranging in size from as large as several hundred miles (e.g. Milly et al., 2005), to as little as eight miles (e.g. Christensen and Lettenmaier, 2007). Such studies have discerned the hydrologic response to climate change from General Circulation Model (GCM) output and macro-scale hydrologic models, respectively, and do not include comprehensive analyses of processes important at the watershed scale. The overall goal of this study is to predict the impacts of climate change on the hydrology and water resources in Colorado, but to do so at a localized, watershed scale through use of a

comprehensive physically-based model. Specifically, the four study watersheds of interest include the Cache la Poudre, Gunnison, San Juan, and Yampa River basins. Several objectives critical to the success of the research were (i) to develop a comprehensive, process-based watershed model for each of the study watersheds through incorporation of detailed watershed characteristics and necessary modifications for mountainous basins; (ii) to downscale, in space and time, an ensemble of climate projections in a manner which addresses both the error involved and uncertainty inherent in climate modeling through incorporation of numerous models and diverse emissions scenarios; and (iii) to objectively identify the direction and degree of potential impacts on water resources, namely water yield, in Colorado and associate specific climate projections with low and high conditions of freshwater availability.

## 3.2 METHODS

Typical approaches for projecting the hydrologic response to climate change include several pathways leading from GCM outputs to specific physical processes (e.g. streamflow), as outlined in Figure 3.1. At a large, global scale the hydrology component of coarse-resolution General Circulation Models (GCMs) may be taken directly (e.g. Milly et al., 2005). However, this is an atypical method for more local scale studies, where climate projections must be either hypothetically created through the application of incremental changes (Fontaine et al., 2002; Stonefelt et al., 2000) or unbiased and downscaled, either statistically or dynamically (e.g. Wood et al., 2004), for use in the regional or watershed setting. Finally, to determine the implications of such downscaled projections to hydrologic response, the projections must be driven by either process-based hydrologic models (e.g. Christensen and Lettenmaier, 2007) or by regression and

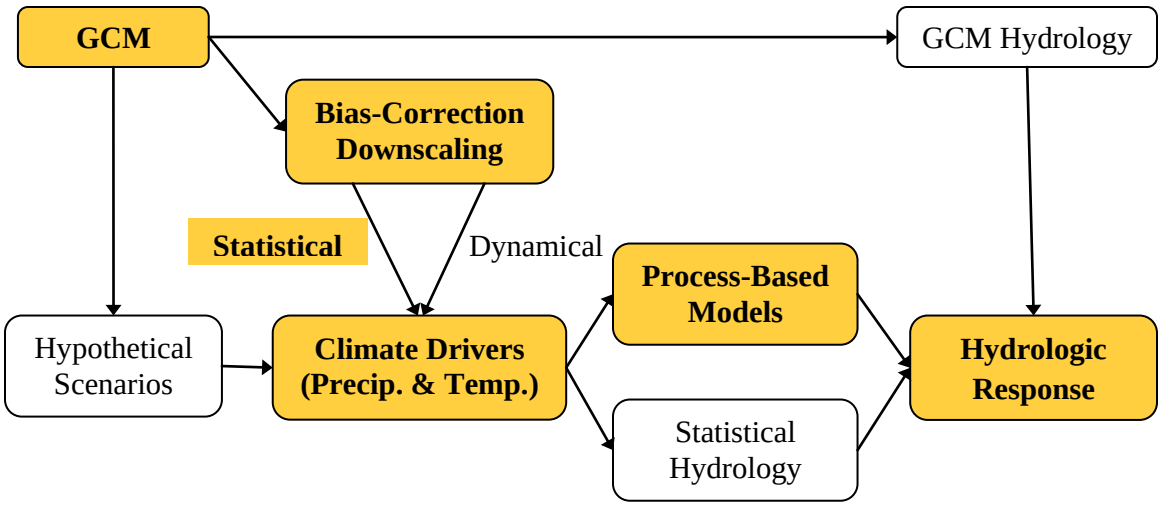


**Figure 3.1** - Several general approaches for discerning the impacts of climate change on hydrologic response with the approach taken in this study shaded in orange. Figure modified after Ray et al. (2008).

empirically-based statistical hydrology (e.g. Hoerling and Eischeid, 2007). The approach taken herein is highlighted in orange, and includes forcing a process-based hydrologic model with future climatic data that have been statistically downscaled, both spatially and temporally, and unbiased from its original GCM output.

An extensive collection of 112 separate climate projections, composed of 16 GCMs covering 3 emissions path scenarios, were obtained for the study. The projections, characterized at a monthly time scale and 1/8° spatial resolution, were first corrected for areal average to point bias. This ensured that initial conditions of areal-averaged future climate projections were consistent with actual observations of precipitation and temperature at a given meteorological stations within the area. Next, each scenario was temporally downscaled to a daily time step using a resampling and scaling/incrementing technique. The final climate simulations, downscaled to a point location and daily time-step, were used to run the process-based Soil and Water Assessment Tool (SWAT) for a period of 90 years from 2010 – 2099. The SWAT model specific to each study

watershed was calibrated and tested over a period of 16 years (1990 – 2005), and further details regarding development, calibration, and testing of the model may be found in the preceding chapter. Each model was then driven with the downscaled projections of precipitation and temperature, for a total of 112 simulations in each of the four watersheds, and the results were analyzed for hydrologic response to climate change.

### 3.2.1 FUTURE CLIMATE PROJECTIONS

*GENERAL CIRCULATION MODELS AND EMISSIONS PATH SCENARIOS*

The World Climate Research Programme's (WCRP's) Coupled Model Intercomparison Project phase 3 (CMIP3) multi-model dataset provides a broad set of climate projections, which include both a multitude of GCMs and range of emissions path scenarios. The CMIP3 dataset represents the largest and most comprehensive international global coupled climate model [atmospheric-ocean general circulation model (AOGCM)] experiment and multi-model analysis effort ever attempted, with initial participation of 16 modeling groups representing 11 countries who produced 23 models for assessment (Meehl et al., 2007). Of the 23 GCMs embodied in the CMIP3 dataset, 16 were utilized for this study and represented work of 14 modeling groups from 10 countries (Table 3.1).

**Table 3.1** – Characteristics of the 16 GCMs utilized in this study.

| Modeling Group | Country | Name | Runs | | | Primary Reference |
|---|---|---|---|---|---|---|
| | | | A2 | A1B | B1 | |
| Bjerknes Centre for Climate Research | Norway | BCCR-BCM2.0 | 1 | 1 | 1 | (Furevik et al., 2003) |
| Canadian Centre for Climate Modeling & Analysis | Canada | CGCM3.1 (T47) | 5 | 5 | 5 | (Flato and Boer, 2001) |
| Meteo-France / Centre National de Recherches Meteorologiques | France | CNRM-CM3 | 1 | 1 | 1 | (Salas-Mélia et al., 2005) |
| CSIRO Atmospheric Research | Australia | CSIRO-Mk3.0 | 1 | 1 | 1 | (Gordon et al., 2000) |
| US Dept. of Commerce / NOAA / Geophysical Fluid Dynamics Laboratory | USA | GFDL-CM2.0 | 1 | 1 | 1 | (Delworth et al., 2006) |
| US Dept. of Commerce / NOAA / Geophysical Fluid Dynamics Laboratory | USA | GFDL-CM2.1 | 1 | 1 | 1 | (Delworth et al., 2006) |
| NASA / Goddard Institute for Space Studies | USA | GISS-ER | 1 | 2 | 1 | (Russell et al., 2000) |
| Institute for Numerical Mathematics | Russia | INM-CM3.0 | 1 | 1 | 1 | (Diansky and Volodin, 2002) |
| Institut Pierre Simon Laplace | France | IPSL-CM4 | 1 | 1 | 1 | (Marti et al., 2006) |
| Center for Climate System Research (The University of Tokyo), National Institute for Environmental Studies, and Frontier Research Center for Global Change (JAMSTEC) | Japan | MIROC3.2 (medres) | 3 | 3 | 3 | (Hasumi and Emori, 2004) |
| Meteorological Institute of the University of Bonn, Meteorological Research Institute of KMA | Germany/Korea | ECHO-G | 3 | 3 | 3 | (Legutke and Voss, 1999) |
| Max Planck Institute for Meteorology | Germany | ECHAM5/ MPI-OM | 3 | 3 | 3 | (Jungclaus et al., 2006) |
| Meteorological Research Institute | Japan | MRI-CGCM2.3.2 | 5 | 5 | 5 | (Yukimoto et al., 2001) |
| National Center for Atmospheric Research | USA | CCSM3 | 4 | 6 | 7 | (Collins et al., 2006) |
| National Center for Atmospheric Research | USA | PCM | 4 | 4 | 2 | (Washington et al., 2000) |
| Hadley Centre for Climate Prediction and Research / Met Office | UK | UKMO-HadCM3 | 1 | 1 | 1 | (Gordon et al., 2002) |

Each of the GCMs utilize conditions from a multitude of emissions path scenarios, as described by the Intergovernmental Panel on Climate Change (IPCC) Special Report on Emissions Scenarios (SRES) (IPCC, 2000). Additionally, within each emissions path scenarios, there are one or more runs representing unique initial conditions, which are dependent upon the 20th century "control" simulations as described by the WCRP (more information may be found at the WCRP website http://www-pcmdi.llnl.gov/ipcc/time_correspondence_summary.htm). The scenarios characterize projections of future greenhouse gas (GHG) emissions, and are based on storylines of demographic and economic development, technological change, energy resources and demand, and land use change with no additional implementation of climate policies. Three different emissions scenarios were used in this study (SRES A2, SRES A1B, and SRES B1), which correspond to a range of conditions from high GHG emissions to low GHG emissions, respectively (Figure 3.2). A description of the storylines from Climate Change 2007: Synthesis Report (Bernstein et al., 2007) is as follows:

> **SRES A2** ("higher" emissions path) – very heterogeneous world with high population growth, slow economic development, and slow technologic change;
>
> **SRES A1B** ("middle" emissions path) – very rapid economic growth with a global population that peaks in the mid-21st century and fast introduction of new and more efficient technologies, balanced between fossil intensive and non-fossil energy sources;
>
> **SRES B1** ("lower" emissions path) – convergent world with the same population as A1B, but with more rapid changes in economic structures toward and service and information based economy.

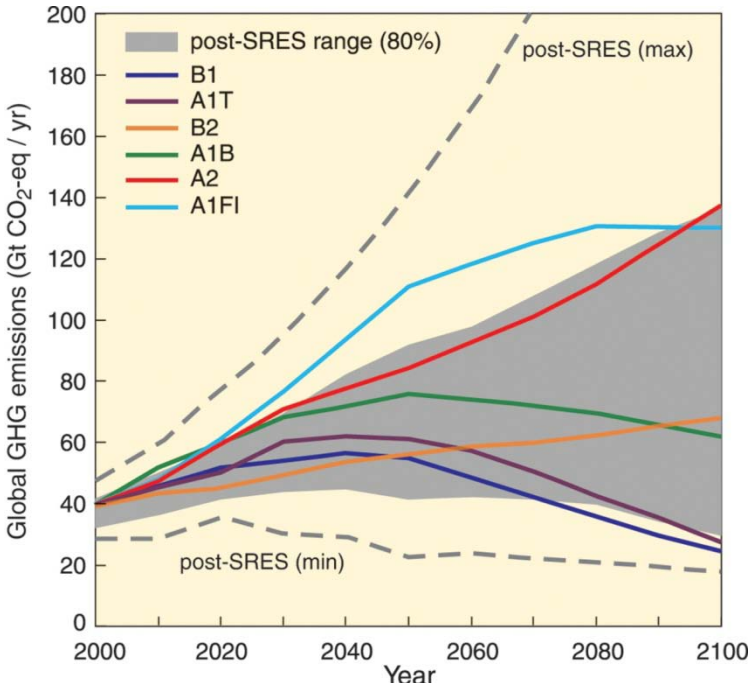


**Figure 3.2 –** Global GHG emissions (gigatons $CO_2$-equivalent per year) in the absence of future climate policies: six SRES 2000 scenarios (colored lines), 80$^{th}$ percentile range of recent scenarios since publication of SRES 2000 (gray shaded area), and complete range of post-2000 scenarios (gray dashed lines). The emissions include $CO_2$, $CH_4$, $N_2O$ and F-gases. Figure adapted from Bernstein et al. (2007).

*STATISTICALLY DOWNSCALED DATA*

The spatial scales of the CMIP3 data correspond to the various spatial scales of the respective GCMs, and are not adequate to discern the impacts of climate change at a watershed-scale, especially in the complex, mountainous terrain of Colorado. Thus, an archive of bias-corrected and spatially downscaled climate projections derived from CMIP3 data and served at http://gdo-dcp.ucllnl.org/downscaled_cmip3_projections/, as described by Maurer et al. (2007), were utilized for this study. These data were created by a collaborative effort between the Lawrence Livermore National Laboratory (LLNL), United States Bureau of Reclamation (USBR), Santa Clara University (SCU), and Climate Central (CC), and will be referred to as the LLNL/USBR dataset hereafter. The LLNL/USBR dataset contains 112 climate projections spanning the contiguous United

States, culminating from 16 GCMs, 3 emissions path scenarios, and one or more runs with unique initial conditions (Table 3.1). Each climate projection was bias-corrected and spatially downscaled using a two-step procedure (Maurer et al., 2007; Wood et al., 2004; Wood et al., 2002) applied to both monthly precipitation rate (mm/day) and monthly surface air temperature (°C).

The first step in creation of the LLNL/USBR data was to correct the bias between each projection's past climate simulation and actual observations, based on a gridded dataset of 20th century (1950-1999) climatic conditions described in Maurer, Wood et al. (2002). The spatial resolution of each of the datasets under comparison had to be rectified in order to be comparable, such that the observationally based gridded dataset was aggregated from 1/8° to 2° and the GCM gridded dataset was spatially interpolated (in the same manner) from its original spatial resolution to 2°. A quantile map was created from the probability thresholds between cumulative distribution functions of GCM and observed grids (on a monthly basis) for both precipitation and temperature during the overlapping period (1950-1999). Bias-correction was completed by adjusting each climate projection (both past and future simulations) using the previously defined quantile maps. This step ensured that adjusted GCM datasets were statistically consistent with the observed datasets during the overlapping period.

The second, and final, step in creation of the LLNL/USBR data was to spatially downscale the bias-corrected GCM data (1950-2099) from a 2° grid (~200 km), to a higher resolution, watershed-scale of 1/8° (~12 km). Factor values were computed at each 2° grid between the bias-corrected GCM projection (precipitation and temperature) and the corresponding observational datum, computed as the given month's 1950-1999

mean from the 2° observational dataset. The 2° factor values were then spatially downscaled using a modified inverse-distance-squared interpolation known as the SYMAP algorithm (Shepard, 1984), and applied to the mean of the original 1/8° observed dataset for each month (1950-1999).

The previously summarized methodology ensured that the final GCM projections were both statistically consistent with the observed datasets during the overlapping period as well as spatially correlated with large and fine-scale climate. By interpolating the 2° factor values (from 1950-1999) to 1/8° and applying them to future periods, an assumption was introduced that the topographic and climatic features acting in the historical record will be analogous in the future.

Further methods for downscaling the LLNL/USBR climate projections, both spatially and temporally, were required to implement the climate projections into SWAT and meet the objectives of this study. First, an additional bias-correction technique was required to spatially downscale the data from a 1/8° grid to a point location within the grid, as SWAT utilizes climatic input data from meteorological stations. The use of meteorological stations allows for representation of orographic effects through application of temperature and precipitation lapse rates because each station has an associated elevation. Conversely, application of lapse rates from gridded temperature and precipitation data is more difficult, as a representative elevation from each area must be established. Second, a temporal downscaling methodology was required to produce daily patterns of precipitation, maximum temperature, and minimum temperature, as SWAT requires climatic input data at a daily time-step to simulate those processes occurring over smaller time scales (e.g. snow accumulation and snowmelt).

*AREAL AVERAGE TO POINT BIAS-CORRECTION TECHNIQUE*

The spatial downscaling method, which removed the bias between LLNL/USBR climate projections at 1/8° grid and a meteorological station location within the grid (Figure 3.3), ensured that projections of precipitation and temperature were consistent with observations of the late 20th century. Observations of precipitation and temperature from meteorological stations in and around the study watersheds were compared to the

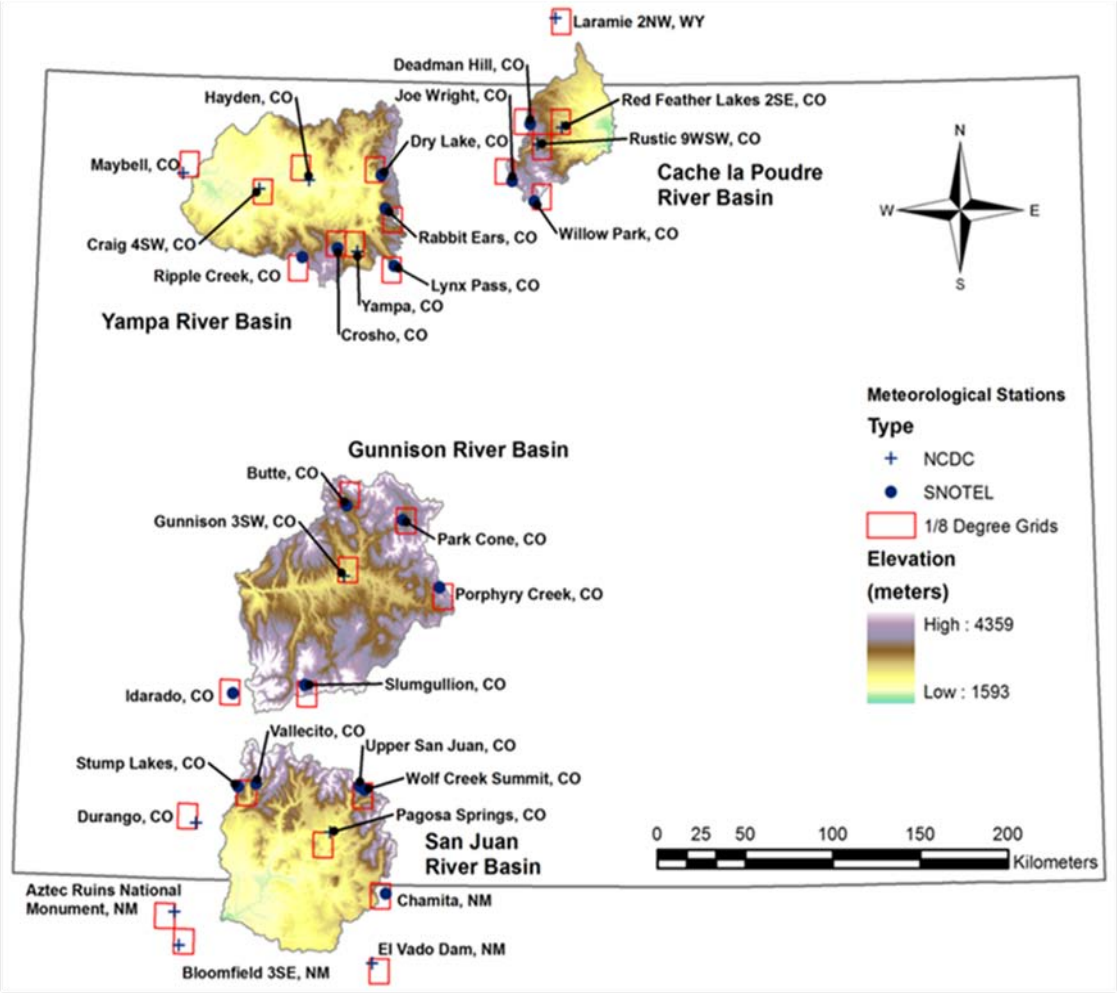


**Figure 3.3** – Topography, as represented by a digital elevation model (DEM), location of meteorological stations (SNOTEL and NCDC), and 1/8° grids corresponding to future climate projections in each of the headwater basins of Colorado.

LLNL/USBR data from the single latitudinal/longitudinal grid cell encompassing the station, and the bias between the two was removed through scaling (precipitation) and incrementing (temperature) on a monthly basis. This method was applied on a monthly time-scale in such a fashion that months with a complete observation record of precipitation and temperature were averaged and compared to the averaged values of the same months from the LLNL/USBR dataset. From this comparison a single ratio (for precipitation) and a single increment (temperature) was applied to all future monthly projections. Equations 3.1 and 3.2, below, display the computations necessary to remove bias from the LLNL/USBR climate projections of the 21st century.

$$P_{corrected,i} = \frac{\sum_{m=1}^{N} P_{observed,m}}{\sum_{m=1}^{N} P_{projected,m}} \times P_{uncorrected,i} \qquad \textit{Equation 3.1}$$

where $P_{corrected,i}$ is the bias-corrected average daily precipitation for future month *i* (mm/day), $P_{observed,m}$ is the observed average daily precipitation for month *m* with a complete record (mm/day), *N* is the total number of months with a complete record of observed data, $P_{projected,m}$ is the projected average daily precipitation from LLNL/USBR dataset of the corresponding month *m* (mm/day), and $P_{uncorrected,i}$ is the biased average daily precipitation for future month *i* from LLNL/USBR dataset (mm/day).

$$T_{corrected,i} = \left(\frac{\sum_{m=1}^{N} T_{observed,m}}{N} - \frac{\sum_{m=1}^{N} T_{projected,m}}{N}\right) + T_{uncorrected,i} \qquad \textit{Equation 3.2}$$

where $T_{corrected,i}$ is the bias-corrected average daily temperature for future month *i* (ºC), $T_{observed,m}$ is the observed average daily temperature for month *m* with a complete record (ºC), $T_{projected,m}$ is the projected average daily temperature from LLNL/USBR dataset of the corresponding month *m* (ºC), and $T_{uncorrected,i}$ is the biased average daily temperature for future month *i* from LLNL/USBR dataset (ºC).

*MONTHLY TO DAILY TEMPORAL DOWNSCALING TECHNIQUE*

Following the spatial downscaling/bias-correction method previously described, a dataset consisting of average monthly values of precipitation (mm/day) and temperature (°C) at each meteorological station were available. However, the hydrologic model utilized to assess the impacts of climate change on water resources, SWAT, requires daily values of precipitation, maximum temperature, and minimum temperature. Therefore, an existing resampling technique (Bureau of Reclamation, 2009; Maurer et al., 2007; Wood et al., 2002) was refined for utilization in this study to downscale monthly values of precipitation and temperature into daily values of precipitation, maximum temperature, and minimum temperature. This method creates daily values of climatic variables that both preserve observed spatial and temporal correlations and aggregate to future monthly projections.

The basic premise of this technique involved moving through a number of meteorological stations' simulated projections (2010 – 2099) and associating a randomly selected corresponding historical month with each month simulated in the future. The historical month's daily series were then scaled (precipitation) and incremented (temperature) to create a future month's daily series which satisfy the future monthly projection.

$$P_{future,j} = \frac{P_{future,k}}{P_{historical,l}} \times P_{historical,j} \qquad \textit{Equation 3.3}$$

where $P_{future,i}$ is the future precipitation on day $j$ of future month $k$ (mm), $P_{future,k}$ is the projected average daily precipitation in future month $k$ (mm/day), $P_{historical,l}$ is the

observed average daily precipitation in resampled historical month *l* (mm/day), and $P_{historical,j}$ is the observed precipitation on day *j* of resampled historical month *l* (mm).

$$T_{future,j} = \left(T_{future,k} - T_{historic,l}\right) + T_{historical,j} \qquad \textit{Equation 3.4}$$

wherein $T_{future,i}$ is the future temperature on day *j* of future month *k* (°C), $T_{future,k}$ is the projected average daily temperature in future month *k* (°C), $T_{historical,l}$ is the observed average daily temperature in resampled historical month *l* (°C), and $T_{historical,j}$ is the observed temperature on day *j* of resampled historical month *l* (°C).

In order to maintain the space-time correlation amongst individual meteorological stations in a watershed, the same resampled historical month was applied to all stations in a given future month. This process was completed in each watershed, separately, and for all future monthly scenarios from 2010 – 2099. As may be seen in Equations 3.3 and 3.4 one of the key components of this technique was in the resampling of an appropriate historical month *l* for simulated future month *k*. Although the historical month was "randomly" selected, the pool of candidate historic months were determined based on several conditions. The conditions were that the resample historical month had to (i) be the same calendar month as the future simulated month (e.g. for a January in the future, only historical Januaries could be resampled), (ii) have the same qualitative precipitation-temperature classification, (iii) have observed historical data in at least half of the meteorological stations, and (iv) have non-zero precipitation in all meteorological stations (to avoid infinite scaling ratios).

*Month Classifications*

In order to avoid resampling a "wet-cool" historical month to generate a daily series of climatic variables in a "dry-warm" projected month, or vice-versa, a wetness and warmth classification scheme was used (Bureau of Reclamation, 2009). This scheme separated months, future and historic separately, into four general classifications: "wet-warm", "wet-cool", "dry-warm", and "dry-cool". The first component of the classification, which refers to the wetness of a given month, was determined by comparing the precipitation of that month with the median precipitation of the same calendar month over the period of record. For historical months the period of record differed between climate stations, and was determined by the availability of data at each station. The period of record for future months was consistent between all stations, and was composed of a 90 year set of data (2010 – 2099) for a given calendar month and a given climate projection. A month with precipitation greater than the median from the period of record was classified as "wet", while a month with a precipitation less than the median was classified as "dry". Similarly, the temperature of a given month was classified as "warm" or "cool" by comparing the average monthly temperature to the median average monthly temperature over the period of record. Thus, a set of monthly classifications was created for each meteorological station within each basin for both historical and future months. However, due to the classification of each climate station separately, it was not a guarantee that all stations in a given month, either future or historical, had the same classification. Therefore, the final classification of a given month in a watershed was taken to be the mode of the individual station classifications.

*Missing Data*

Missing daily measurements of precipitation, maximum temperature, and/or minimum temperature were found to be prevalent among many of the basins' meteorological stations. Such data was either completely missing in a given month, or more commonly was missing on only several occasions within an otherwise complete record of a month. Several features were added to the technique in an effort to handle the missing daily values in either case.

*Missing Precipitation*

When a day, or multiple days, of precipitation were found to be missing in a resampled month, an effort was necessary to fill-in the day(s) with a reasonable value(s). This was done through a two-step procedure that first determined if the day of missing data was wet or dry, and if wet, determined the amount of precipitation that fell during the day. The day was determined to be wet or dry depending on the status of that day in a surrogate station. The surrogate station for precipitation occurrence was found using the Jaccard similarity index (Equation 3.5), as first developed by Jaccard (1908) and later summarized by McCormick et al. (1992). The index expresses the similarity, or dissimilarity, of nonzero datasets as:

$$J(A,B) = \frac{|A \cap B|}{|A \cup B|} = \frac{\sum_{j=1}^{T}\left[\left(\vartheta_{A,i} = \vartheta_{B,i}\right) \wedge \left(\vartheta_{A,i} \neq 0 \vee \vartheta_{B,i} \neq 0\right)\right]}{\sum_{j=1}^{T}\left(\vartheta_{A,i} \neq 0 \vee \vartheta_{B,i} \neq 0\right)} \qquad \textit{Equation 3.5}$$

where *J(A,B)* is the Jaccard similarity coefficient between stations *A* and *B*, $|A \cap B|$ is the size of the intersection between station *A* and station *B*, $|A \cup B|$ is the size of the union between the two stations, $\vartheta_{A,i}$ is a binary variable depicting the wet or dry status of day *i* at station *A* (0 for a dry day, 1 for a wet day), $\vartheta_{B,i}$ is a binary variable depicting the wet or

dry status of day *i* at station *B*, and *T* is the number of historic days that both stations *A* and *B* have data. The end result was a list of surrogate stations ordered by the Jaccard similarity index and based on correlation of precipitation occurrence. If the first surrogate station (most closely related) also had missing data, the next surrogate station (second most closely related) was looked at, and if that station had missing data, the third surrogate was examined, and so on, until the day was determined to be wet or dry. If the day was determined to be dry the resampling procedure continued, but if the day was determined to be wet, a value of precipitation had to be calculated for that day. The amount of precipitation that fell on a wet day was taken from a Gamma distribution function (Equation 3.6) fit to the specific station, month, and wet-warmth classification. The use of the Gamma distribution for determination of a given wet day's rainfall amount has been previously proposed by Buishand (1978), and was recently used in a climate change study in West Africa (Schuol and Abbaspour, 2007).

$$y = f(x|a,b) = \frac{1}{b^a \Gamma(a)} x^{a-1} e^{-\frac{x}{b}} \qquad \textit{Equation 3.6}$$

where *y* is the gamma probability density function, *x* is the amount of precipitation on a given wet day (mm), *a* is the gamma distribution shape parameter, and *b* is the gamma distribution scale parameter.

In several rare cases, precipitation was missing in all stations on a given day, and the wet or dry status of the day had to be reconciled in a different manner. In this case, transitional probabilities, calculated for each wet-warmth classification within each calendar month within each station, were used to quantify the probability of a wet day following a dry day and the probability of a wet day following a wet day. Then, a random number was calculated and compared with the appropriate transitional

probability (depending on the state of the previous day), and if the random number was less than the transitional probability, the day was deemed wet. If the random number was greater than the transitional probability, the day was determined to be dry.

*Missing Temperature*

Missing daily temperature data came in three forms (a) maximum temperature missing, minimum temperature measured, (b) minimum temperature missing, maximum temperature measured, and (c) both maximum and minimum temperature missing. Situations (a) and (b) were rectified in the same manner, while a different methodology had to be used in case (c). In both cases (a) and (b), when either minimum or maximum temperature was missing, the difference between the maximum and minimum temperature from the previous day was either added to, or subtracted from whichever temperature had a measurement on that day. However, if no measurement was made for maximum or minimum temperature on a given day a surrogate station for temperature was determined. Surrogate stations were based on the correlation between daily mean temperatures, and sorted from most closely to least correlated. Then, when a day with both maximum and minimum temperatures missing was encountered, the corresponding temperatures from the first surrogate station were used. If the first surrogate station had no data, the second surrogate station was used, and so on until a station with data was found. The temperatures from the surrogate station (either maximum or minimum) were then adjusted by the difference between the future projected monthly temperature of that station and the future monthly projected temperature of the station with missing data. As a last case scenario, if no stations had temperature data on a given day, a regression between the maximum and mean daily temperatures from each station (and calculated

separately for wet and dry days) was used to add a random residual to the future monthly projected temperature of the given station.

*Specific Modification for the San Juan Watershed*

In the San Juan River basin, a specific modification to the temporal downscaling methodology had to be made to account for the prevalence of months with zero precipitation. Located in the southwestern portion of Colorado and the northern portion of New Mexico, the climate in parts of the watershed, especially at lower elevations, is quite arid. In five of the ten meteorological stations (Pagosa Springs, CO, Stump Lakes, CO, Chamita, NM, Aztec, NM, and Bloomfield, NM) it was observed that the month of June had zero precipitation in numerous years on record. However, one of the conditions in creating a pool of eligible months to be resampled from is that the month must have nonzero precipitation, to avoid issues associated with infinite scaling. Typically in the other basins of Colorado this was not an issue, as a different year for a given month and wet-warmth classification would be chosen. This could not be done at the five specified stations in the San Juan watershed because all Junes in a given classification had zero precipitation. Therefore, if a resampled month in one of the five stations had zero precipitation, the given future month was also given zero precipitation. This was considered to be a reasonable assumption as the prevalence of months in the historical record with zero precipitation made it realistic. Additionally, other climate stations with higher elevations in the watershed were simulating precipitation over these months, so that the entire basin was not being simulated as dry.

### 3.2.2 HYDROLOGIC SIMULATION OF FUTURE PROJECTIONS

The Soil and Water Assessment Tool (SWAT) is a comprehensive, process-based hydrologic model that was utilized to drive the downscaled and bias-corrected climate scenarios. Future daily projections of precipitation and temperature were used as input to the models, and were represented at meteorological stations throughout each study watershed (Figure 3.3). Development, calibration, and testing of the model specific to each study watershed is described in thorough detail in the previous chapter, and is therefore not described herein. The model was run on a daily time-step for 90 years from 2010 – 2099 and various model outputs at a monthly resolution will be discussed in the forthcoming sections.

*STATISTICAL TREND TESTS*

Two statistical tests were utilized to discern the impacts of climate change on hydrologic response, specifically through measures of trend in annually averaged streamflow over the period 2012 - 2099. The statistical tests were calculated with MAKESENS, a spreadsheet application developed by the Finish Meteorological Institute and available at http://www.fmi.fi/organization/contacts_25.html, with methods as outlined in Salmi et al. (2002). The first method, known as the Mann-Kendall test (Mann, 1945), is a nonparametric method with the ability to detect monotonic trends in non-seasonal time series. The null hypothesis, $H_0$, of no trend in the data was tested against the alternative hypothesis, $H_1$, of an increasing or decreasing trend in the data. From the series of $n$ years ($n$ = 88) of average annual streamflows for each future scenario the Mann-Kendall test statistic ($S$) was calculated as:

$$S = \sum_{q=1}^{n-1} \sum_{p=q+1}^{n} sgn(x_p - x_q) \qquad \textit{Equation 3.7}$$

where $x_p$ and $x_q$ are annual average streamflows in years $p$ and $q$, respectively, and:

$$sgn(x_p - x_q) = \begin{cases} 1 & if\ x_p - x_q > 0 \\ 0 & if\ x_p - x_q = 0 \\ -1 & if\ x_p - x_q < 0 \end{cases} \qquad \textit{Equation 3.8}$$

In order to calculate the test Z-statistic, VAR(S) was calculated as:

$$VAR(S) = \frac{1}{18}\left[n(n-1)(2n+5) - \sum_{s=1}^{r} t_s(t_s-1)(2t_s+5)\right] \qquad \textit{Equation 3.9}$$

where r is the number of tied groups and $t_s$ is the number of values in the $s^{th}$ tied group.

Previous calculations of S and VAR(S) were then used to compute the test Z-statistic:

$$Z = \begin{cases} \dfrac{S-1}{\sqrt{VAR(S)}} & if\ S > 0 \\ 0 & if\ S = 0 \\ \dfrac{S+1}{\sqrt{VAR(S)}} & if\ S < 0 \end{cases} \qquad \textit{Equation 3.10}$$

The Z-statistic was then compared to $Z_{1-\alpha/2}$, which was obtained from a normal cumulative distribution table at the desired significance level ($\alpha$). Each scenario trend was tested at the significance levels 0.001, 0.01, 0.05, and 0.1; of which the lowest value was taken when $H_0$ was rejected.

For all future scenarios with a statistically significant trend in projected annual streamflow ($\alpha \leq 0.1$), Sen's slope estimator (Sen, 1968) was used to quantify the rate of the trend, along with a 95% confidence interval around the slope. Through the assumption of a linear trend, an estimate of Sen's slope ($Q$) was calculated by first computing the slopes between all pairs as of points in the series:

$$Q_i = \frac{x_p - x_q}{p - q} \qquad \textit{Equation 3.11}$$

wherein $p > q$. The number ($N$) of slope estimates ($Q_i$) from a time series of $n$ years is equal to $n(n\text{-}1)/2$. The Sen's method takes the median of all slopes $Q_i$ as the final estimate of the trend. The 100(1-$\alpha$)% two-sided confidence interval was determined for each Sen's slope estimate first, by calculating:

$$C_\propto = Z_{1-\propto/2}\sqrt{VAR(S)} \qquad \textit{Equation 3.12}$$

where *VAR(S)* is calculated in *Equation 3.9* and $Z_{1-\alpha/2}$ is taken from the standard normal distribution. The confidence interval boundaries, $Q_{min}$ and $Q_{max}$, are taken from an ordered list of the $N$ slope estimates $Q_i$ as the $M_1^{th}$ largest and the $(M_2 + 1)^{th}$ values.

$$M_1 = \frac{N - C_\propto}{2} \qquad \textit{Equation 3.13}$$

$$M_2 = \frac{N + C_\propto}{2} \qquad \textit{Equation 3.14}$$

where $M_1$ and $M_2$ resulting in decimal numbers required interpolation of the respective limit.

### 3.3 RESULTS & DISCUSSIONS

Model simulations driven by downscaled future climate projections were analyzed for their respective changes in basin average temperature and precipitation, in addition to changes in hydrologic response, over the course of the 21st century. The direction, magnitude, and variability of impacts were analyzed by combining SRES emissions scenarios and computing ensemble means, medians, and quartiles. The 21st century was split into three periods including near-future (2012 – 2039), mid-century (2040 – 2069), and late-century (2070 – 2099) of which averages were taken for analysis of results.

Additionally, statistical trend tests were performed on annual streamflow for each of the 112 scenarios in order to correlate specific scenarios with bounds of hydrologic response.

### 3.3.1 DOWNSCALED TEMPERATURE & PRECIPITATION

Figure 3.4 displays the annual basin averaged temperature and precipitation throughout the 21st century in each of the study basins. The grey lines represent annual projections from each of the 112 climate scenarios and the colored lines represent the ensemble averaged annual values for each of the three SRES emissions paths.

The individual projected changes in temperature over the 21st century are variable in nature, but appear to follow a general pattern when grouped by SRES emissions scenario in each of the basins. The ensemble averaged temperature from each of the three scenarios appears to increase at approximately the same rate until about 2039, when the paths begin to diverge. From 2040–2069, the increase in temperature in B1 is substantially lower than that of A1B and A2, which appear to continue increasing at nearly the same rate. After 2070, A1B and A2 begin to diverge with A2 showing greater increasing temperatures by the end of the century. Conversely, projected changes in precipitation over the 21st century do not appear to differ drastically when grouped by SRES emissions scenarios, but do display a large amount of variability between individual projections.

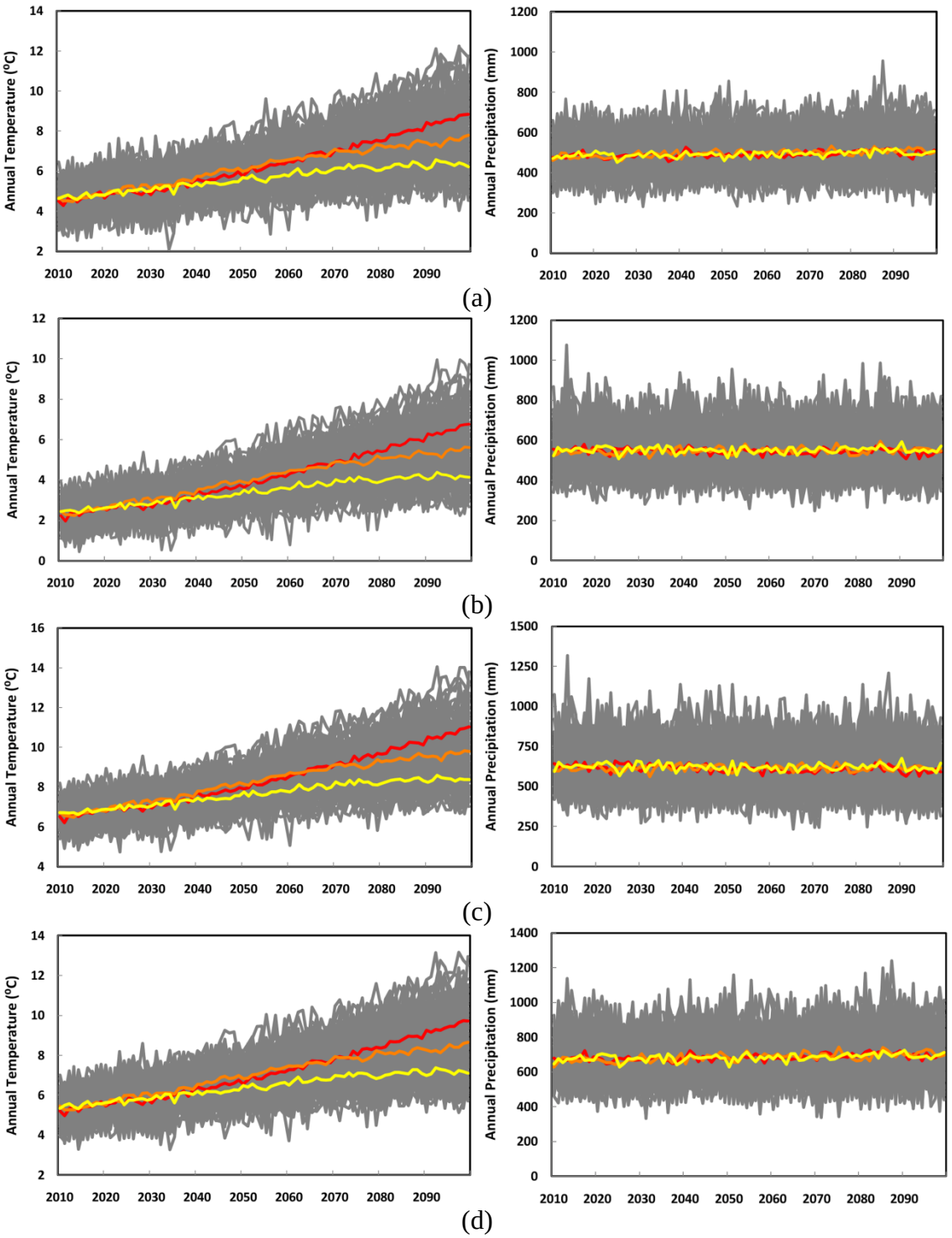


**Figure 3.4 -** Basin averaged annual temperature and precipitation in the (a) Cache la Poudre, (b) Gunnison, (c) San Juan, and (d) Yampa River basins. The grey lines represent annual values from each of the 112 projections and the colored lines represent the ensemble averaged annual values from SRES emissions scenarios A2 (red), A1B (orange), and B1 (yellow).

### 3.3.2 IMPLICATIONS TO HYDROLOGIC RESPONSE

*PROJECTION VARIABILITY*

As depicted in Figure 3.4, there is considerable variability associated with projections of precipitation and temperature in each of the study basins. This variability of climatic drivers appears to be translated into a range of hydrologic responses via model simulations. Figures 3.5 shows the variability in projected temperature, precipitation, ET, and the resulting water yield in each of the study basins. The box and whisker plots represent the minimum, maximum, upper and lower quartile, and median of period averaged annual values within each SRES emissions scenario.

Two patterns from Figure 3.5 were immediately apparent. The first is the general increasing range in projections, regardless of the variable, that appears over time. This makes intuitive sense, as the variability in simulations should increase over time as the results from individual scenarios diverge due to different GCM configurations, specific initial conditions used in GCM runs, and different emissions scenarios. Additionally, the uncertainty involved in long-term projections of climatic variables, especially precipitation, would be expected to increase as the forecast period progresses into the future. The second pattern noticed was the similarity in both range and direction of change between precipitation and water yield. This relationship between precipitation and water yield is not surprising, as precipitation is more highly correlated with total yield than other hydroclimatic variables such as temperature and ET (Stonefelt et al., 2000).

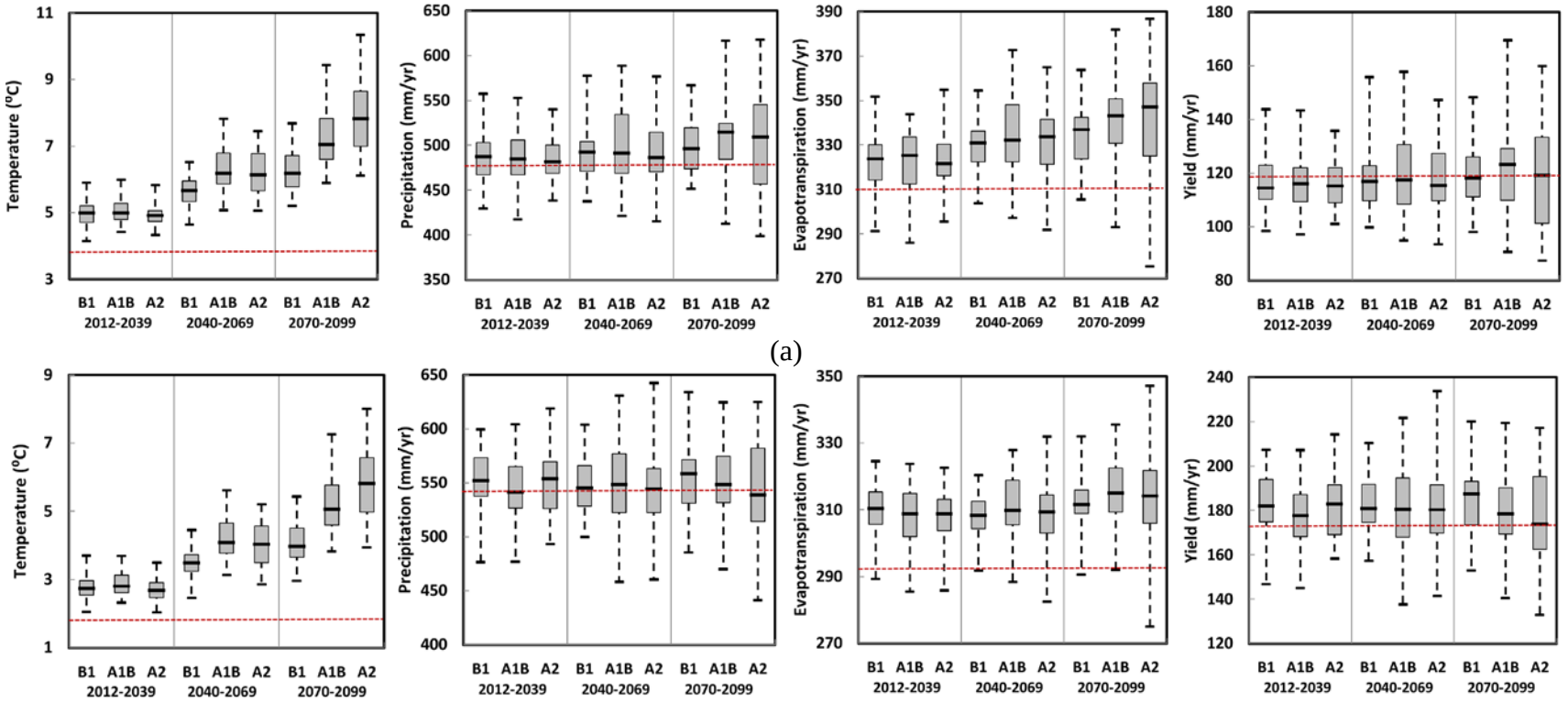


**Figure 3.5 -** Variability in temperature, precipitation, evapotranspiration, and water yield projections in the (a) Cache la Poudre and (b) Gunnison River basins from 112 scenarios consisting of 16 GCMs. The traditional box and whisker plots represent the minimum and maximum, upper and lower quartiles, and median of the data; annual averages of the SRES B1, A1B, and A2 emissions scenarios over the three future periods 2012-2039 (28 years), 2040-2069 (30 years), and 2070-2099 (30 years). The dashed red line represents the average annual value over the 1990 – 2005 historic period (1990 – 2004 in Yampa).

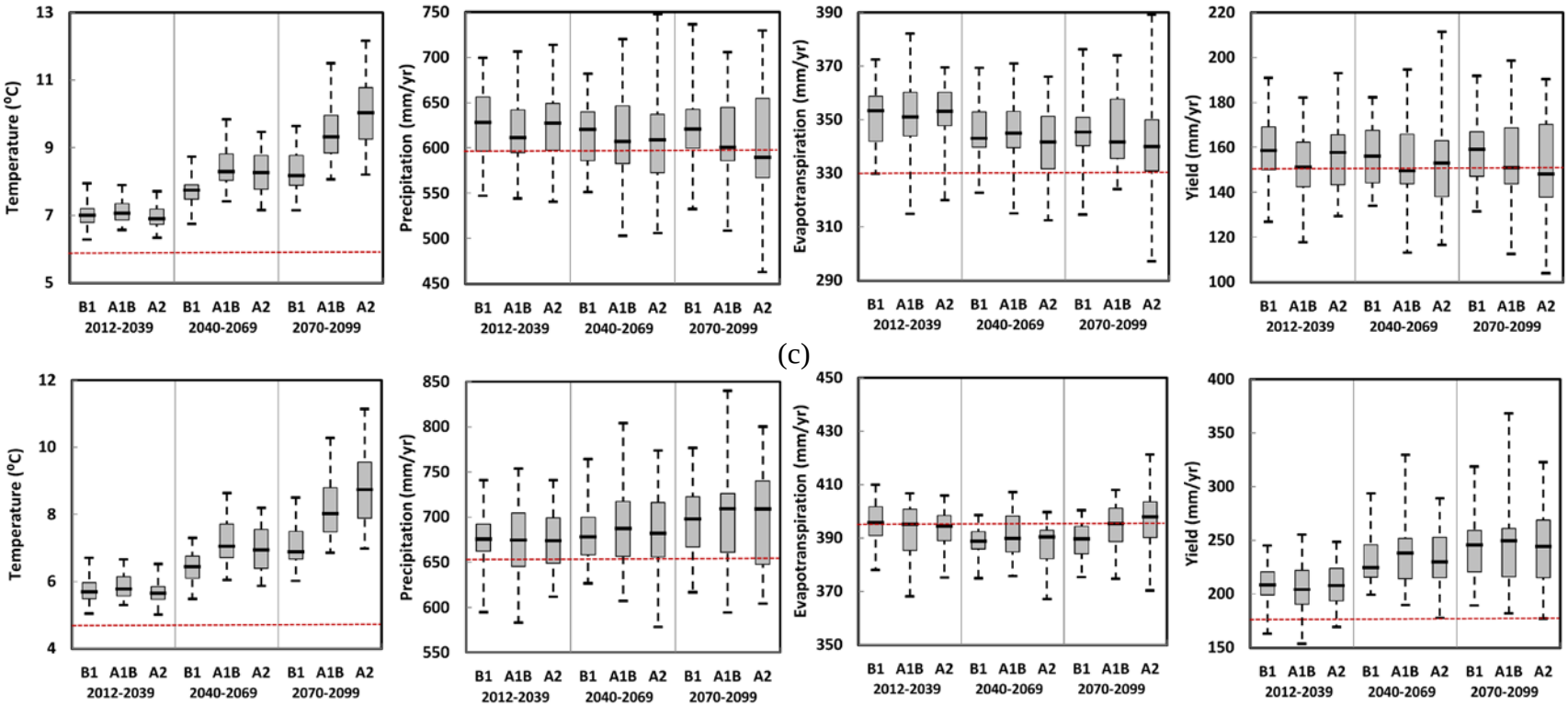


**Figure 3.5 (contd)** - Variability in temperature, precipitation, evapotranspiration, and water yield projections in the (c) San Juan and (d) Yampa River basins from 112 scenarios consisting of 16 GCMs. The traditional box and whisker plots represent the minimum and maximum, upper and lower quartiles, and median of the data; annual averages of the SRES B1, A1B, and A2 emissions scenarios over the three future periods 2012-2039 (28 years), 2040-2069 (30 years), and 2070-2099 (30 years). The dashed red line represents the average annual value over the 1990 – 2005 historic period (1990 – 2004 in Yampa).

Figure 3.6 shows the variability in future projections of the precipitation to potential evapotranspiration (PET) ratio (P:PET). This ratio is often used as a measure of aridity of a landscape, and was shown to decrease throughout the 21st century in all four study basins. As expected, decreasing trends in the aridity index corresponded well with increasing trends in temperature, as the A2 ensemble average had the highest projected increase in temperature and therefore the highest projected decrease in aridity index over the 21st century. Although all four study basins are expected to become more arid over the 21st century, the shift is more pronounced in the watersheds on the west side of the Continental Divide when compared to the Cache la Poudre watershed, which was the most arid study watershed over the historic simulation period (1990 – 2005).

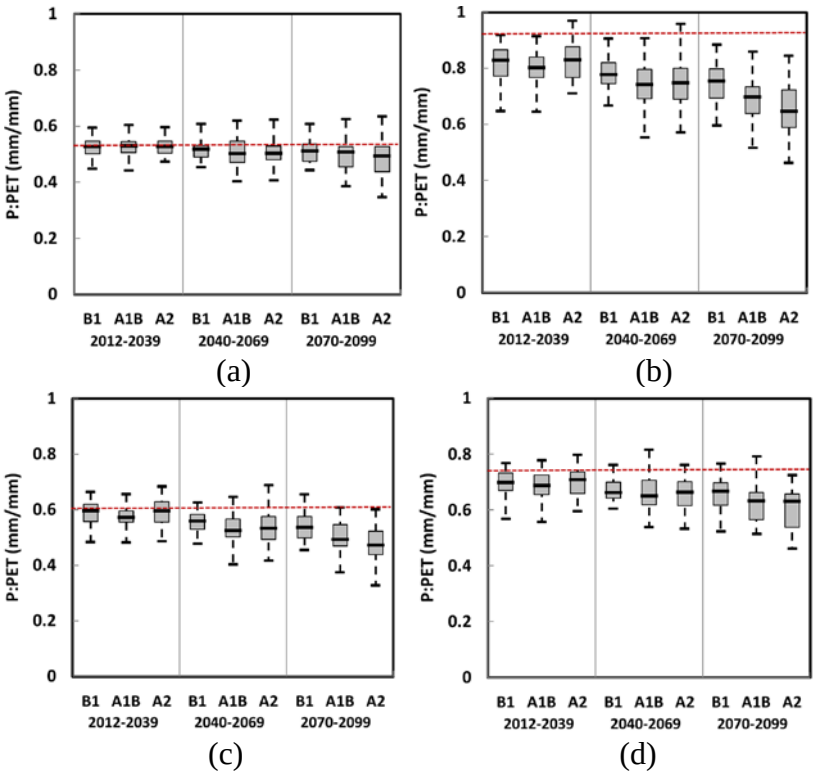


**Figure 3.6** - Variability of the aridity index in the (a) Cache la Poudre, (b) Gunnison, (c) San Juan, and (d) Yampa River basins from 112 scenarios consisting of 16 GCMs. The box and whisker plots represent annual averages of the SRES B1, A1B, and A2 emissions scenarios over the three future periods 2012-2039 (28 years), 2040-2069 (30 years), and 2070-2099 (30 years). The dashed red line represents the average annual value over the 1990 – 2005 historic period (1990 – 2004 in Yampa).

The variability amongst future projections stems from two sources of uncertainty; the uncertainty associated with projections of future temperature and precipitation and the uncertainty associated with hydrologic modeling using SWAT. Additionally, it is clear that the impacts of climate change on hydrologic fluxes will vary amongst study watersheds across the state. The localized effects will have different implications to the management of water resources within each of the study basins, and are presented in the following section.

*BASIN-SPECIFIC IMPACTS*

The monthly distributions of basin-averaged annual temperature, precipitation, snow to precipitation ratio (S:P), ET, and streamflow for SRES emissions ensemble averages over three future periods and the historic baseline period are presented in Figures 3.7 – 3.11. Changes over the 21$^{st}$ century were quantified as an increment (for temperature) or percentage change (for all other variables) between ensemble averages from the near-future (2012-2039) and the late-century (2070-2099).

In the Cache la Poudre River basin, the ensemble averaged annual temperature increases by 3°C, 2.2°C, and 1.3°C from the near-future period to the late-century period in scenarios A2, A1B, and B1, respectively. The most pronounced changes in temperature appear to occur during the summer months (June – September) and winter months (January – Precipitation), while less dramatic changes were simulated during the remaining fall and spring months. This general pattern of greater increases in temperature during the summer and winter months than during spring and fall months applies to all study watersheds. Annual precipitation is also projected to increase over the same periods by 4%, 4.7%, and 2.9% in scenarios A2, A1B, and B1, respectively.

Most of the increase in precipitation is attributed to increases occurring over the winter, from November – March. As would be anticipated with an increase in both temperature and precipitation, annual ET is projected to increase by 5.5%, 5.7%, and 3.8% in scenarios A2, A1B, and B1, respectively. Ensemble-averaged annual streamflow increases in the Cache la Poudre River basin by 2.8%, 5.6%, and 3.7% in scenarios A2, A1B, and B1, respectively. An increase in streamflow over the 21$^{st}$ century came with an earlier and larger peak, which is most likely resultant of increased winter precipitation and warmer temperatures. Thus, the recession of the annual hydrograph also appeared earlier in the year and resulted in decreased streamflows over the summer months. Generally, streamflow appeared to increase from October – May and decrease from June – September in the Cache la Poudre River basin.

Ensemble-averaged temperature in the Gunnison River basin shows an increase over the 21$^{st}$ century of 3°C, 2.3°C, and 1.3°C in SRES A2, A1B, and B1, respectively. Changes in precipitation are not consistent in direction, and include changes of -1.5%, +1.3%, and +0.4% in paths A2, A1B, and B1, respectively. Unlike the Cache la Poudre River basin, S:P did not appear to be affected in all months snow fell. While the ratio did decrease during the spring and fall months, all precipitation continued to fall as snow in the deep winter months of December, January, and February. This is not surprising, as the Gunnison watershed is higher in elevation than the Cache la Poudre, thus deep-winter temperatures remain well below freezing. Surprisingly, even with a decrease in precipitation in the A2 ensemble average, ET is projected to increase across all three ensembles, which includes increases of 1.6%, 2.4%, and 0.7%. Similar to projections of precipitation, results from the SRES ensembles did not agree on a direction in change of

annual average streamflow from the late-century period to the near-future period, and include changes of -2.4%, +1.4%, and +1% in SRES A2, A1B, and B1, respectively. The relationship between the direction of change in precipitation and that of water yield is identified in the Gunnison River basin, as the only emissions scenario ensemble that results in a decrease in streamflow (A2) was the only ensemble that projects a decrease in precipitation. Similarly to the Cache la Poudre watershed, the snowmelt hydrograph of the Gunnison River basin is shifted to earlier in the year with a slight increase in peak.

Annual basin-wide temperature in the San Juan River basin is projected to increase by 3°C, 2.2°C, and 1.4°C in ensembles A2, A1B, and B1, respectively. Precipitation in the watershed is anticipated to decrease across all emissions ensemble averages, and includes declines of 3.5%, 0.2%, and 0.8%. Unlike the other three study basins, which predict a noticeable increase in precipitation over the winter months, the San Juan watershed predicts a very small increase in precipitation over the winter, if any, over the course of the 21$^{st}$ century. With decreases in ensemble-averaged annual precipitation occurring in all three emissions scenarios, it was not surprising to find decreases of 3.2%, 1.7%, and 1.8% in annual ET in scenarios A2, A1B, and B1, respectively. Interestingly, the majority of such annual decreases in ET appear to occur in the months of June and July, which have no intuitive explanation as no appreciable changes in precipitation occur during those months. The direction of change in streamflow across the three emissions scenarios was inconsistent, and included alterations of -3.9%, +1.5%, and 0% between near-future and late-century periods. Although an increase of 1.5% in streamflow was simulated from the near-future to the late-century in the average of A1B scenarios, the calculation is slightly misleading as the

increase in streamflow actually occurred between the near-future and mid-century periods (2%) and was followed by a decrease in streamflow between the mid-century and late-century periods (-0.5%). Similarly, the net change of 0 % between near-future and late-century periods in scenario B1 was actually a decrease of 1.4% (from near-future to mid-century) followed by an increase of 1.4% (from mid-century to late-century).

Similar to the other three study watersheds, the ensemble-averaged projections of temperature in the Yampa River basin include increases of 3°C, 2.4°C, and 1.4°C in ensembles A2, A1B, and B1, respectively. Future changes of precipitation in the watershed include increases of 3.7%, 4.7%, and 2.9%. The S:P ratio declined in all months that snow fell, with the greatest changes pronounced in the spring and fall months. Similarly to the Gunnison River basin, S:P is projected to only decrease slightly during the deep winter months of December, January, and February as the temperatures during these months were projected to be well below freezing through the end of the 21$^{st}$ century. As anticipated from increases in both temperature and precipitation in all ensemble averages, an increase in ET of 0.8% and 0.3% were calculated for scenarios A2 and A1B, respectively. However, a change in ET of -1.5% was calculated for ensemble B1, which was surprising with increases in both precipitation and temperature calculated for that scenario. Regardless of the change in ET between future periods, annual streamflow increases of 13.6%, 19.6%, and 16% were found for ensemble-averaged emissions scenarios A2, A1B, and B1, respectively. The projected increases in ensemble-averaged streamflow were appreciably higher in the Yampa watershed than either of the other three study basins, which correspond to the projected increases in precipitation over the basin.

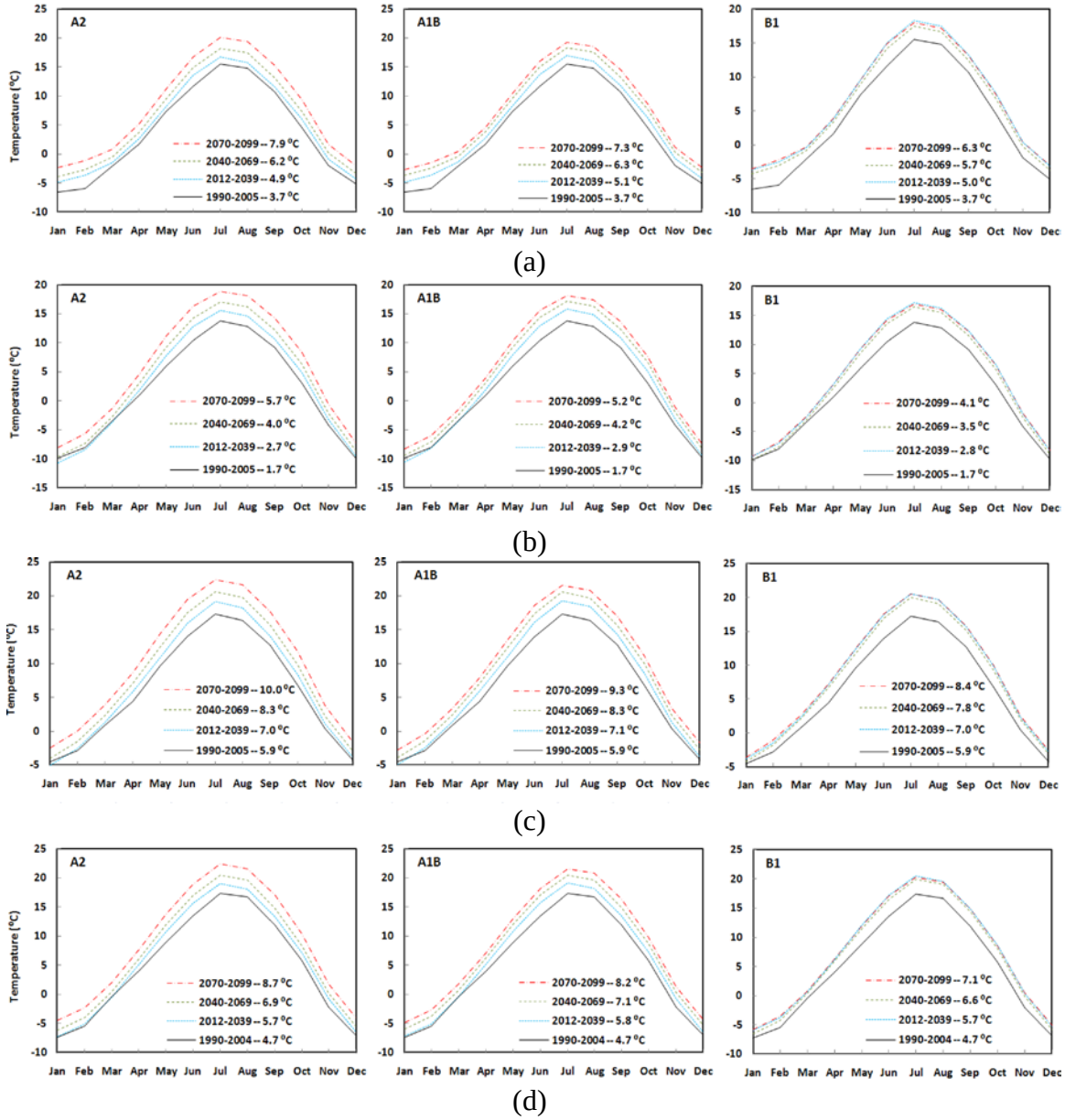


**Figure 3.7 -** Projections of average monthly temperature in the (a) Cache la Poudre, (b) Gunnison, (c) San Juan, and (d) Yampa River basins over three future periods. The graph shows the ensemble-averaged monthly temperature for each emissions scenario (dashed colored lines) and historic period (solid black line), in addition to reporting the average annual temperature over each respective period.

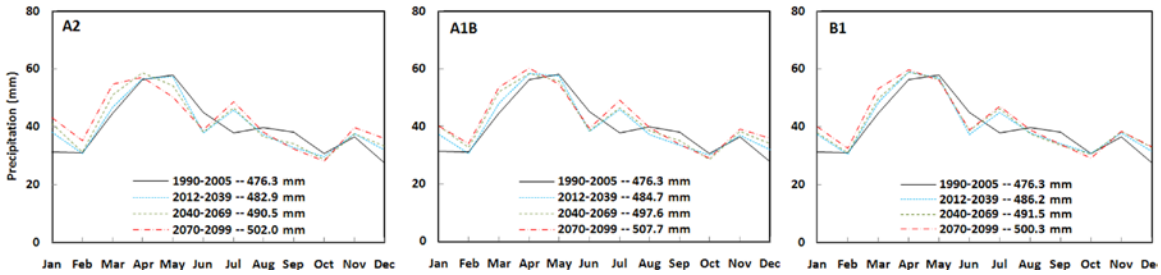


(a)

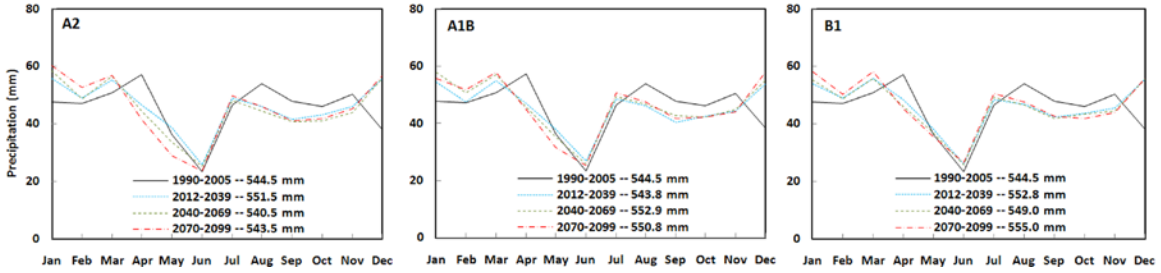


(b)

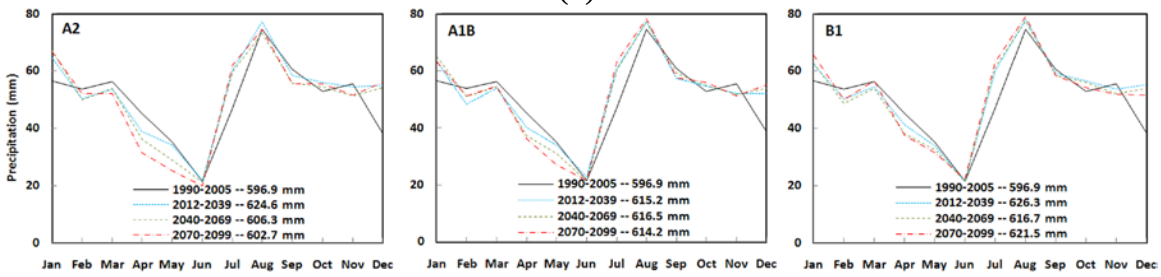


(c)

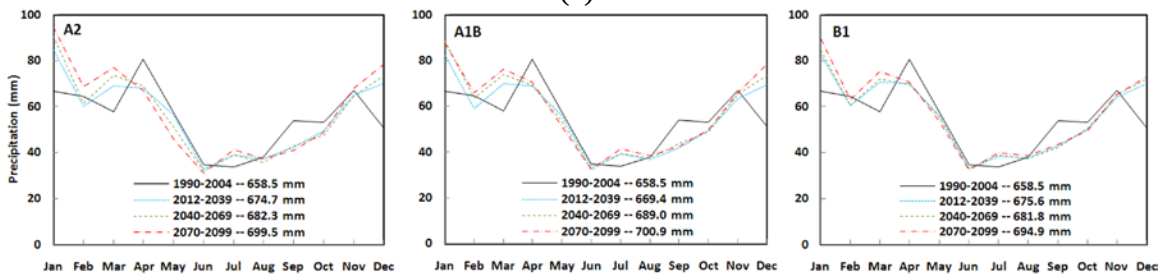


(d)

**Figure 3.8 -** Projections of average monthly precipitation in the (a) Cache la Poudre, (b) Gunnison, (c) San Juan, and (d) Yampa River basins over three future periods. The graph shows the ensemble-averaged monthly precipitation for each emissions scenario (dashed colored lines) and historic period (solid black line), in addition to reporting the average annual precipitation over each respective period.

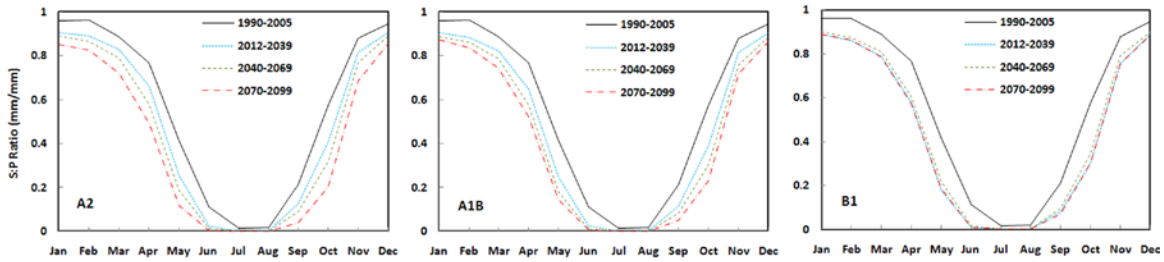


(a)

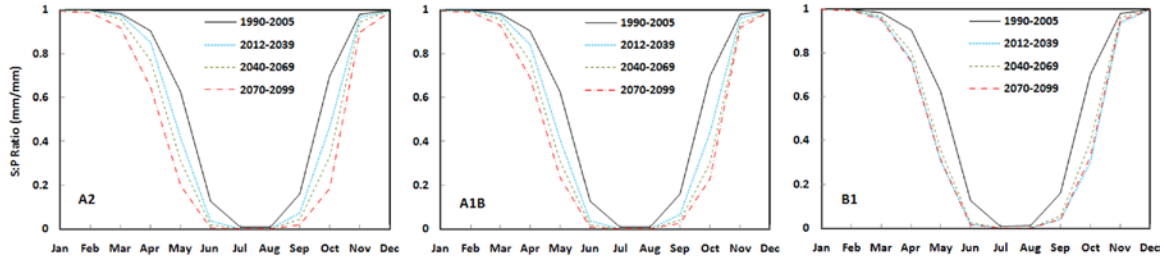


(b)

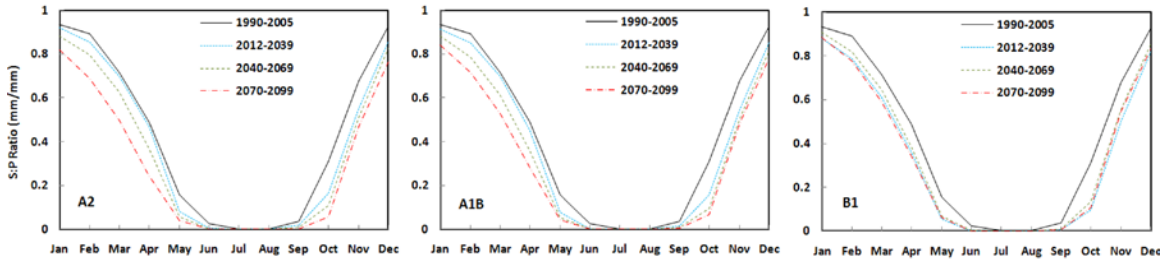


(c)

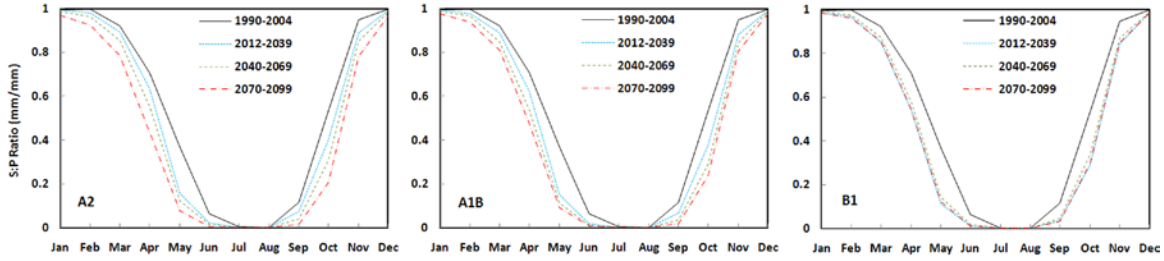


(d)

**Figure 3.9** - Projections of average monthly snowfall to precipitation ratio (S:P) in the (a) Cache la Poudre, (b) Gunnison, (c) San Juan, and (d) Yampa River basins over three future periods. The graph shows the ensemble-averaged monthly S:P for each emissions scenario (dashed colored lines) and historic period (solid black line).

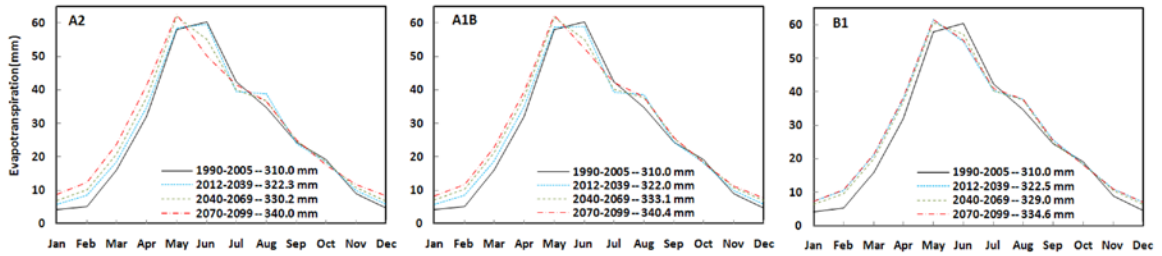


(a)

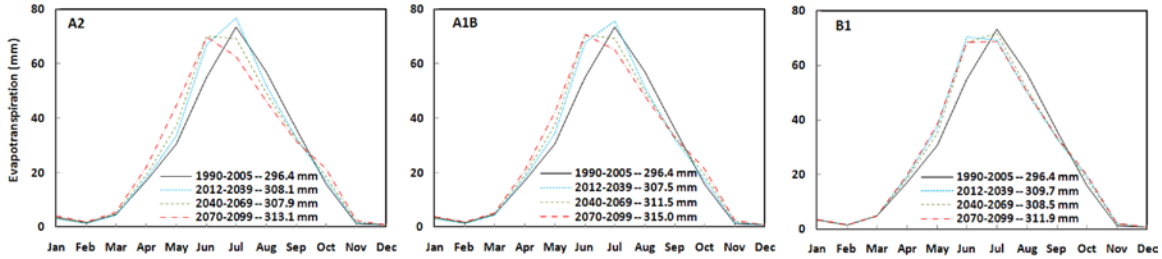


(b)

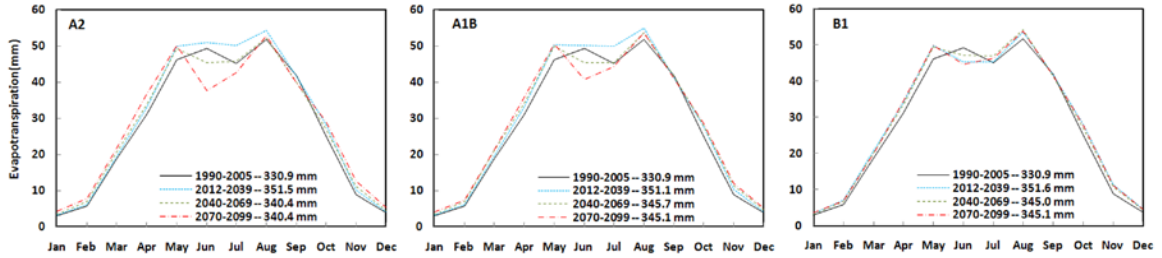


(c)

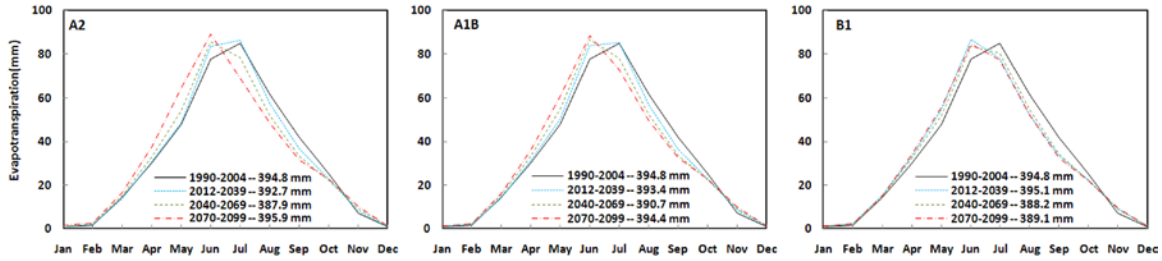


(d)

**Figure 3.10** - Projections of average monthly ET in the (a) Cache la Poudre, (b) Gunnison, (c) San Juan, and (d) Yampa River basins over three future periods. The graph shows the ensemble-averaged monthly ET for each emissions scenario (dashed colored lines) and historic period (solid black line), in addition to reporting the average annual ET over each respective period.

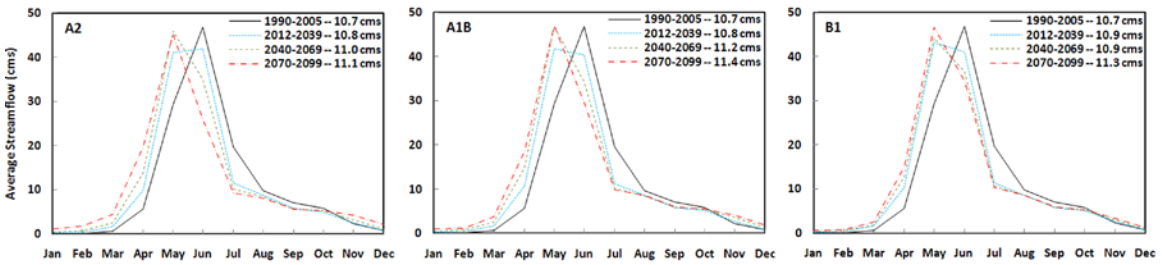


(a)

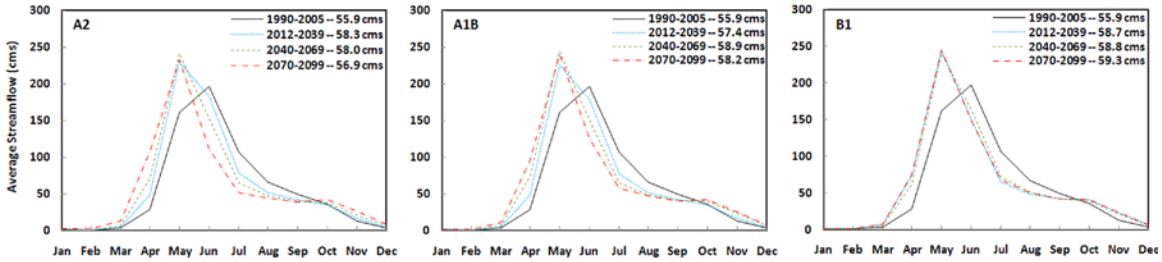


(b)

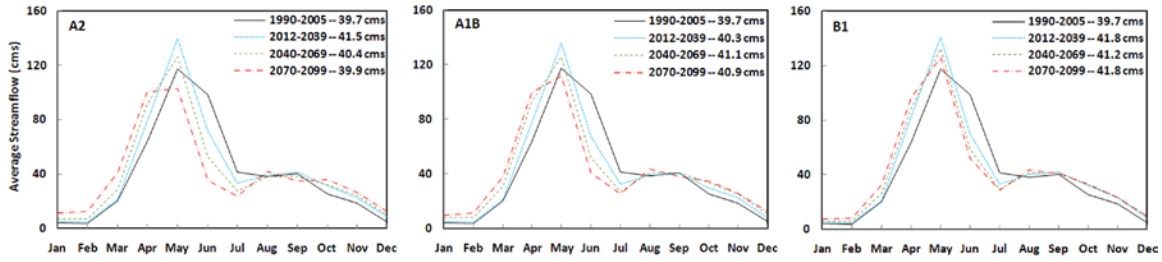


(c)

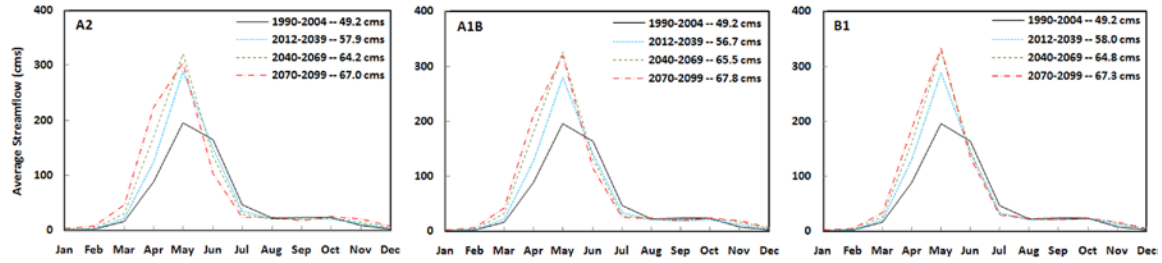


(d)

**Figure 3.11 -** Projections of the average annual hydrograph in the (a) Cache la Poudre, (b) Gunnison, (c) San Juan, and (d) Yampa River basins over three future periods. The graph shows the ensemble-averaged monthly streamflow for each emissions scenario (dashed colored lines) and historic period (solid black line), in addition to reporting the average annual streamflow over each respective period.

*SENSITIVITY OF STREAMFLOW TO PRECIPITATION VARIABILITY*

The sensitivity of streamflow to future projections of precipitation varied amongst the four study basins. Figure 3.12 shows a plot of annual precipitation versus annual yield (streamflow) from the annual emissions scenario ensemble averages over 88 years (2012 – 2099) and historic baseline (1990 – 2005). A linear trend line was fit to each study basin, and the resulting equation and coefficient of determination ($R^2$) are presented in the figure. The trend lines for the Yampa and Gunnison River basins exhibit the steepest slopes, which correspond to a greater sensitivity of streamflow to precipitation. Physically, this makes sense as these watersheds were shown to be less arid than the Cache la Poudre and Gunnison watersheds (Figure 3.6), and thus have less capacity to store and evaporate/transpire an increase in precipitation. Therefore, increasing precipitation results in a greater increase in streamflow than would be observed in a more arid watershed. Alternately, the Cache la Poudre River basin exhibits the mildest slope, which corresponds to less sensitivity of streamflow to precipitation. Again, this makes sense as more arid watersheds have a greater capacity to store and evaporate/transpire an increase in precipitation, and streamflow will not increase as much as it would in a less arid watershed.

Another notable observation in Figure 3.12 is the variability in annual precipitation and streamflow of the observed period versus that of the emissions scenario ensemble averages over the future. Caution should be used when analyzing emissions scenario ensemble averages, as they do not represent the variability associated with a single climate projection. Thus, emissions scenario ensemble averages make the data appear less variable than they actually are.

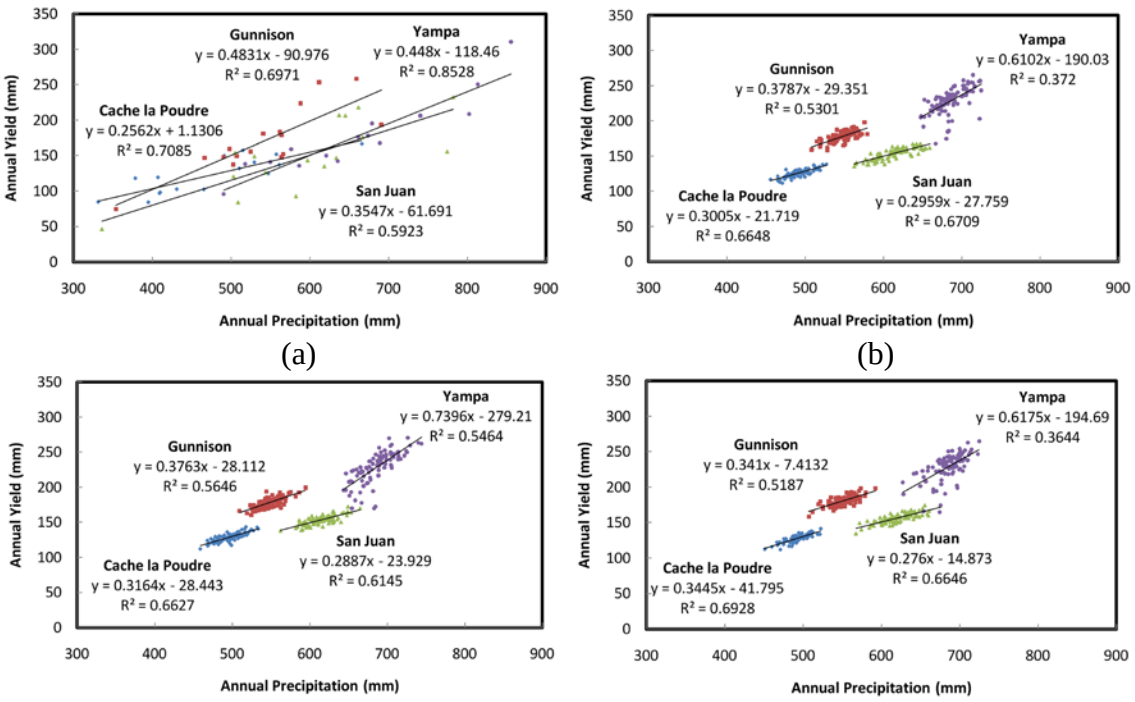


**Figure 3.12 –** Sensitivity of streamflow to precipitation, as depicted by plots of annual precipitation versus annual yield (streamflow) for the (a) baseline period 1990 – 2005 (1990 – 2004 in Yampa), (b) SRES A2 annual ensemble averages from 2012 – 2099, (c) SRES A1B annual ensemble averages from 2012 – 2099, and (d) SRES B1 annual ensemble averages from 2012 – 2099. The Cache la Poudre basin is depicted by blue diamonds, Gunnison basin by red squares, San Juan basin by green triangles, and Yampa basin by purple dots.

*TRENDS IN STREAMFLOW*

Up to this point, the results from model simulations have been analyzed using ensemble statistics from each of the three SRES emissions scenarios. Although this is a common method to represent climate projections and their resultant hydrologic impacts (e.g. Christensen and Lettenmaier, 2007; Milly et al., 2005; Ray et al., 2008), one of the objectives of this study was to identify specific GCMs and emissions scenarios that resulted in the extremes, or in this case the bounds of trends in average annual streamflow over the study period (2012-2099). Figure 3.13 displays the number of statistically significant ($\alpha<0.1$) increasing (dark grey) and decreasing (light grey) trends in average

annual streamflow at the outlet of each basin over 88 years in the 21st century. All 112 simulations driven by separate climate scenarios in each basin were tested for trends using the non-parametric Mann-Kendall test.

As expected, the four basins yielded different results regarding the direction and magnitude of streamflow trends over the 21st century. The Cache la Poudre basin yielded 40 statistically significant trends of streamflow, of which 26 were increasing and 14 were decreasing. However, at the highest significance level tested ($\alpha = 0.001$) there were 6 trends, of which 3 were increasing and 3 were decreasing. The Gunnison watershed was determined to have a total of 26 significant trends in annual streamflow, of which 11 were positive and 15 were negative. The San Juan River basin had 32 significant trends, which half (16) were increasing and the other half (16) were decreasing. The Yampa River basin had 72 significant trends, of which all were increasing with the exception of 1 that was decreasing (at the lowest acceptable significance level of 10%).

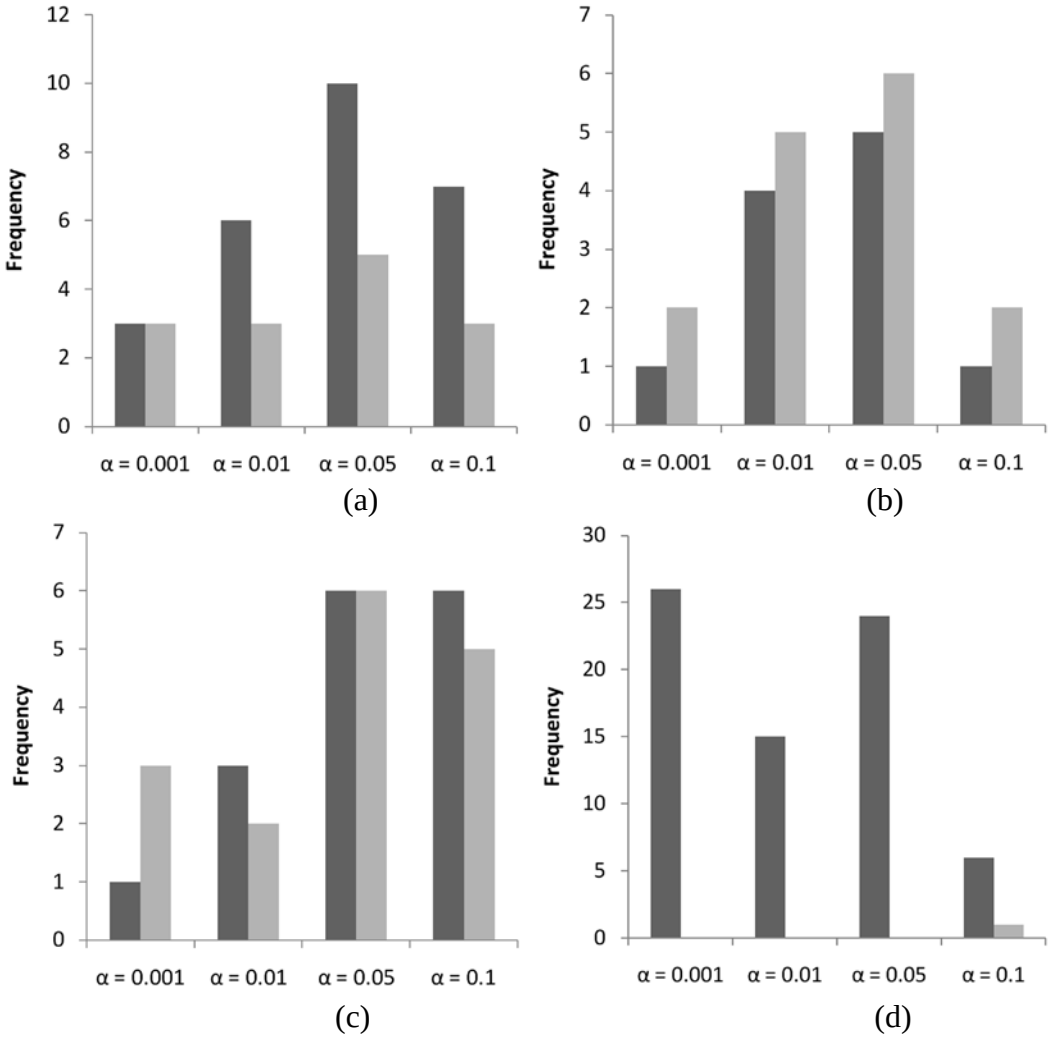


**Figure 3.13 -** Histogram of significant trends in future average annual streamflows (dark grey bars indicate the number of increasing trends and light grey bars indicate the number of decreasing trends) during the period 2012 – 2099 in the (a) Cache la Poudre, (b) Gunnison, (c) San Juan, and (d) Yampa River basins. Each of the 112 projections in each watershed was tested separately for a monotonic trend in average annual streamflow. Significant trends were determined using the nonparametric Mann-Kendall test, and are grouped by the significance level in which they rejected the null hypothesis of no trend.

Estimates of the change in average annual streamflow (cms/year) through 2099 were taken from Sen's slope estimate and as expected, varied in both magnitude and direction amongst the study basins. In the Cache la Poudre watershed, increasing trends are between 0.02 and 0.06 cms/year, while decreasing trends are between -0.02 and -0.05 cms/year. The range in positive trends correspond to an increase in average annual streamflow between 1.8 cms and 5.3 cms from 2012 – 2099 (88 years), and the negative trends correspond to a decrease between 1.8 cms and 4.4 cms over the same period. Positive trends in both the Gunnison and San Juan basins vary between approximately 0.1 and 0.25 cms/year and negative trends vary between approximately -0.1 and -0.2 cms/year. These ranges correspond to an increase in average annual streamflow between 8.8 cms and 22 cms, and a decrease in average annual streamflow between 8.8 cms and 17.6 cms over the 88 year future period. Furthermore, positive trends in the Yampa watershed vary between 0.2 and 0.55 cms/year, which correspond to an increase in average annual streamflow between 17.6 cms and 48.4 cms. As may be seen from the figure, there appears to be no correlation between the projections with significant positive or negative trends, and the emissions scenarios they represent. Additionally, there also appears to be no pattern between the significance level at which a trend was determined and the direction of that trend.

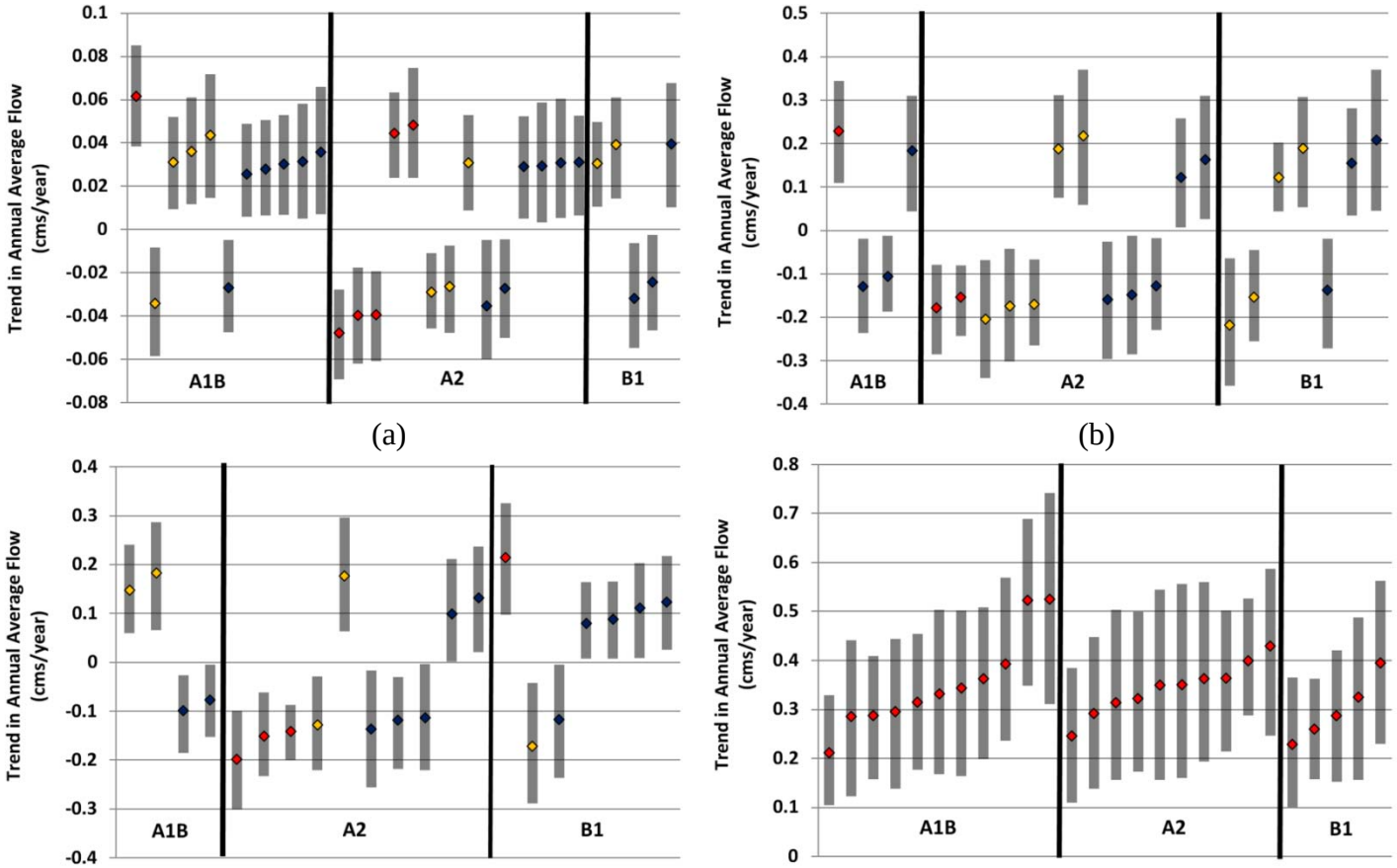


**Figure 3.14** - Change in average annual streamflow (cms/year) for individual scenarios with statistically significant trends during 2012 – 2099 in the (a) Cache la Poudre, (b) Gunnison, (c) San Juan, and (d) Yampa River basins. The projections were grouped by their respective emissions path scenarios. All trends determined to be significant were quantified using Sen's slope, of which the most significant are displayed here. The diamond represents the trend slope, which is enclosed by a grey shaded box to show the associated 95% confidence interval. The color of the diamond indicates the significance level associated with the Mann-Kendall test and include red ($\alpha = 0.001$), yellow ($\alpha = 0.01$), and dark blue ($\alpha = 0.05$).

Twelve individual projections were found to have the same direction of significant ($\alpha<0.05$) trend across all study basins (Table 3.2). Six of the projections corresponded to significant positive trends in average annual streamflow across all basins, while the other six were related to significant negative trends in average annual streamflow across all basins (except for Yampa, which had only one significant negative trend with $\alpha = 0.10$). The table depicts the GCM, SRES emissions scenario, run number (when applicable), and Sen's slope in each basin for each of the 12 projections.

**Table 3.2** – Individual projections with similar trends in streamflow for all study basins.

| GCM | SRES | Run # | Sen's slope (cms/year) | | | |
|---|---|---|---|---|---|---|
| | | | Poudre | Gunnison | San Juan | Yampa |
| CNRM-CM3 | A2 | NA | -0.04 | -0.20 | -0.14 | -0.14 |
| CNRM-CM3 | B1 | NA | -0.03 | -0.22 | -0.17 | -0.14 |
| IPSL-CM4 | A2 | NA | -0.04 | -0.15 | -0.20 | 0.04 |
| MIROC3.2 | A2 | 1 | -0.04 | -0.17 | -0.12 | -0.03 |
| MIROC3.2 | A2 | 2 | -0.05 | -0.18 | -0.15 | -0.06 |
| MIROC3.2 | A2 | 3 | -0.03 | -0.15 | -0.14 | -0.04 |
| ECHAM5/MPI-OM | A2 | 1 | 0.03 | 0.12 | 0.10 | 0.36 |
| MRI-CGCM2.3.2 | B1 | 4 | 0.03 | 0.16 | 0.11 | 0.29 |
| PCM | A2 | 2 | 0.04 | 0.19 | 0.13 | 0.40 |
| PCM | B1 | 3 | 0.04 | 0.19 | 0.12 | 0.40 |
| PCM | A1B | 4 | 0.06 | 0.23 | 0.15 | 0.52 |
| UKMO-HadCM3 | A1B | NA | 0.03 | 0.18 | 0.18 | 0.36 |

### 3.3.3 ASSUMPTIONS & LIMITATIONS

Inherent in any field of research, especially that concerning projection of future climate and hydrologic modeling at the watershed-scale, is the need to both make assumptions and recognize limitations of the study. One of several assumptions regarding the downscaling methodology taken herein was from the resampling technique used to temporally downscale future projections. By resampling historical daily patterns and

implementing them in future scenarios (after scaling/incrementing), an assumption in stationarity, of a sort, was made. The stationarity assumed was that the relative magnitude of temperature and precipitation fluctuations on a day to day basis remains constant in the future. Although the occurrence of extreme events is expected to be impacted by climate change, this assumption was determined to be relatively insignificant as analysis of the results was performed on a monthly scale.

One assumption immediately recognized during hydrologic simulation of future climate projections was that of a time-invariant land use throughout the future. The SWAT model for each study watershed was developed based on the 2001 National Land Cover Dataset (NLCD). It is apparent that the land use distribution throughout the study basins will change over time, but such change may be relatively minor in high elevation mountain watersheds. However, the current outbreak of Mountain Pine Beetle in a substantial portion of all the watersheds could potentially impact water yield in the future (e.g. Potts, 1984), which was beyond the scope of this study to quantify. Additionally, time-invariant parameters were assumed in the SWAT model. Although it is recognized that some of the SWAT parameters are climate dependent, it was beyond the scope of this study to modify them based on future climate scenarios. One final assumption in using the SWAT model was that of stationary lapse rates, which were utilized to model orographic effects on temperature and precipitation. The lapse rates of the future were assumed to be similar to those computed over the historical period, and therefore were not modified for future simulations over the 21$^{st}$ century. Furthermore, it is recognized that orographic effects are not necessarily constant throughout the year or over all elevations in a watershed. For instance, one study in southwest Idaho found the strongest

orographic effects on precipitation to occur during advective storms of winter, than compared to summer precipitation driven by convection (Hanson, 1982).

## 3.4 CONCLUSIONS

In order to project the impacts of climate change on hydrologic response over a spatial scale relevant to Colorado watersheds, 112 individual climate projections from 16 GCMs and 3 emissions scenarios were downscaled, in both space and time, and corrected for bias. The resulting projections of daily precipitation and temperature at point locations were used to drive a comprehensive, process-based watershed model (SWAT), which was calibrated and tested for monthly simulation of streamflow in four mountainous headwater river basins located throughout the state. The model was run for 90 years through the end of the 21$^{st}$ century, and results were analyzed from both emissions scenarios ensemble averages and individual scenarios. The results display a substantial amount of variability amongst future projections of temperature and precipitation, which resulted in variability in simulated hydrologic response. However, several generalities found across all four basins in Colorado through the end of the 21$^{st}$ century include a greater increase in temperature over winter and summer months relative to spring and fall months, an increase in winter precipitation and a decrease in late spring precipitation, a decrease in the ratio of snow fall to total precipitation, especially in the fall and spring months, a shift in the annual snowmelt hydrograph to earlier times in the year, and a progression towards more arid environments. Additionally, trends in average annual streamflow through the end of the century did not agree upon a direction, either increasing or decreasing, in the Poudre, Gunnison, and San Juan River basins. The

Yampa River basin, on the other hand, had better agreement on trends of average annual streamflow, which appeared to increase from 2012-2099. Finally, 12 individual climate scenarios were identified as the worst-case or best-case scenarios for water yield across all study basins through the 21st century, which may direct future work in bounding of water availability.

## 3.5 REFERENCES


Bernstein, L., Bosch, P., Canziani, O.F., Chen, Z., Christ, R., Davidson, O., Hare, W., Huq, Q., Karoly, D., Kattsov, V., Coauthors, 2007. 3.1 Emissions scenarios. In: Allali, A., Bojariu, R., Diaz, S., Elgizouli, I., Griggs, D., Hawkins, D., Hohmeyer, O., Jallow, B.P., Kajfez-Bogataj, L., Leary, N., Lee, H., Wratt, D. (Eds.), Climate Change 2007: Synthesis Report. IPCC, Geneva, pp. 44.

Buishand, T.A., 1978. Some remarks on the use of daily rainfall models. Journal of Hydrology, 36(3-4): 295-308.

Bureau of Reclamation, U.S., 2009. Long-Term Planning Hydrology based on Various Blends of Instrumental Records, Paleoclimate, and Projected Climate Information.

Cayan, D.R., Kammerdiener, S.A., Dettinger, M.D., Caprio, J.M., Peterson, D.H., 2001. Changes in the onset of spring in the western United States. Bulletin of the American Meteorological Society, 82(3): 399-416.

Christensen, N.S., Lettenmaier, D.P., 2007. A multimodel ensemble approach to assessment of climate change impacts on the hydrology and water resources of the Colorado River Basin. Hydrology and Earth System Sciences, 11(4): 1417-1434.

Collins, W.D., Bitz, C.M., Blackmon, M.L., Bonan, G.B., Bretherton, C.S., Carton, J.A., Chang, P., Doney, S.C., Hack, J.J., Henderson, T.B., 2006. The community climate system model: CCSM3. Journal of Climate, 19(11): 2122-2143.

Delworth, T.L., Broccoli, A.J., Rosati, A., Stouffer, R.J., Balaji, V., Beesley, J.A., Cooke, W.F., Dixon, K.W., Dunne, J., Dunne, K.A., 2006. GFDL's CM2 global coupled climate models. Part I: Formulation and simulation characteristics. Journal of Climate, 19(5): 643-674.

Diansky, N.A., Volodin, E.M., 2002. Simulation of present-day climate with a coupled atmosphere-ocean general circulation model. Izvestiya Atmospheric and Oceanic Physics, 38(6): 732-747.

Flato, G.M., Boer, G.J., 2001. Warming asymmetry in climate change simulations. Geophysical Research Letters, 28(1): 195-198.

Fontaine, T.A., Cruickshank, T.S., Arnold, J.G., Hotchkiss, R.H., 2002. Development of a snowfall-snowmelt routine for mountainous terrain for the soil water assessment tool (SWAT). Journal of Hydrology, 262(1-4): 209-223.

Furevik, T., Bentsen, M., Drange, H., Kindem, I.K.T., Kvamstø, N.G., Sorteberg, A., 2003. Description and evaluation of the Bergen climate model: ARPEGE coupled with MICOM. Climate Dynamics, 21(1): 27-51.

Gordon, C., Cooper, C., Senior, C.A., Banks, H., Gregory, J.M., Johns, T.C., Mitchell, J.F.B., Wood, R.A., 2000. The simulation of SST, sea ice extents and ocean heat transports in a version of the Hadley Centre coupled model without flux adjustments. Climate Dynamics, 16(2-3): 147-168.

Gordon, H.B., Rotstayn, L.D., McGregor, J.L., Dix, M.R., Kowalczyk, E.A., O'Farrell, S.P., Waterman, L.J., Hirst, A.C., Wilson, S.G., Collier, M.A., Watterson, I.G., Elliot, T.I., 2002. The CSIRO Mk3 climate system model, Victoria, Australia.

Hamlet, A.F., Mote, P.W., Clark, M.P., Lettenmaier, D.P., 2005. Effects of temperature and precipitation variability on snowpack trends in the western United States. Journal of Climate, 18: 4545-4561.

Hanson, C., 1982. Distribution and stochastic generation of annual and monthly precipitation on a mountainous watershed in southwest Idaho. Journal of the American Water Resources Association, 18(5): 875-883.

Hasumi, H., Emori, S., 2004. K-1 coupled model (MIROC) description.

Hoerling, M., Eischeid, J., 2007. Past peak water in the Southwest. Southwest Hydrology, 6(1): 18-19.

IPCC, 2000. Special Report on Emissions Scenarios, Cambridge, UK, 612 pp. pp.

Jaccard, P., 1908. Nouvelles recherches sur la distribution florale. Bulletin de la Société Vaudoise des Sciences Naturelles, 44(163): 223-269.

Jungclaus, J., Keenlyside, N., Botzet, M., Haak, H., Luo, J., Latif, M., Marotzke, J., Mikolajewicz, U., Roeckner, E., 2006. Ocean circulation and tropical variability in the coupled model ECHAM5/MPI-OM. Journal of Climate, 19(16): 3952-3972.

Knowles, N., Dettinger, M.D., Cayan, D.R., 2006. Trends in snowfall versus rainfall in the western United States. Journal of Climate, 19(18): 4545-4559.

Kundzewicz, Z.W., Mata, L.J., Arnell, N.W., Doll, P., Kabat, P., Jiménez, B., Miller, K., Oki, T., Sen, Z., Shiklomanov, I., 2007. Freshwater resources and their management. In: Parry, M.L., Canziani, O.F., Palutikof, J.P., van der Linden, P.J., Hanson, C.E. (Eds.), Climate Change 2007: Impacts, Adaptation and Vulnerability. Contribution of Working Group II to the Fourth Assessment Report of the Intergovernmental Panel on Climate Change. Cambridge University Press, Cambridge, UK, pp. 173-210.

Legutke, S., Voss, R., 1999. The Hamburg atmosphere-ocean coupled circulation model-ECHO-G, Hamburg.

Mann, H.B., 1945. Nonparametric tests against trend. Econometrica: Journal of the Econometric Society, 13(3): 245-259.

Marti, O., Braconnot, P., Bellier, J., Benshila, R., Bony, S., Brockmann, P., Cadule, P., Caubel, A., Denvil, S., Dufresne, J.L., Fairhead, L., Filiberti, M.A., Foujols, M.A., T. Fichefet, T., Friedlingstein, P., Gosse, H., Grandpeix, J.Y., F. Hourdin, F., Krinner, G., Lévy, C., Madec, G., Musat, I., de Noblet, N., Polcher, J., Talandier, C., 2006. The new IPSL climate system model: IPSL-CM4, Paris, France.

Maurer, E.P., Brekke, L., Pruitt, T., Duffy, P.B., 2007. Fine-resolution climate projections enhance regional climate change impact studies. EOS Transactions American Geophysical Union, 88(47): 504.

Maurer, E.P., Wood, A.W., Adam, J.C., Lettenmaier, D.P., Nijssen, B., 2002. A long-term hydrologically based dataset of land surface fluxes and states for the conterminous United States. Journal of Climate, 15(22): 3237-3251.

McCormick, W.P., Lyons, N.I., Hutcheson, K., 1992. Distributional properties of jaccard's index of similarity. Communications in Statistics-Theory and Methods, 21(1): 51-68.

Meehl, G.A., Covey, C., Delworth, T., Latif, M., McAvaney, B., Mitchell, J.F.B., Stouffer, R.J., Taylor, K.E., 2007. The WCRP CMIP3 multimodel dataset. Bulletin of the American Meteorological Society, 88(9): 1383-1394.

Milly, P.C.D., Dunne, K.A., Vecchia, A.V., 2005. Global pattern of trends in streamflow and water availability in a changing climate. Nature, 438(17): 347-350.

Mote, P.W., Hamlet, A.F., Clark, M.P., Lettenmaier, D.P., 2005. Declining Mountain Snowpack in Western North America. Bulletin of the American Meteorological Society, 86(1): 39-49.

Potts, D.F., 1984. Hydrologic impacts of a large-scale Mountain Pine Beetle (*Dendroctonus Ponderosae*) epidemic. American Water Resources Association, 20(3): 373-377.

Praskievicz, S., Chang, H., 2009. A review of hydrological modelling of basin-scale climate change and urban development impacts. Progress in Physical Geography, 33(5): 650-671.

Ray, A.J., Barsugli, J.J., Averyt, K.B., Wolter, K., Hoerling, M., Doesken, N., Udall, B., Webb, R.S., 2008. Climate Change in Colorado: A Synthesis to Support Water Resources Management and Adaptation.

Russell, G.L., Miller, J.R., Rind, D., Ruedy, R.A., Schmidt, G.A., Sheth, S., 2000. Comparison of model and observed regional temperature changes during the past 40 years. Journal of Geophysical Research, 105(D11): 14,891-14,898.

Salas-Mélia, D., Chauvin, F., Déqué, M., Douville, H., Gueremy, J.F., Marquet, P., Planton, S., Royer, J.F., Tyteca, S., 2005. Description and validation of the CNRM-CM3 global coupled model. Climate Dynamics (in review).

Salmi, T., Määttä, A., Anttila, P., Ruoho-Airola, T., Amnell, T., 2002. Detecting Trends of Annual Values of Atmospheric Pollutants by the Mann-Kendall Test and Sen's Slope Estimates - The Excel Template Application MAKESENS, Helinski.

Schuol, J., Abbaspour, K.C., 2007. Using monthly weather statistics to generate daily data in a SWAT model application to West Africa. Ecological Modelling, 201(3-4): 301-311.

Sen, P., 1968. Estimates of the regression coefficient based on Kendall's tau. Journal of the American Statistical Association, 63(324): 1379-1389.

Serreze, M.C., Clark, M.P., Armstrong, R.L., McGinnis, D.A., Pulwarty, R.S., 1999. Characteristics of the western United States snowpack from snowpack telemetry (SNOTEL) data. Water Resources Research, 35(7): 2145-2160.

Shepard, D., 1984. Computer mapping: The SYMAP interpolation algorithm. In: Gaile, G.L., Willmott, C. (Eds.), Spatial Statistics and Models. Springer, pp. 133–145.

Stewart, I.T., 2009. Changes in snowpack and snowmelt runoff for key mountain regions. Hydrological Processes, 23(1): 78-94.

Stewart, I.T., Cayan, D.R., Dettinger, M.D., 2004. Changes in snowmelt runoff timing in western North America under abusiness as usual'climate change scenario. Climatic Change, 62(1-3): 217-232.

Stonefelt, M.D., Fontaine, T.A., Hotchkiss, R.H., 2000. Impacts of climate change on water yield in the Upper Wind River Basin. Journal of the American Water Resources Association, 36(2): 321-336.

Trenberth, K.E., Jones, P.D., Ambenje, P., Bojariu, R., Easterling, D., Tank, A.K., Parker, D., Rahimzadeh, F., Renwick, J.A., Rusticucci, M., Soden, B., Zhai, P., 2007. Observations: surface and atmospheric climate change. In: Solomon, S., Qin, D., Manning, M., Chen, Z., Marquis, M., Averyt, K.B., Tignor, M., Miller, H.L. (Eds.), Climate Change 2007: The Physical Science Basis: Contribution of Working Group I to the Fourth Assessment Report of the Intergovernmental Panel on Climate Change. Cambridge University Press, Cambridge, UK, pp. 236-336.

United Nations Committee on Economic, S.a.C.R., 2003. General Comment No. 15 (2002). United Nations Economic and Social Council, Geneva, pp. 1-18.

Washington, W.M., Weatherly, J.W., Meehl, G.A., Semtner Jr, A.J., Bettge, T.W., Craig, A.P., Strand Jr, W.G., Arblaster, J., Wayland, V.B., James, R., 2000. Parallel climate model (PCM) control and transient simulations. Climate Dynamics, 16(10): 755-774.

Wood, A.W., Leung, L.R., Sridhar, V., Lettenmaier, D.P., 2004. Hydrologic implications of dynamical and statistical approaches to downscaling climate model outputs. Climatic Change, 62(1-3): 189-216.

Wood, A.W., Maurer, E.P., Kumar, A., Lettenmaier, D.P., 2002. Long range experimental hydrologic forecasting for the eastern US. Journal of Geophysical Research, 107(D20): ACL 6-1 - 6-15.

Yukimoto, S., Noda, A., Kitoh, A., Sugi, M., Kitamura, Y., Hosaka, M., Shibata, K., Maeda, S., Uchiyama, T., 2001. The new Meteorological Research Institute coupled GCM(MRI-CGCM 2) - Model climate and variability. Papers in Meteorology and Geophysics, 51(2): 47-88.

## CHAPTER 4: CONCLUSIONS

The headwater basins of Colorado are heavily relied upon for freshwater resources, of which the demand for is only projected to increase in the future. However, knowledge concerning the generation of such resources and the implications of climate change on their availability is not well understood. Thus, this research was undertaken to investigate the potential hydrologic response to a changing climate at the watershed scale in mountainous Colorado over the course of the 21$^{st}$ century. Specifically, the objectives of this study were (i) to develop and test a comprehensive process-based watershed model that can, with a high level of confidence, represent important hydrologic processes in the snowmelt-dominated headwater catchments of Colorado; (ii) to observe the dominance of various hydrologic fluxes in the study watersheds based on observed conditions in the past; (iii) to downscale, in space and time, an ensemble of climate projections in a manner which addresses both the error involved and uncertainty inherent in climate modeling through incorporation of numerous models and diverse emissions scenarios; and (iv) to objectively identify the direction and degree of potential impacts on water resources, namely water yield, in Colorado and associate specific climate projections with low and high conditions of freshwater availability.

The Soil and Water Assessment Tool (SWAT) was used for simulation of hydrologic processes on a daily time-step in headwater basins of Colorado. The study watersheds are located on both sides of the Continental Divide and represent various

physiographic and climatic conditions occurring across the state. The SWAT model was calibrated and tested over a 16 year period (1990 – 2005) at multiple nested locations within each basin to ascertain the robustness of the simulation approach at varying spatial scales. Naturalized streamflows were utilized for calibration and testing in order to unambiguously discern the impacts of climate variability on hydrologic fluxes from alterations caused by diversions, dams, and other man-made storage and transfer structures. Calibration was performed over the first 8 years (1990 – 1997), and compared the more common Shuffled Complex Evolution – University of Arizona (SCE-UA) parameter optimization technique to a Markov Chain Monte Carlo (MCMC) method known as the Gibbs Sampler Algorithm (GSA). Hydrologic fluxes including evapotranspiration (ET), water yield, surface runoff, subsurface lateral flow, and groundwater discharge (baseflow) were quantified over the 16 year simulation period to evaluate their respective dominance in Colorado basins. The calibrated and tested model was then forced with a suite of General Circulation Model (GCM) projections of precipitation and temperature to take into account the range of aleatory and epistemic uncertainties inherent in predicting future conditions. The suite of projections, consisting of 112 individual scenarios, was downscaled in both space and time in a manner that preserved the observed spatial and temporal correlations of temperature and precipitation. Each watershed model was run for a period of 90 years over the 21$^{st}$ century, from 2010 – 2099. Results from the model were used to quantify the range and emission scenario ensemble averages (emission paths A2, A1B, and B1) of changes in temperature, precipitation, snowfall, ET, potential evapotranspiration (PET), and streamflow (yield). Additionally, trends in average annual streamflow for each of the 112 individual

projections were tested for statistical significance over the 21st century, and specific projections resulting in a similar response across all study watersheds in CO were identified.

Satisfactory results from the calibration and testing periods indicate a high level of confidence in simulation of streamflow, with Nash-Sutcliffe efficiency coefficients ($E_{NS}$) at the watershed outlets ranging from 0.86 – 0.95 and 0.70 – 0.90 over the calibration and validation periods, respectively. The most dominant hydrologic flux observed in all study basins was ET, with 55% – 65% of precipitation going to ET on an average annual basis over the 16 year period. Lateral flow was simulated to be a major source of gross water yield, with 64% – 82% contributions on an average annual basis during the same period. Future projections of climate showed an increase in temperature and variable responses in precipitation across the three emissions scenarios A2, A1B, and B1 over the 21st century. Emissions scenario ensemble averages depicted a general increase in winter precipitation, a lower snow to total precipitation ratio, and an earlier occurrence of the snowmelt-dominated hydrograph in all study basins. Statistically significant trends in average annual streamflow were variable across the region. The Yampa basin showed strong evidence of increasing streamflow over the 21st century, while the other three basins showed mixed results. Generally, the projections suggest a decrease in streamflow in the San Juan and Gunnison basins and an increase in streamflow in the Cache la Poudre basin. Twelve individual projections were found to produce the same trend direction of annual streamflow across all four study basins, with six corresponding to increasing trends and six corresponding to decreasing trends. Regardless of the trends in streamflow, emissions path ensemble averages show a

decrease in the ratio of precipitation to PET in all study basins, which suggests all watersheds moving towards more arid environments in the future.

The results of this research show variable hydrologic response to climate change across the region depending on the geographic location and specific characteristics of a given watershed. Implications of this study are considerable, as management of water resources, both within the state and across the West, will be affected by the availability of freshwater in the future. The amount and timing of diversion, transfer, and storage of water in addition to the infrastructure required by such, will all be reliant on future hydrologic conditions. Thus, predictive tools that can represent hydrologic processes at smaller scales will continue to become more important to expose basin-specific hydrologic response to climate change, especially in mountainous headwater catchments of Colorado.

# APPENDIX A – SUPPLEMENTARY FIGURES

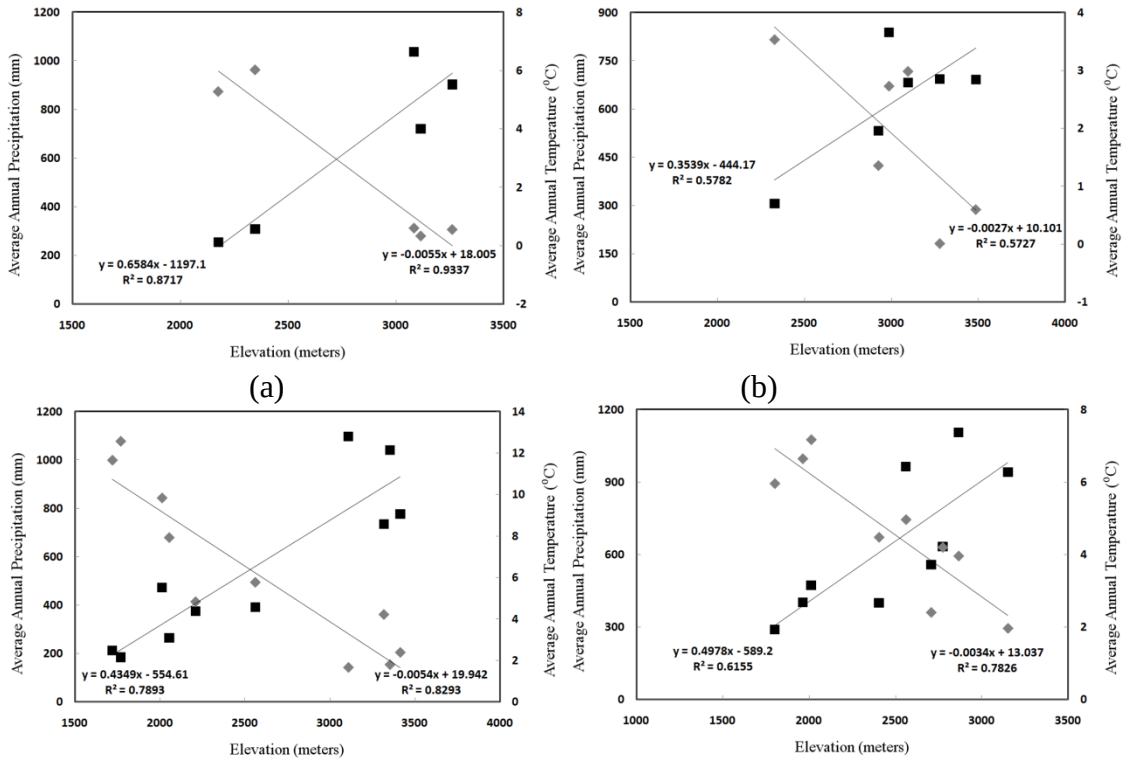


**Figure A.1** – Temperature and precipitation lapse rates in the (a) Cache la Poudre, (b) Gunnison, (c) San Juan, and (d) Yampa River basins. Lapse rates were computed using linear regression in Microsoft Excel with the coefficient of determination ($R^2$) displayed below the equation.

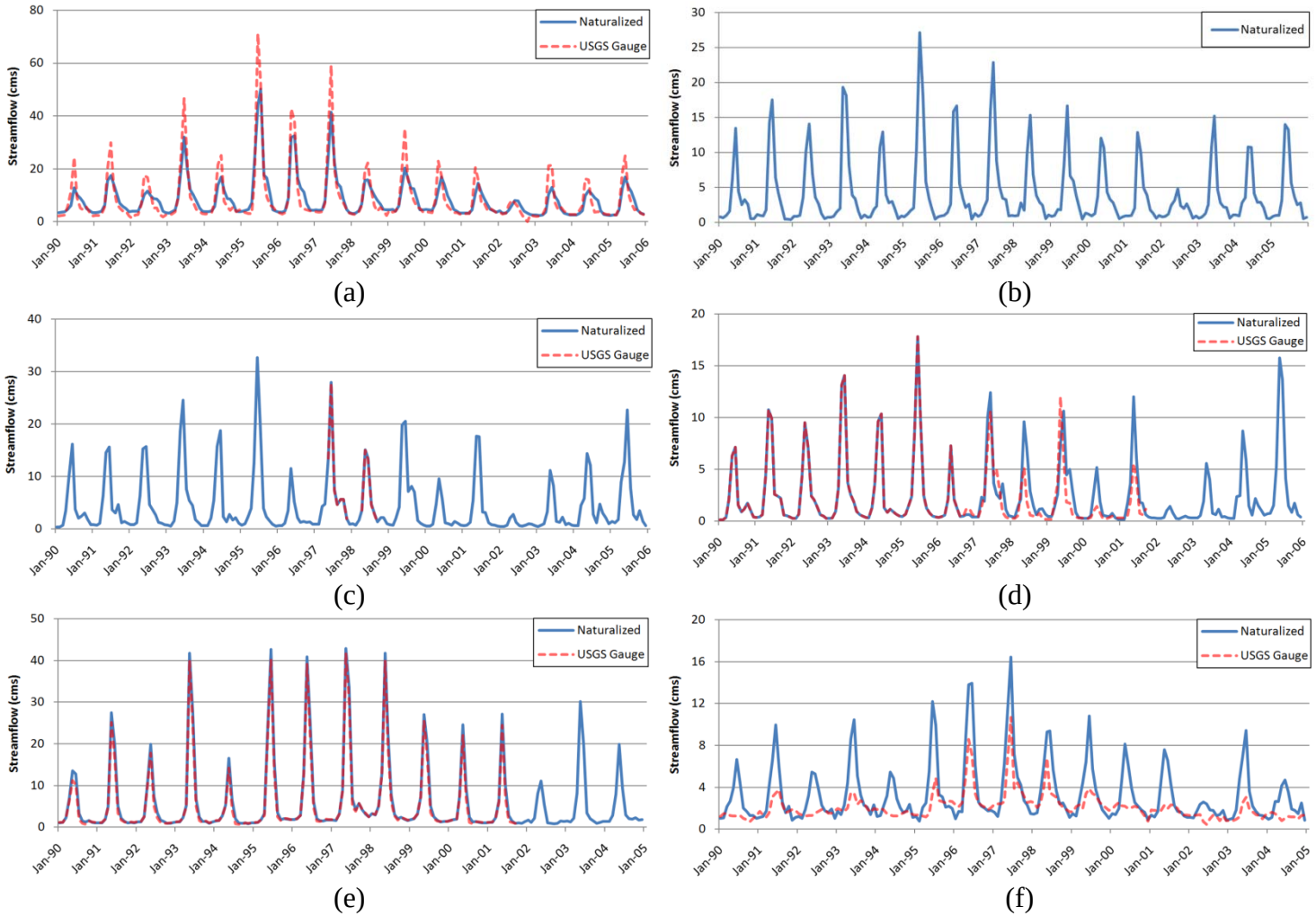


**Figure A.2** - A comparison between simulated naturalized and measured USGS gauge streamflows at multiple sites within each watershed; Gunnison (a) USGS 09110000, (b) USGS 09126500; San Juan (c) USGS 09341500, (d) USGS 09339900; and Yampa (e) USGS 09249750 (f) USGS 09237500. Several sites had either limited or no record of measured streamflow over the study period.

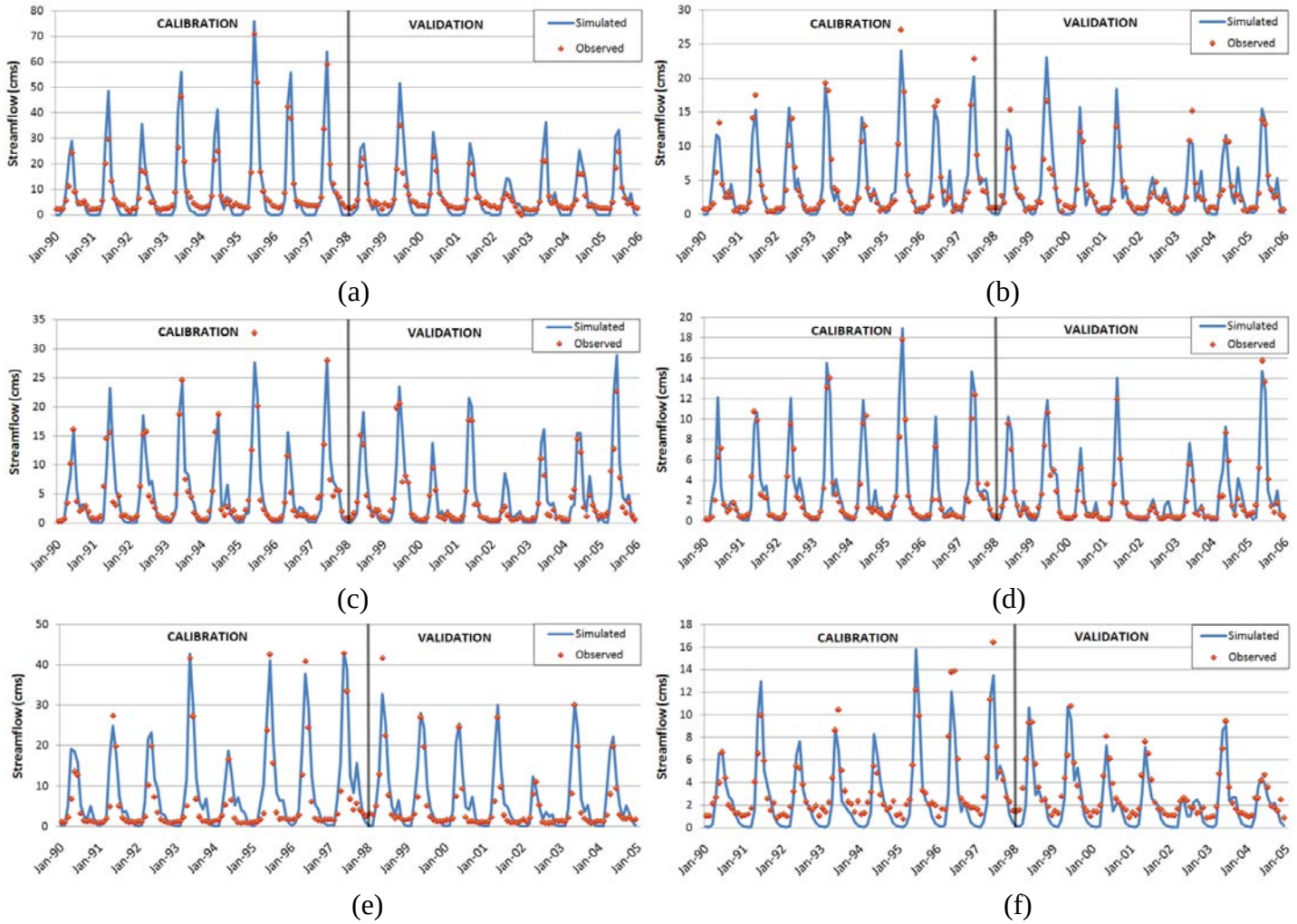


**Figure A.3** - Time series of simulated and observed (naturalized) streamflows over the calibration and validation periods at multiple sites within each watershed; Gunnison (a) USGS 09110000, (b) USGS 09126500; San Juan (c) USGS 09341500, (d) USGS 09339900; and Yampa (e) USGS 09249750 (f) USGS 09237500.

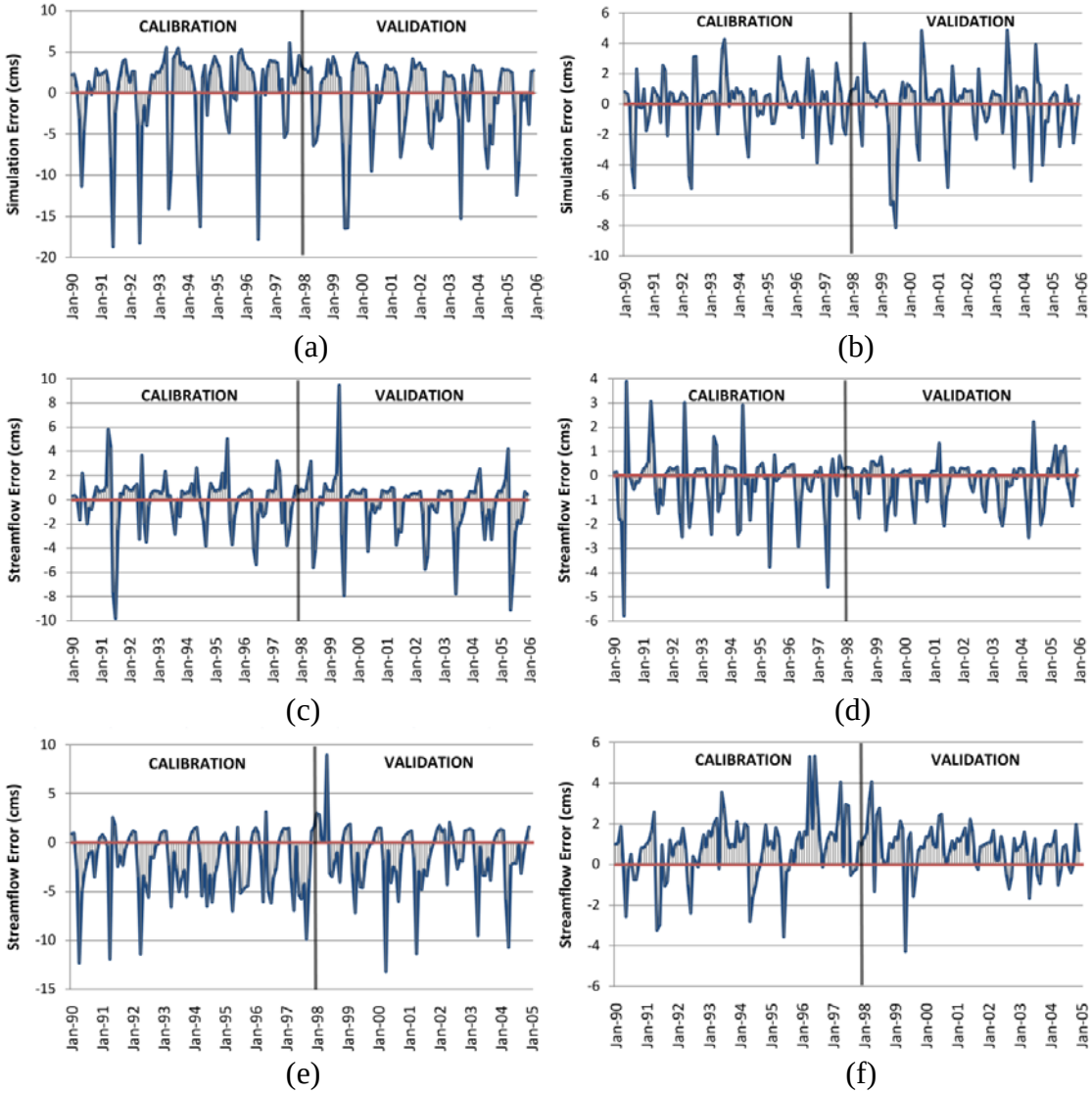


**Figure A.4** - Time series of streamflow error (observed – simulated) over the calibration and validation periods at multiple sites within each watershed; Gunnison (a) USGS 09110000, (b) USGS 09126500; San Juan (c) USGS 09341500, (d) USGS 09339900; and Yampa (e) USGS 09249750 (f) USGS 09237500.

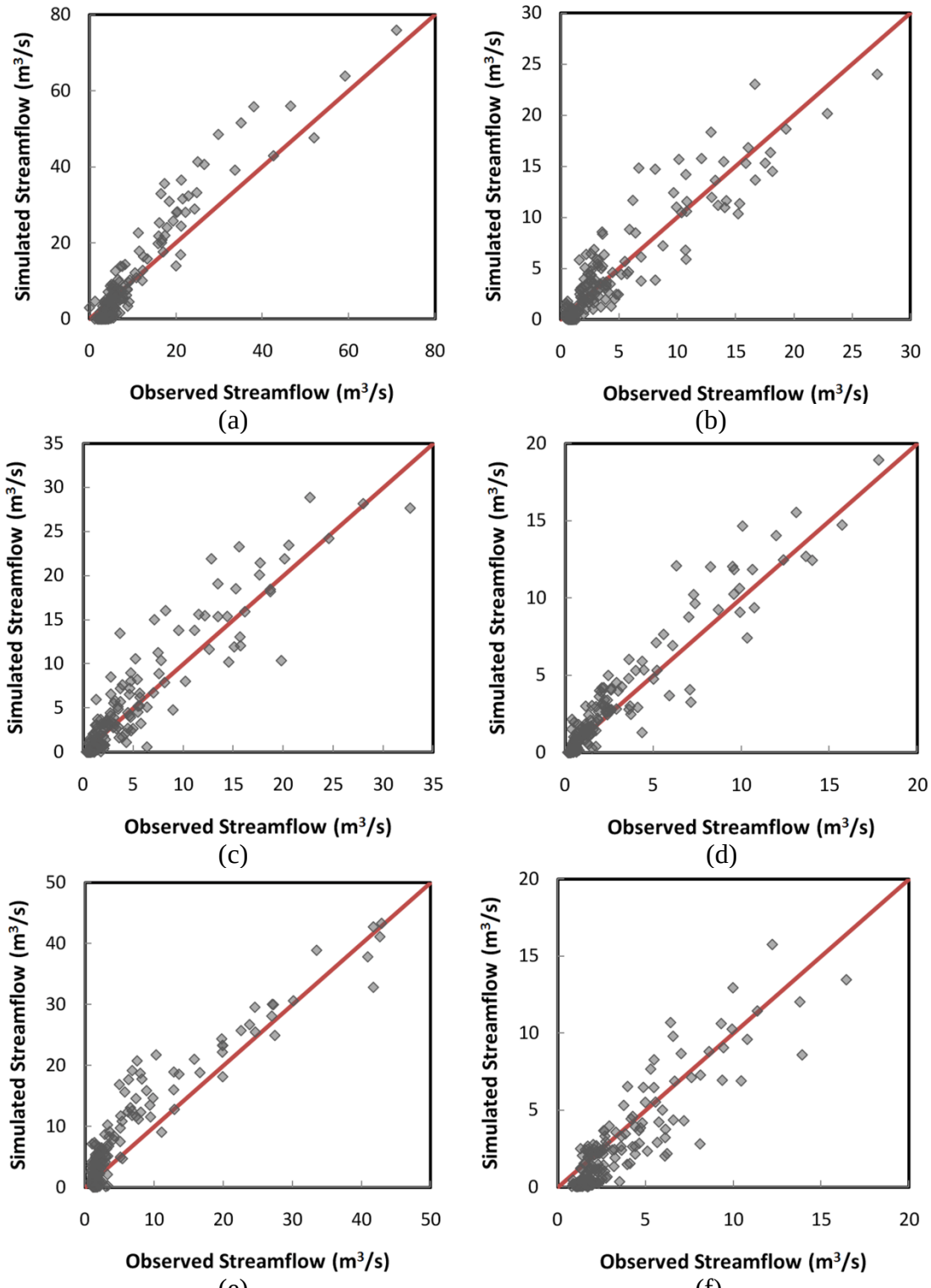


**Figure A.5 -** Observed versus simulated monthly streamflows over the 1990 – 2005 (1990 – 2004 in Yampa) study period at multiple sites within each study watershed; Gunnison (a) USGS 09110000, (b) USGS 09126500; San Juan (c) USGS 09341500, (d) USGS 09339900; and Yampa (e) USGS 09249750 (f) USGS 09237500.

# APPENDIX B: SUPPLEMENTARY TABLES

**Table B.1 –** NLCD 1992 land use/land cover lookup table.

| NLCD 1992 Type | SWAT LULC Code | SWAT LULC Description |
|---|---|---|
| Open Water | WATR | Water |
| Perennial Ice/Snow | WATR | Water |
| Low-Intensity Residential | URLD | Residential-Low Density |
| High-Intensity Residential | URHD | Residential-High Density |
| Commercial/Industrial/Transportation | UCOM | Commercial |
| Bare Rock/Sand/Clay | SWRN | Southwestern US (Arid) Range |
| Quarries/Strip Mines/Gravel Pits | SWRN | Southwestern US (Arid) Range |
| Transitional | SWRN | Southwestern US (Arid) Range |
| Deciduous Forest | FRSD | Forest-Deciduous |
| Evergreen Forest | FRSE | Forest-Evergreen |
| Mixed Forest | FRST | Forest-Mixed |
| Shrubland | RNGB | Range-Brush |
| Orchards/Vineyards/Other | ORCD | Orchard |
| Grasslands/Herbaceous | RNGE | Range-Grasses |
| Pasture/Hay | HAY | Hay |
| Row Crops | AGRR | Agricultural Land-Row Crops |
| Small Grains | WWHT | Winter Wheat |
| Fallow | PAST | Pasture |
| Urban/Recreational Grasses | URLD | Residential-Low Density |
| Woody Wetlands | WETF | Wetlands-Forested |
| Emergent Herbaceous Wetlands | WETN | Wetlands-Non-Forested |

**Table B.2 –** NLCD 2001 Land use/land cover lookup table.

| NLCD 2001 Type | SWAT LULC Code | SWAT LULC Description |
|---|---|---|
| Open Water | WATR | Water |
| Perennial Ice/Snow | WATR | Water |
| Developed, Open Space | URLD | Residential-Low Density |
| Developed, Low Intensity | URMD | Residential-Medium Density |
| Developed, Medium Intensity | URHD | Residential-High Density |
| Developed, High Intensity | UIDU | Industrial |
| Barren Land (Rock/Sand/Clay) | SWRN | Southwestern US (Arid) Range |
| Unconsolidated Shore* | SWRN | Southwestern US (Arid) Range |
| Deciduous Forest | FRSD | Forest-Deciduous |
| Evergreen Forest | FRSE | Forest-Evergreen |
| Mixed Forest | FRST | Forest-Mixed |
| Dwarf Scrub | RNGB | Range-Brush |
| Shrub/Scrub | RNGB | Range-Brush |
| Grassland/Herbaceous | RNGE | Range-Grasses |
| Sedge/Herbaceous | RNGE | Range-Grasses |
| Lichens | RNGE | Range-Grasses |
| Moss | RNGE | Range-Grasses |
| Pasture/Hay | HAY | Hay |
| Cultivated Crops | AGRR | Agricultural Land-Row Crops |
| Woody Wetlands | WETF | Wetlands-Forested |
| Palustrine Forested Wetland* | WETF | Wetlands-Forested |
| Palustrine Scrub/Shrub Wetland* | WETL | Wetlands-Mixed |
| Estuarine Forested Wetland* | WETF | Wetlands-Forested |
| Estuarine Scrub/Shrub Wetland* | WETL | Wetlands-Mixed |
| Emergent Herbaceous Wetlands | WETN | Wetlands-Non-Forested |
| Palustrine Emergent Wetland (Persistent)* | WETN | Wetlands-Non-Forested |
| Estuarine Emergent Wetland* | WETN | Wetlands-Non-Forested |
| Palustrine Aquatic Bed* | WATR | Water |
| Estuarine Aquatic Bed* | WATR | Water |

* Indicates the NLCD description is applicable to coastal areas only.

**Table B.3 –** SWAT streamflow parameters with their allowable ranges and corresponding processes.

| No. | Parameter | Min | Max | Definition | Process |
|---|---|---|---|---|---|
| $x_1$ | DEPIMP_BSN | 0 | 6000 | Depth to impervious layer (mm) | Groundwater |
| $x_2$ | EPCO | 0.01 | 1 | Plant evaporation compensation factor | Evaporation |
| $x_3$ | SFTMP | -5 | 5 | Snowfall temperature (°C) | Snow cover |
| $x_4$ | SMFMN | 0 | 10 | Melt factor on June 21 (mm /°C/day) | Snowmelt |
| $x_5$ | SMFMX | 0 | 10 | Melt factor on Dec 21(mm/°C/day) | Snowmelt |
| $x_6$ | SMTMP | -5 | 5 | Threshold temperture for snowmelt (°C) | Snowmelt |
| $x_7$ | SNOCOVMX | 0 | 650 | Minimum snow water content that corresponds to 100% snow cover (mm) | Snow cover |
| $x_8$ | SNO50COV | 0 | 1 | Fraction of snow volume represented by SNOCOVMX that corresponds to 50% snow cover | Snow cover |
| $x_9$ | SURLAG | 1 | 24 | Surface runoff lag coefficient | Runoff |
| $x_{10}$ | TIMP | 0.01 | 1 | Snow temperature lag factor | Snowmelt |
| $x_{11}$ | ALPHA_BF | 0 | 1 | Baseflow recession constant | Groundwater |
| $x_{12}$ | GW_DELAY | 0 | 500 | Groundwater delay (days) | Groundwater |
| $x_{13}$ | GW_REVAP | 0.02 | 0.2 | Groundwater Revap coefficient | Groundwater |
| $x_{14}$ | GW_SPYLD* | -0.5 | 1 | Fraction change in specific yield of the shallow aquifer | Groundwater |
| $x_{15}$ | GWHT | 0 | 25 | Initial groundwater height (m) | Groundwater |
| $x_{16}$ | GWQMN | 0 | 5000 | Threshold water level in shallow aquifer for baseflow to occur (mm) | Groundwater |
| $x_{17}$ | RCHRG_DP | 0 | 1 | Groundwater recharge to deep aquifer (fraction) | Groundwater |
| $x_{18}$ | REVEP_MN | 0 | 500 | Threshold water level in the shallow aquifer for Revap to occur (mm) | Groundwater |
| $x_{19}$ | ESCO | 0.01 | 1 | Soil evaporation compensation factor | Evaporation |
| $x_{20}$ | CANMX | 0 | 10 | Maximum canopy storage | Runoff |
| $x_{21}$ | OV_N | 0.01 | 0.3 | Manning's n for overland flow | Runoff |
| $x_{22}$ | SLOPE* | -0.1 | 0.1 | Fraction change in slope of HRU | Geomorphology |

**Table B.3 (contd) –** SWAT streamflow parameters with their allowable ranges and corresponding processes.

| No. | Parameter | Min | Max | Definition | Process |
|---|---|---|---|---|---|
| $x_{23}$ | CN_F* | -0.15 | 0.15 | Fraction change in curve number | Runoff |
| $x_{24}$ | CH_KII | -0.01 | 500 | Effective hydraulic conductivity of channel (mm/hr) | Channel |
| $x_{25}$ | CH_NII | 0.01 | 0.3 | Manning's n for main channel | Channel |
| $x_{26}$ | CH_SII* | -0.05 | 0.05 | Fraction change in average channel slope along channel length | Channel |
| $x_{27}$ | SOL_AWC* | -0.1 | 2 | Fraction change in available water capacity of the soil layer | Groundwater |
| $x_{28}$ | SOL_K* | -0.5 | 5 | Fraction change in soil conductivity | Groundwater |
| $x_{29}$ | CH_KI | 0 | 300 | Effective hydraulic conductivity of channel (mm/hr) | Channel |
| $x_{30}$ | CH_NI | 0.008 | 0.3 | Manning's n for tributary channel | Channel |
| * These parameters were varied as a percentage of their default values to maintain their relative spatial variability. | | | | | |

**Table B.4** – Meteorological stations implemented into the SWAT models.

| Basin | Station Name | Source | Latitude | Longitude | Elevation (m) | Period of Record |
|---|---|---|---|---|---|---|
| Cache la Poudre | Deadman Hill, CO | SNOTEL | 40.80 | -105.77 | 3115.1 | 10/1/1978 - Present |
| | Joe Wright, CO | SNOTEL | 40.53 | -105.88 | 3084.6 | 10/1/1978 - Present |
| | Laramie 2NW, WY | NCDC | 41.33 | -105.60 | 2176.3 | 5/1/1966 - Present |
| | Red Feather Lakes 2SE, CO | NCDC | 40.78 | -105.55 | 2488.7 | 8/1/1948 - 7/1/1990 |
| | Red Feather Lakes, CO* | NCDC | 40.80 | -105.58 | 2529.8 | 7/1/1991 - 5/27/1997 |
| | Rustic 9WSW, CO | NCDC | 40.70 | -105.72 | 2347.0 | 4/1/1993 - Present |
| | Willow Park, CO | SNOTEL | 40.43 | -105.73 | 3261.4 | 7/5/1980 - Present |
| Gunnison | Butte, CO | SNOTEL | 38.90 | -106.95 | 3096.8 | 10/1/1981 - Present |
| | Gunnison 3SW, CO | NCDC | 38.53 | -106.97 | 2323.8 | 8/1/1948 - Present |
| | Idarado, CO | SNOTEL | 37.93 | -107.68 | 2987 | 7/23/1980 - Present |
| | Park Cone, CO | SNOTEL | 38.82 | -106.58 | 2926.1 | 8/10/1980 - Present |
| | Porphyry Creek, CO | SNOTEL | 38.48 | -106.33 | 3279.6 | 10/1/1978 - Present |
| | Slumgullion, CO | SNOTEL | 37.98 | -107.20 | 3486.9 | 8/19/1980 - Present |
| San Juan | Aztec Ruins National Monument, NM | NCDC | 36.83 | -108.00 | 1720.3 | 7/1/1946 - Present |
| | Bloomfield 3SE, NM | NCDC | 36.67 | -107.97 | 1769.7 | 7/1/1946 - Present |
| | Chamita, NM | SNOTEL | 36.95 | -106.65 | 2560.3 | 10/1/1979 - Present |
| | Durango, CO | NCDC | 37.28 | -107.88 | 2011.7 | 12/1/1904 - 2/27/1991 |
| | Durango, CO** | NCDC | 37.28 | -107.85 | 2060.8 | 2/27/1991 - Present |
| | El Vado Dam, NM | NCDC | 36.60 | -106.73 | 2054.4 | 7/1/1946 - Present |
| | Pagosa Springs, CO | NCDC | 37.25 | -107.02 | 2209.8 | 8/1/1948 - 11/18/1998 |
| | Pagosa Springs 2W, CO*** | NCDC | 37.27 | -107.05 | 2319.5 | 10/1/1999 - Present |
| | Stump Lakes, CO | SNOTEL | 37.48 | -107.63 | 3413.8 | 10/1/1986 - Present |
| | Upper San Juan, CO | SNOTEL | 37.48 | -106.83 | 3108.9 | 10/1/1978 - Present |
| | Vallecito, CO | SNOTEL | 37.48 | -107.50 | 3316.2 | 10/1/1986 - Present |
| | Wolf Creek Summit, CO | SNOTEL | 37.48 | -106.80 | 3352.8 | 10/1/1986 - Present |

**Table B.4 (contd)** – Meteorological stations implemented into the SWAT models.

| Basin | Station Name | Source | Latitude | Longitude | Elevation (m) | Period of Record |
|---|---|---|---|---|---|---|
| Yampa | Craig 4SW, CO | NCDC | 40.45 | -107.58 | 1980.0 | 5/5/1977 - Present |
| | Crosho, CO | SNOTEL | 40.17 | -107.05 | 2773.7 | 10/1/1986 - Present |
| | Dry Lake, CO | SNOTEL | 40.53 | -106.78 | 2560.3 | 10/1/1980 - Present |
| | Hayden, CO | NCDC | 40.50 | -107.25 | 1971.1 | 8/1/1948 - Present |
| | Lynx Pass, CO | SNOTEL | 40.08 | -106.67 | 2706.6 | 10/1/1980 - Present |
| | Maybell, CO | NCDC | 40.52 | -108.10 | 1811.7 | 6/1/1958 - Present |
| | Rabbit Ears, CO | SNOTEL | 40.37 | -106.73 | 2865.1 | 10/1/1986 - Present |
| | Ripple Creek, CO | SNOTEL | 40.10 | -107.30 | 3151.6 | 10/1/1986 - Present |
| | Yampa, CO | NCDC | 40.15 | -106.92 | 2394.8 | 8/1/1948 - Present |

*Combined with prior Red Feather Lakes 2SE station
**Combined with prior Durango station
***Combined with prior Pagosa Springs station